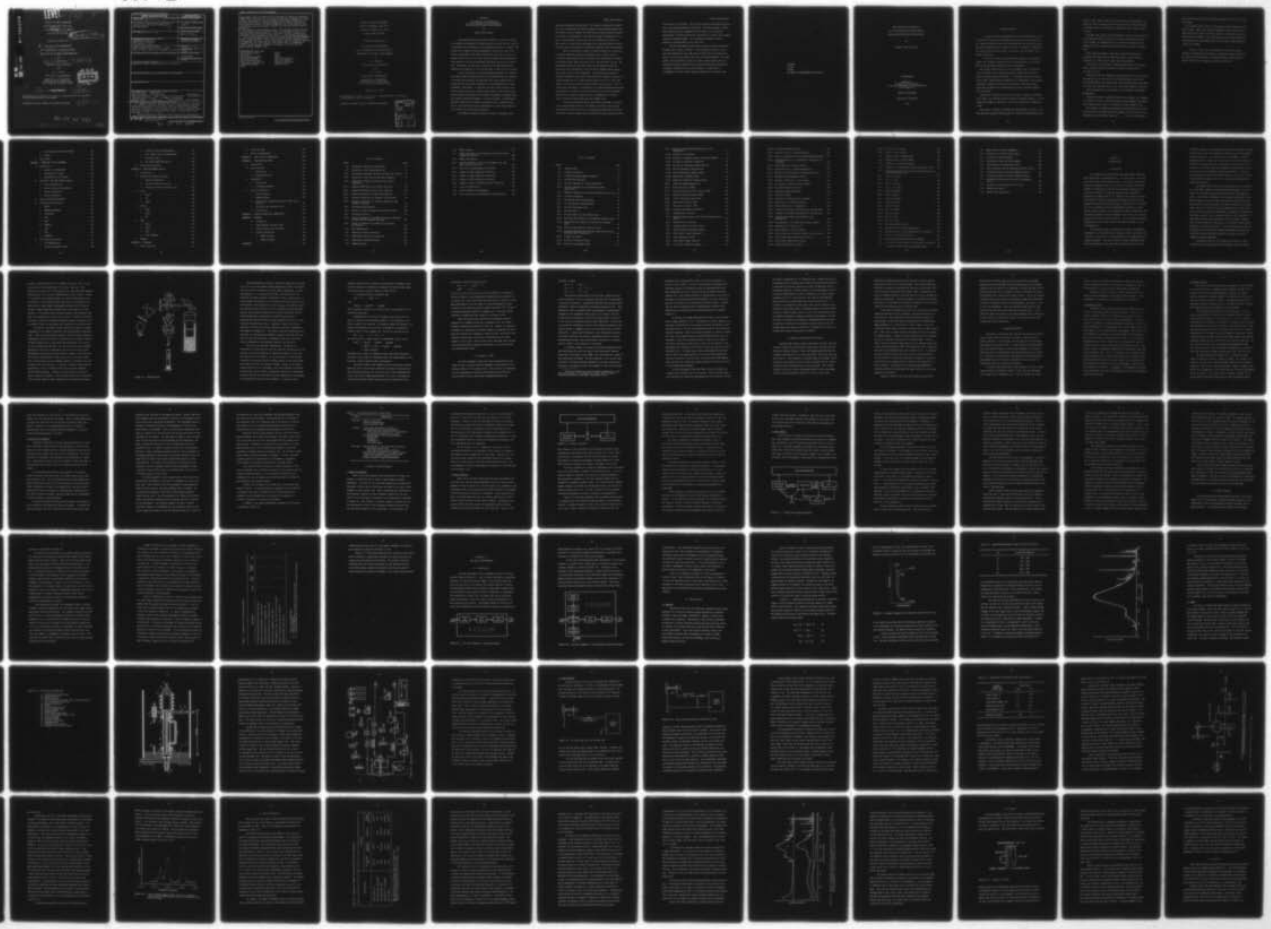
AD-A056 269 MICHIGAN STATE UNIV EAST LANSING DEPT OF CHEMISTRY F/G 14/2
THE DESIGN AND OPERATION OF AN AUTOMATED, HIGH-EFFICIENCY PHOTO--ETC(U)
FEB 78 E J DARLAND, G E LEROI N00014-76-C-0434
UNCLASSIFIED TR-1 NL




OF
6269

AD A056269
DDC FILE COPY
AU NO.

LEVEL II

(12)

OFFICE OF NAVAL RESEARCH

PHYSICS PROGRAM (Code 421)

(15) Contract N00014-76-C-0434

Project NR 394-009

(9) Doctoral thesis,

(1) Technical Report No. 1

(6) THE DESIGN AND OPERATION OF AN AUTOMATED, HIGH-EFFICIENCY PHOTOIONIZATION MASS SPECTROMETER.

by

(10) E. J. Darland, G. E. Leroi

(Doctoral Dissertation)

and

G. E. Leroi

(Principal Investigator)

Department of Chemistry
Michigan State University
East Lansing, Michigan 48824

DDC
RECEIVED
JUL 14 1978
A

(11) 24 February 24, 1978

(12) 528 p.

Reproduction in whole or in part is permitted for any purpose of the United States Government.

Approved for public release; distribution unlimited.

(14) TR-1

78 07 14 041

268563

JOB

SECURITY CLASSIFICATION OF THIS PAGE *(When Data Entered)*

REPORT DOCUMENTATION PAGE		READ INSTRUCTIONS BEFORE COMPLETING FORM
1. REPORT NUMBER Technical Report No. 1	2. GOVT ACCESSION NO.	3. RECIPIENT'S CATALOG NUMBER
4. TITLE *(and Subtitle)* The Design and Operation of an Automated, High-Efficiency Photoionization Mass Spectrometer		5. TYPE OF REPORT & PERIOD COVERED Interim 6. PERFORMING ORG. REPORT NUMBER
7. AUTHOR(s) E. J. Darland and G. E. Leroi		8. CONTRACT OR GRANT NUMBER(s) N00014-76-C-0434
9. PERFORMING ORGANIZATION NAME AND ADDRESS Department of Chemistry Michigan State University East Lansing, MI 48824		10. PROGRAM ELEMENT, PROJECT, TASK AREA & WORK UNIT NUMBERS Project No. NR 394-009
11. CONTROLLING OFFICE NAME AND ADDRESS Office of Naval Research, Physics Program (Code 421) 800 N. Quincy St., Arlington, VA 22217		12. REPORT DATE February 24, 1978 13. NUMBER OF PAGES 525
14. MONITORING AGENCY NAME & ADDRESS *(if different from Controlling Office)*		15. SECURITY CLASS. *(of this report)* Unclassified 15a. DECLASSIFICATION/DOWNGRADING SCHEDULE

16. DISTRIBUTION STATEMENT *(of this Report)*
Approved for public release; distribution unlimited

17. DISTRIBUTION STATEMENT *(of the abstract entered in Block 20, if different from Report)*

18. SUPPLEMENTARY NOTES

19. KEY WORDS *(Continue on reverse side if necessary and identify by block number)*
Photoionization Automation
Mass Spectrometry Data Acquisition (for more key
Efficiency, Operating Signal-to-Noise Ratio Expressions words see over)
Efficiency, Data Acquisition Artifacts, Instrumental
Computer Clocks Lamps (vuv) Vacuum Ultraiolet Vacuum Systems

20. ABSTRACT *(Continue on reverse side if necessary and identify by block number)*
A computer-controlled photoionization mass spectrometer is described, as are operating procedures designed to achieve maximum possible efficiency during data acquisition, and very high efficiency overall. The software necessary to implement these procedures as well as a set of guidelines which have been developed for facilitating user-computer interaction are also described. → next page

The data acquisition software includes provisions for performing at regular intervals during the experiment, any of several types of "correction

DD FORM 1 JAN 73 1473 EDITION OF 1 NOV 65 IS OBSOLETE
S/N 0102-LF-014-6601

SECURITY CLASSIFICATION OF THIS PAGE *(When Data Entered)*

78 07 14 041

measurements" that are necessary for eliminating the effects of scattered light, long term drifts, etc. The data are partially corrected and plotted as they are acquired so that their quality may be judged immediately. The software also includes a variable integration time option, which allows the integration time to be varied automatically on a point-by-point basis so that it is just long enough to acquire data with the desired signal-to-noise ratio.

An extensive safety interlock system, which monitors and controls the complex vacuum system and other utilities, is described in detail, as are the computer-interface electronics. The latter includes a unique pulse amplifier circuit designed for fast photon - or ion-counting applications.

The new instrument has been used to study the mixed chlorofluoromethanes $CFCl_3$, CF_2Cl_2 and CF_3Cl. There is some evidence that the observed parent ion appearance potentials may be significantly above the adiabatic ionization potentials for all three molecules, and further work is recommended to resolve several apparent paradoxes in presently available data for both parent and fragment ions.

Additional key words (#19)
Vacuum system control
Interlocks
Photon Counting/Counter
Ion Counting/Counter
Pulse Counting/Counter
Interaction, Computer-user
Chlorofluoromethanes
$CFCl_3$
CF_2Cl_2
$CFCl_3$
Freons
Ionization Potentials
Heats of Formation
Appearance Potentials
Software Design

OFFICE OF NAVAL RESEARCH

PHYSICS PROGRAM (Code 421)

Contract NOOO14-76-C-0434

Project NR 394-009

Technical Report No. 1

THE DESIGN AND OPERATION OF AN AUTOMATED, HIGH-EFFICIENCY PHOTOIONIZATION MASS SPECTROMETER

by

E. J. Darland

(Doctoral Dissertation)

and

G. E. Leroi

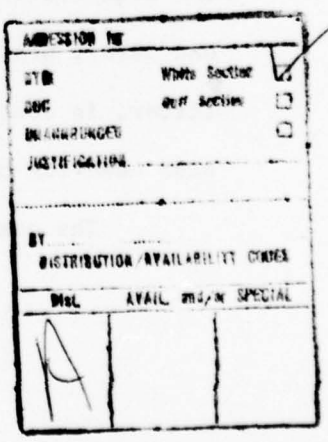
(Principal Investigator)

Department of Chemistry
Michigan State University
East Lansing, Michigan 48824

February 24, 1978

Reproduction in whole or in part is permitted for any purpose of the United States Government.

Approved for public release; distribution unlimited.



ABSTRACT

THE DESIGN AND OPERATION
OF AN AUTOMATED, HIGH-EFFICIENCY
PHOTOIONIZATION MASS SPECTROMETER

By

Edward James Darland

Photoionization mass spectrometry (PIMS) is a powerful technique for studying the energetics of atoms and small molecules and the kinetics of polyatomic ion decomposition and ion-molecule reactions. However, PIMS suffers from a number of severe experimental difficulties which often result in experiments that either provide data with poor precision (low signal-to-noise ratio) or are very long and tedious, even neglecting the time required to set up the experiment and reduce the data to a useable form. Maximizing the efficiency of operation of PIMS instruments is therefore very important if the full potential of PIMS is to be realized.

In this dissertation, operating procedures designed to achieve a very high overall operating efficiency (while maintaining high standards of accuracy and precision) are discussed, and a new, automated photoionization mass spectrometer designed to allow implementation of these procedures is described. A comparison of several types of data acquisition systems shows that a computer-based system is the simplest automated system which provides the flexibility necessary to implement fully the required operating procedures. The new instrument, incorporating a one-meter, near-normal incidence monochromator and a quadrupole mass filter, is controlled during the experiments by a minicomputer which is also used for data reduction and analysis.

The computer programs (software) required to implement these

operating procedures are described. The software is moderately complex, but a set of guidelines has been developed for facilitating computer-user interaction, and all software has been written following these guidelines. As a result, the complexity of the system is largely transparent to the user; the instrument is very easy to use, and this ease of use is a major factor in reducing the experiment set-up and data reduction time so that more time can be spent in actual data acquisition and interpretation.

The data acquisition software includes provisions for recording, at regular intervals during the experiment, any of several types of "correction measurements" that are necessary for eliminating the effects of scattered light, long term drifts, etc., from the final results. The data being acquired are partially corrected and plotted as they are acquired so that the quality of the data may be judged without waiting until after the end of the experiment. The software also includes a variable integration time option, which allows the integration time to be varied automatically on a point-by-point basis so that it is just long enough to acquire data with the desired signal-to-noise ratio. The procedure used, equivalent to "integrating to a constant background-corrected ion intensity", is shown to make more efficient use of data acquisition time than the constant integration time or "integration to constant photon intensity" methods which are more commonly used.

So that the instrument may be left safely unattended, the status of the vacuum system as well as the "general utilities" (high voltage power supplies, water flow, etc.) is continuously monitored by an extensive safety interlock system, which automatically takes appropriate action

in the event of any failure. The interlock system is described in detail, as are the computer-interface electronics. The latter include a unique pulse amplifier circuit designed for fast photon- or ion-counting applications. The pulse counter has a sensitivity of 250 μV and a maximum count rate exceeding 90 MHz. It is entirely DC-coupled so that it exhibits no baseline shift at any count rate.

The new instrument has been used to study the mixed chlorofluoromethanes $CFCl_3$, CF_2Cl_2, and CF_3Cl. Photoionization efficiency curves have been obtained for the first time for $CFCl_3^+$, which is produced only rarely, as well as for twelve other ions from these compounds. All three parent ions are therefore stable, but there is some evidence that the observed ionization potentials may be significantly above the adiabatic ionization potentials for all three molecules. Further work is recommended to resolve several apparant paradoxes in the present data.

To Susan

To Mom

To Dad

For whom no acknowledgment can suffice.

THE DESIGN AND OPERATION OF AN AUTOMATED, HIGH-EFFICIENCY PHOTOIONIZATION MASS SPECTROMETER

By

Edward James Darland

A DISSERTATION

Submitted to
Michigan State University
in partial fulfillment of the requirements
for the degree of

DOCTOR OF PHILOSOPHY

Department of Chemistry

1978

ACKNOWLEDGMENTS

It would be virtually impossible for me to acknowledge all of the people who have had a part in making the past six years so enjoyable for me. However, among those who have contributed most to my personal growth and to the preservation of my sanity (if any), I owe Mike and Joan Kelsey, Jon Powers, Marv and Sylvia Reimer, Frank Tully, and Pat Dehmer a very special "thank you".

I would also like to offer my heartfelt thanks to the following people, all of whom have made more direct contributions to the development of the instrument described in this dissertation:

Bill Chupka, Warren Jivery, Pat and Joe Dehmer, and Joe Berkowitz--for the information they shared unstintingly during several months I spent at Argonne National Laboratory; for showing me how their instruments worked, making numerous suggestions for improvements, and answering innumerable questions on the practical aspects of PIMS methodology. Their help and advice were indispensable in getting the MSU instrument "off the ground".

George Leroi and Chris Enke--for their support, guidance, encouragement, advice, and patience during my years as a graduate student; for the things they taught me, and most of all for the things they allowed me to learn.

Russ Geyer, Len Eisele, Dick Menke and Dick Watters, the staff of the MSU Chemistry Department Machine Shop--for carefully machining the vacuum

chambers, lamp, and all other non-trivial parts of the instrument, for taking the time to teach me many of the principles of mechanical design and drawing, and for building what I wanted even when I didn't draw it correctly.

Ron Haas, Dick Johnson, and Rick Sandford, the staff of the MSU Chemistry Department Electronic Shop--for carefully etching many printed circuit boards, for assembling much of the interlock system, and for keeping much of the commercial electronics gear in our lab in running order.

Marty Rabb, MSU Chemistry Department Electronics Designer--for designing and building the new lamp power supply, and for helpful discussions on a wide range of other electronic problems.

Stan Crouch--for his careful reading of many parts of this dissertation, and many helpful discussions on "photon counting and the futility of it all".

Frank Tully--for his inestimable aid in getting the vacuum system up and running, and for many hours spent discovering new and ever more interesting hardware and software bugs, characterizing them so thoroughly that they were relatively easy to fix. Also, many thanks to Frank and ...

Paula Kronebusch--for acquiring much of the earliest chlorofluoromethane data.

Gary Ray--for help in assembling some of the plumbing, for designing the current ion source, sodium salycilate detector assembly, and sample inlet system, and for help in a multitude of other thankless tasks.

Dave Rider--for keeping the instrument running during recent months while Gary and I were preoccupied with getting in that "last run" or in finishing the "final figure, except for . . . ", for his willingness to

dig in and find out what was wrong when something quit, and for his many fresh ideas.

Tom Atkinson and Rick Yost--for writing many useful programs for the PDP-11 system. Many of the schematic diagrams in this theses were prepared using Rick's LAYOUT, and final copies of all data plots were produced with Tom's MULPLT. Other subroutines written by Tom and Rick are used extensively in transferring data from the PDP8 to PDP11 computers as well as in PIMS11.

Finally, I would like to acknowledge the financial support provided by Michigan State University, the National Science Foundation, the Office of Naval Research, the Associated Midwest Universities of Argonne "Thesis Parts" Program, my parents, and my wife.

TABLE OF CONTENTS

page

List of Tables xi

List of Figures xiii

CHAPTER I. INTRODUCTION 1

A. The Thesis 1

B. Photoionization Mass Spectrometry 3

C. Advantages of PIMS 9

D. Fundamental Experimental Difficulties 12

E. Design Requirements 14

1. Precision of Data 15

2. Accuracy of Data 16

3. Efficiency of Operation 19

F. Merits of Previous Designs 22

1. Basis of Comparison 22

2. Manual Operation 23

3. Data Logging 26

G. The MSU Instrument 30

CHAPTER II. THE MASS SPECTROMETER 37

A. Introduction 37

B. Photon Sources 39

1. Overview 39

2. Lamps 44

3. Power Supplies 52

C. Photon Optics 59
D. Photon Transducers 63
E. Ion Source 70
F. Ion Optics 72
G. Ion Transducers 76
H. Vacuum System 80
CHAPTER III. THE INTERLOCK SYSTEM 90
A. Introduction 90
B. Capabilities and General Discussion 93
1. Master Control Module 94
2. Vacuum System Control Modules 97
3. Sequencing 99
C. Master Control Module 103
D. Vacuum System Control Module 109
1. Operation of a 115 VAC, Fully Automated System . 112
2. Wiring for Other Options 115
CHAPTER IV. CONTROL AND DATA ACQUISITION 119
A. Introduction 119
B. The Wavelength Drive 124
C. Shutter 130
D. Pressure Measurement 134
E. DC Current Measurement 140
F. The Pulse Counter 151
1. Introduction 151
2. The Pulse Counter 156
3. Pulse Counter Performance 172
4. Recommended Modifications 179

5. Pulse Counting System Performance 181
6. Summary 199
G. Dual Counter 200
CHAPTER V. OPERATION OF THE INSTRUMENT 210
A. Introduction 210
1. Stages of the Experiment 210
2. Progression of Stages 212
3. Organization of the Chapter 213
B. Overview of the PIMS Software System 213
1. Basic Considerations 213
2. Specific Software Requirements 216
3. General Description 218
4. System Conventions 221
C. Typical Operating Procedures 225
D. Interactive Setup Options 231
1. CLOSE 231
2. CURRENT WAVELENGTH 232
3. INITIALIZE 232
4. MOVE 234
5. OPEN 235
6. PRESCALE 235
7. SCAN 235
8. TEST 236
9. TRANSFER 237
E. Data Acquisition Options 243
1. The RECORD Option 243
2. Variable Integration Time 248

3. Periodic Correction Measurements 251
4. Stray Light Correction Measurements 254
5. Real-Time Output 255
6. The TIMED ACQUISITION Option 256
F. Data Reduction Options 260
CHAPTER VI. SOME PRELIMINARY RESULTS 272
A. Introduction 272
B. Results and General Discussion 275
1. Relative Intensities 275
2. Photoionization Efficiencies 277
3. Formation of Positive Chlorine Ions 295
C. CF_3Cl 298
1. CF_3Cl^+ 299
2. CF_3^+ 301
3. CF_2Cl^+ 304
D. CF_2Cl_2 305
1. CF_2Cl^+ 305
2. $CFCl_2^+$ 305
3. CF_2^+ 308
E. $CFCl_3$ 309
1. $CFCl_3^+$ 310
2. $CFCl_2^+$ 312
3. CCl_3^+ 313
4. Other Fragments 314
F. Summary 314
APPENDIX A. ARTIFACTS 317
A. Finite Slit Width 317

B. Scattered Light 319

C. Detector Misalignment 324

APPENDIX B. BASIC PDP 8/I INTERFACING 329

APPENDIX C. THE REAL-TIME CLOCK 336

A. Introduction 336

B. Basic Operation 338

1. Decade Clock 340

2. Programmable Clock 340

C. Programming 341

1. Instructions 342

2. Programming Examples 346

D. Circuit Description 348

1. Control Register 348

2. Command Decoder 350

3. Preset Latch, Presettable Counter, Output Latch, and Drive 353

4. Oscillator and Time Base Select 355

5. Flag Circuits 355

APPENDIX D. SIGNAL-TO-NOISE RATIO EXPRESSIONS 359

APPENDIX E. SOFTWARE 365

A. Introduction 365

B. PIMS8 Programs and Subroutines 367

C. PIMS11 Programs and Subroutines 451

D. Variable Definitions 490

1. PIMS8 Variables 490

2. PIMS11 Variables 492

REFERENCES 497

LIST OF TABLES

table		page
I-1.	Requirements Imposed by Design Goals.	22
I-2.	Comparison of Four Design Approaches.	35
II-1.	Approximate Wavelength Limits of the Rare Gas Continua.	42
II-2.	Comparison of the Cober and ANL Power Supplies.	56
II-3.	Comparison of Common Vacuum Ultraviolet Photon Transducers.	64
III-1.	Summarized MCM Monitor and Control Functions.	96
III-2.	Summarized VCM Monitor and Control Functions.	100
III-3.	Terminal Connections for Main Power Options.	115
III-4.	Terminal Connections for Automatic Valve Options.	116
III-5.	Terminal Connections for Sharing a Mechanical Pump Between Two Systems.	117
IV-1.	Wavelength Reproducibility.	128
IV-2.	Summary of Other Wavelength Reproducibility Tests.	128
IV-3.	Wavelength Accuracy.	129
IV-4.	Relative Stability of the 8850 PC System for Different Voltages and Discriminator Settings.	185
IV-5.	Limits of Linearity for Different Discriminator Coefficients.	196
V-1.	Main PIMS8 Options.	220
V-2.	PIMS8 Input Prompt Conventions.	223
V-3.	PIMS8 Special Character Conventions.	224
V-4.	PIMS8 Data Storage Conventions.	226
V-5.	TRANSFER Options.	238

V-6. PIMS11 Options. 261

V-7. PIMS11 Data Types, Their Possible Corrections and BCE Calculation Methods. 268

V-8. PIMS11 Calculations. 270

VI-1. Relative Abundance of Parent and Fragment Ions from CF_3Cl, CF_2Cl_2, and $CFCl_3$. 276

VI-2. Data Used in Thermodynamic Calculations. 296

VI-3. Summary of CF_3Cl Appearance Potentials. 300

VI-4. Summary of CF_2Cl_2 Appearance Potentials. 306

VI-5. Summary of $CFCl_3$ Appearance Potentials. 311

VI-6. Summary of Heats of Formation Found in This Work. . . 316

C-1. Clock I/O Instructions. 342

C-2. Control Register Bit Assignment. 345

D-1. Error Involved in Using Simplified S/N Expressions . . 364

LIST OF FIGURES

figure		page
I-1.	PIMS Made Easy.	6
I-2.	A Manual Instrument.	24
I-3.	A Simplified Data-Logging Instrument.	26
I-4.	The MSU PIMS Instrument.	31
II-1.	The Basic Elements of a Mass Spectrometer.	37
II-2.	The Basic Elements of a Photoionization Mass Spectrometer.	38
II-3.	Schematic Diagram of the Potential Energy Curves of He_2.	41
II-4.	The Helium Continuum.	43
II-5.	The Hydrogen Many-Lined Spectrum.	45
II-6.	A Π-Type Rare Gas Discharge Lamp.	46
II-7.	The MSU Hinterregger Lamp.	48
II-8.	Lamp Utilities.	50
II-9.	DC Power Supply for the Hydrogen Lamp.	52
II-10.	Spark Gap Power Supply for the Rare Gas Discharge Lamps.	53
II-11.	Vacuum Tube Power Supply for the Rare Gas Discharge Lamps.	58
II-12.	Atomic Nitrogen Emission Lines at 1134 Å.	62
II-13.	The Helium Continuum and Scattered Light Recorded with Different Photon Transducers.	68
II-14.	A Simple Ion Source.	70
II-15.	Top View of Quadrupole Mount.	74
II-16.	Side View of Quadrupole Mount.	75

II-17. Effect of Increasing Mass Resolution on Ion Transmission. 77

II-18. Daly-Type Ion Transducer. 79

II-19. Location of Components Within the Vacuum Chambers. . . 81

II-20. Top View of Instrument, Retracted. 83

II-21. Top View of Instrument, Normal Position. 84

II-22. First Differential Pumping System. 86

II-23. Second Differential Pumping System. 87

II-24. Monochromator Pumping System. 88

II-25. Sample and Quadrupole Pumping Systems. 89

III-1. Interlock System Organization. 93

III-2. Hood Alarm Circuit (MCM). 104

III-3. Diffusion Pump Water Flow Interlock (MCM). 106

III-4. General Utilities Interlock (MCM). 107

III-5. "Local" Mechanical Pump Circuit. 109

III-6. Pump Control Circuit (VCM). 110

III-7. Valve Control Circuit (VCM). 111

III-8. Alternate Interconnection Method. 118

IV-1. Stepping Motor Interface. 124

IV-2. Eight Successive Scans of the Atomic Nitrogen Lines at 1134 Å. 127

IV-3. Shutter Control Interface. 132

IV-4. Auxiliary Shutter Control Circuits. 133

IV-5. Sample Pressure Measurement System. 135

IV-6. Valve Control Signal Generation. 136

IV-7. Valve Timing and Control. 138

IV-8. Valve Enable Signal Selection. 139

IV-9. V-F Current Integration Method. 141

IV-10. V-F Converter Module Circuit. 143

IV-11. Linearity of the V-F Converter Module. 145

IV-12. Effect of Temperature on the Analog Measurement System. 147

IV-13. V-F Nonlinearities as a Percentage of Full Scale and of Reading. 150

IV-14. Block Diagram of the Pulse Counter. 154

IV-15. Anode Pulses from a 1P28 Photomultiplier. 159

IV-16. The Effect of Prescaling on a Random Pulse Train. . . 161

IV-17. Preamplifier/Discriminator Circuit. 162

IV-18. Response of Amplifier to Input Pulses. 163

IV-19. AC Coupling of Amplifier and Comparator. 165

IV-20. Prescaler/Line Driver Circuit. 168

IV-21. Auxiliary Voltage Generation. 170

IV-22. The Pulse Counter. 173

IV-23. Variation of Sensitivity with Frequency. 174

IV-24. Sensitivity vs. Threshold Setting. 174

IV-25. Photon Count Rate vs. Temperature. 178

IV-26. Integral Pulse Height Distribution for the RCA 8850. . 184

IV-27. Integral Pulse Height Distribution for the RCA 1P28. . 187

IV-28. Integral Pulse Height Distribution for the Johnston MM1. 189

IV-29. Non-Linearity of the 8850 Photon Counting System. . . 193

IV-30. Expanded Plot of Figure IV-29. 195

IV-31. Block Diagram of the Dual Counter. 201

IV-32. Control Circuit for 12/24 Bit Select of Dual Counter. . 203

IV-33. Dual Counter Flag and Bit Select Circuit. 204

IV-34. Dual Counter Input Select Circuit. 205

IV-35. Counter and Bus Driver Circuit. 207

IV-36. Counter Enable Circuit. 208

IV-37. Prescale Select Circuit. 209

V-1. TRANSFER Output in PIMS8 Format. 241

V-2. TRANSFER Output in ASCII Format. 242

V-3. RECORD Data Acquisition Flowchart. 246

V-4. Comparison of Variable and Constant Integration Times. 252

V-5. Comparison of Photon and Ion Stripchart Recordings with PIMS8 Real-Time PIE Plot. 257

VI-1. CF_3Cl^+ from CF_3Cl. 278

VI-2. CF_3^+ from CF_3Cl. 279

VI-3. CF_2Cl^+ from CF_3Cl. 280

VI-4. CF_2Cl^+ from CF_2Cl_2. 281

VI-5. $CFCl_2^+$ from CF_2Cl_2. 282

VI-6. CF_2^+ from CF_2Cl_2. 283

VI-7. $CFCl_3^+$ from $CFCl_3$. 284

VI-8. $CFCl_2^+$ from $CFCl_3$. 285

VI-9. CCl_3^+ from $CFCl_3$. 286

VI-10. $CFCl^+$ from $CFCl_3$. 287

VI-11. CCl_2^+ from $CFCl_3$. 288

VI-12. CF^+ from $CFCl_3$. 289

VI-13. CCl^+ from $CFCl_3$. 290

A-1. The Assumed Slit Function. 318

A-2. Measured PIE for Two Overlapping Lines. 320

A-3. Measured PIE for a Line Superimposed on a Continuum. . 321

A-4. Calculated Stray Light Effects. 323

A-5. Experimentally Observed Stray Light Effects. 325

A-6. Calculated PIE for Differing Ion and Photon Linewidths. 327

A-7. Calculated PIE for Offset Ion and Photon Peaks. . . . 328

B-1. Edge Connector Contact Assignments. 333

B-2. Generation of a Device Select Signal. 334

B-3. Gating of DS and IOP Signals. 334

B-4. Generation of Function Select Signals. 335

C-1. Block Diagram of the Real-Time Clock. 339

C-2. Control Register and LED Indicator Decoding Circuits. . 349

C-3. Latch/Drive Control Circuits (Command Decoder). . . . 351

C-4. Counter/Flag Control Circuits (Command Decoder). . . 352

C-5. Latch/Counter/Latch/Driver Circuits (Programmable Clock). 354

C-6. Oscillator and Time Base Select Circuits. 356

C-7. MK5009 Reset Glitch. 357

C-8. Decade Clock Flag Circuit. 358

CHAPTER I

INTRODUCTION

A. The Thesis

The technique of photoionization mass spectrometry (PIMS) has had a wide variety of applications [1]. In recent years, it has been most widely used in three distinct areas: the study of unimolecular kinetics of polyatomic ions [2-4], the study of kinetics and thermodynamics of ion-molecule reactions [5,6], and the determination of ionization potentials of atoms and molecules and of appearance potentials of fragment ions [1,3]. Studies of this latter type have been especially valuable (and frequent) because the ionization and appearance potentials obtained are often of high accuracy (a few meV), and can be combined with other thermodynamic information to yield equally accurate values of such parameters as heats of formation, bond dissociation energies, electron affinities and so forth, not only for molecules but also for ions and radicals. In fact, PIMS has become recognized as one of the most accurate techniques avaliable for such measurements [3].

Photoionization mass spectrometry has a number of remarkable advantages, but also suffers from a number of severe experimental difficulties. At its best, it is characterized by low signal levels and lengthy experiments. The many extremely valuable experiments that have been performed to date have been possible only because of the

incredible patience of the experimenters and the great amount of effort that has been devoted to increasing the efficiency of the instruments and their operation. As in many fields, a large number of useful experiments seems to remain just out of reach no matter how sensitive or efficient the technique becomes. Nevertheless, each increase in efficiency or sensitivity makes more experiments possible, many of which yield very useful and sometimes unexpected information. The information obtained has been sufficiently valuable to justify past efforts at improving the technique, and also to encourage continuing effort toward that same goal.

The Michigan State University photoionization mass spectrometer is, in many ways, similar to most modern PIMS instruments, but it is capable of attaining a significantly higher overall operating efficiency. This thesis is intended to be a complete description of the MSU instrument in which the unique innovations in hardware and operating procedure that make possible the improved efficiency are emphasized. Most of the work that has been performed with the MSU instrument to date has involved the measurement of ionization and appearance potentials, and most of the concepts discussed in later chapters of this thesis were developed specifically for such studies. However, many of these concepts are applicable to other types of PIMS studies, especially ion-molecule reactions. On an even broader scale, many of the guidelines concerning user-computer-instrument interaction described here could be profitably applied to virtually any sort of computer-interfaced experiment.

Succeeding sections of this chapter are devoted to a basic introduction to photoionization mass spectrometry and the concepts

underlying the overall design approach used in the MSU instrument. The basic elements of a photoionization mass spectrometer, the measurements that are made with it, and the information that can be obtained from such measurements are all described briefly in Section B. Section C contains a description of some of the advantages of PIMS and the most important of the experimental difficulties involved are discussed in Section D. Then, in Section E, the capabilities and characteristics that a photoionization mass spectrometer should have if it is to obtain accurate data efficiently are discussed and a list of design requirements is developed. In Section F, the relative merits of several earlier designs are discussed in terms of how well they meet these requirements. Finally, with this background, the general design of the MSU instrument is presented in Section G, along with a brief description of the contents of succeeding chapters.

An attempt has been made to organize the material presented in this thesis so that any of the chapters following this may be read independently. In fact, each chapter is organized insofar as possible so that, once the introductory section has been read, any of the major sections of that chapter can be read without reference to other sections. It is strongly recommended, however, that Chapter I be read in its entirety before any other portions of the thesis are read.

B. Photoionization Mass Spectrometry

No comprehensive reviews of photoionization mass spectrometry have been published since the one by Reid [1] in 1971, which is now rather dated. Nevertheless, that review, together with references [2, 3,5,7-13] provide an excellent introduction to the experimental

methodology of PIMS [1,5,7,8], the processes contributing to the observed signals [2,3,9,13], methods of data analysis [10-13], the applications of the technique [1-3,5] and its relationship to other techniques [3,14,15]. Since the introduction to PIMS presented here is very brief and more than a little abridged, the reader is urged to consult these references for more detailed information.

The first reports describing mass spectrometric analysis of ions produced by photon impact on gaseous samples were published in 1929 [16] and 1932 [17]. At that time, and for years afterwards, the technique was severely limited by the available vacuum and light source technology, and no further PIMS experiments were reported until 1956 [18]. The first really modern instrument (i.e. one incorporating a vacuum monochromator and thus allowing selection of photon energies greater than about 6 eV) was described shortly thereafter [19]. During the next decade or so, the experimental technology was refined and data of ever-increasing quality contributed to a better understanding of the processes that were being observed. This in turn aided the development of more appropriate data analysis methods, which increased the potential of the technique even further.

As awareness of the capabilities of PIMS grew, so did the number of experimental studies. Reid's review of the field [1] indicates that by 1970, more than 130 studies involving "conventional" PIMS had been published, roughly half of them during the previous three years. The power of the technique has attracted increasing numbers of investigators since 1970, in spite of the experimental difficulties that remain even with the best modern equipment.

In the absence of any commercial source for complete PIMS

systems, investigators have had to assemble their own. Thus, no two photoionization mass spectrometers are alike. With only a few exceptions, however, most of them comprise the same functional elements, differing only in the specific implementation of each element. Figure I-1 illustrates the elements present in a basic photoionization mass spectrometer. The radiation from a light source is dispersed so that photons with a known energy (wavelength) distribution can be passed through a sample region which contains one or more gases at a known pressure. If the photons have sufficient energy, their absorption may lead to the production of ions by one or more of a number of processes. The number of photons transmitted through the sample is measured, as is the number of ions of a particular mass (selected by the mass filter).

The ratio of the number of ions formed to the number of photons transmitted by the sample is defined as the photoionization efficiency (PIE). Under typical operating conditions (when the sample pressure is sufficiently low that the amount of absorption by the sample is small), the PIE is proportional to the partial photoionization cross section for the ion being observed [20]. The PIE of an ion is most frequently measured as a function of wavelength, the plot of PIE versus either wavelength or photon energy being referred to simply as the PIE curve. The accurate determination of such curves is one of the most common goals in PIMS because of the tremendous amount of information that can be gained from their analysis. In practice, absolute photon intensity measurements [7] are so difficult that they are rarely attempted during a PIMS experiment. Instead, only the relative variation in photon intensity is measured. The so-called relative PIE curves which result provide almost as much information as the absolute PIE curves.

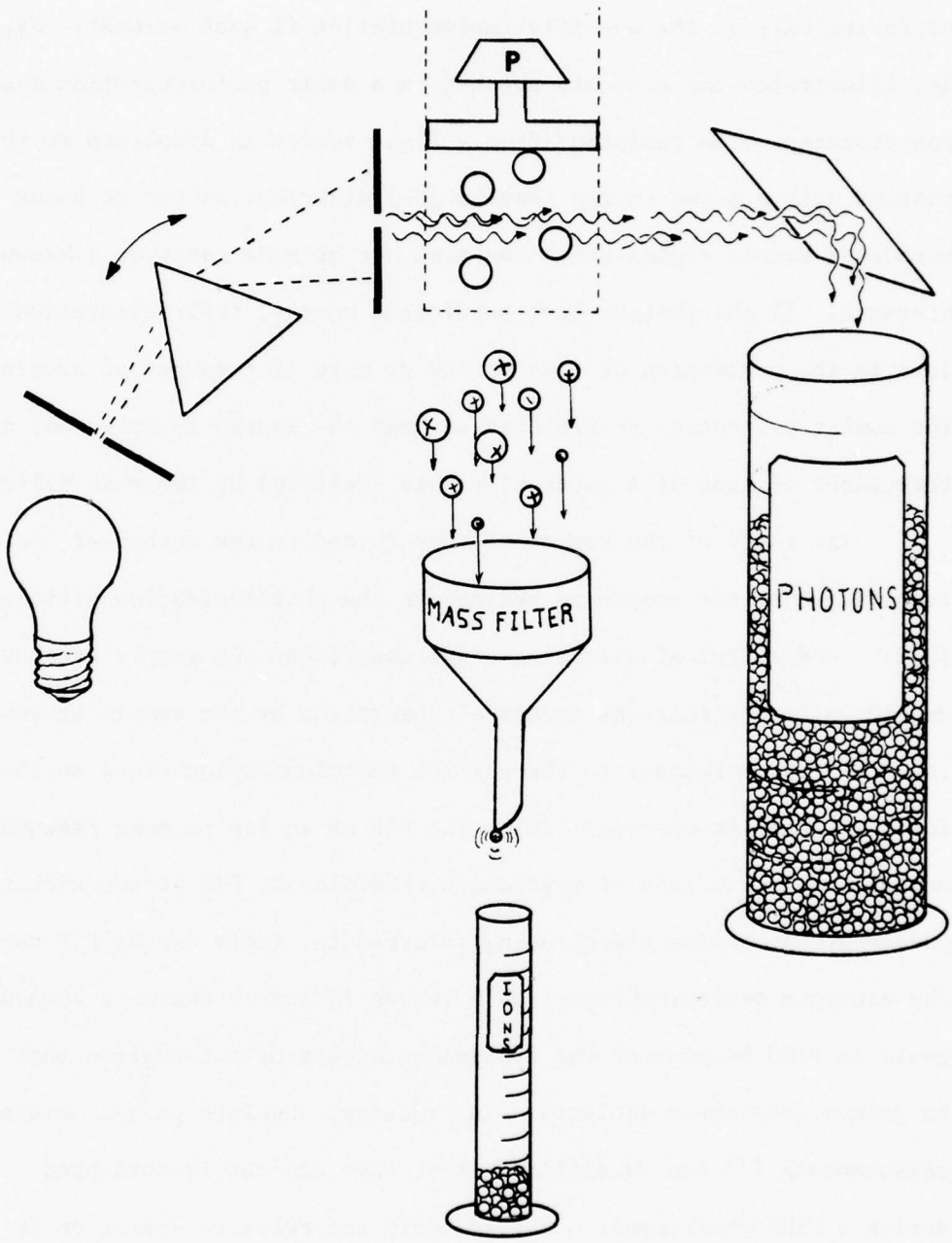


Figure I-1. PIMS Made Easy.

The determination of molecular ionization potentials is an example of one of the most common studies undertaken by PIMS. The threshold law for direct ionization by photon impact corresponds, at least approximately, to a step function [21,22]. The PIE curve for the molecular ion might therefore be expected to show a sudden onset at a photon energy corresponding to the transition from the ground state of the molecule to the ground state of the ion, i.e. the adiabatic appearance potential (IP), and this is in fact observed for some molecules. However, photoionizing transitions are vertical transitions and the Franck-Condon factors governing the transition may allow the ground-ground transition with only small probability relative to transitions to excited ionic states. Therefore, several steps may be observed in the PIE curve, one of which may or may not correspond to the sought-for adiabatic IP. The "extra" structure increases both the difficulty of identifying the adiabatic transition (although this can often be done) and the amount of information that can be extracted from an examination of the threshold region of the PIE curve.

There are other possible complications. Ionization of vibrationally excited molecules from the electronic ground state of the molecule can lead to production of significant numbers of ions below the adiabatic IP ("hot bands"), as can collisional or field induced ionization of molecules excited to Rydberg states of the neutral molecule lying just below the ionization energy. Because of the finite energy resolution of the instrument, what would otherwise be observed as sharp steps can be blurred by unresolved rotational or vibrational structure, and the PIE curve may be further complicated by the presence of autoionization structure above threshold. In spite of these

potential complications, extremely accurate values of adiabatic ionization potentials can frequently be measured [3] and even when complications are severe, accurate limits can often be set.

If the molecule ABC is ionized so that

$$ABC + h\upsilon \rightarrow ABC^+ + e^-$$

then

$$IP(ABC) = \Delta H_f(ABC^+) - \Delta H_f(ABC)$$

and if $\Delta H_f(ABC)$ is known, as is often the case, then $\Delta H_f(ABC^+)$ can be accurately determined.

Examination of PIE curves for fragment ions reveals that the onset of production of measureable numbers of such fragments, while rarely a perfect step function, is frequently rather well defined. The energy corresponding to such an onset is defined as the appearance potential (AP) for that fragment ion. The AP for a process such as

$$ABC + h\upsilon \rightarrow A^+ + BC + e^-$$

can also be used in a wide variety of thermodynamic cycles, such as

$$\begin{aligned} AP(A^+) &= \Delta H_f(A^+) + \Delta H_f(BC) - \Delta H_f(ABC) \\ &= \Delta H_f(A) + IP(A) + \Delta H_f(BC) - \Delta H_f(ABC) \\ &= IP(A) + D(A\text{-}BC). \end{aligned}$$

Equations such as these, in combination with other known information, can yield a wide variety of information about the thermodynamics of the molecules, ions and radicals under consideration.

The actual shapes of the fragment ion PIE curves near threshold depend not only on the relative positions and shapes of molecular and ionic potential surfaces, but also on the rate at which fragmentation occurs, the rates of competing processes, etc.[2,23]. One example is the so-called "kinetic shift" which may raise the measured AP for a

dissociative ionization process such as

$$ABC + h\upsilon \rightarrow ABC^{+*} + e^{-}$$

$$ABC^{+*} \rightarrow AB^{+} + C \ .$$

The rate at which the second step occurs may depend on the amount of energy in excess of the thermochemical threshold that is avaliable in the parent ion. Since the transit time from source to detector in many mass spectrometers is on the order of a few microseconds, the rate constant for the second step must be larger than about $10^5 - 10^6$ sec^{-1} to produce measureable numbers of fragment ions. The excess energy required to produce this rate constant is the kinetic shift.

There are several other reasons why the measured appearance potential of a fragment ion may not correspond to the true thermochemical threshold for production of that ion. However, as pointed out by Chupka [2], dubious data can almost always be recognized, and even when the observed AP is suspected of being in error, the nature of the possible complications is such that the observed value is almost certain to be too high. Even in these cases, when PIMS cannot provide accurate thermochemical appearance potentials, it can still provide very precise upper limits.

C. Advantages of PIMS

The major advantage of PIMS over other photoionization techniques is that is usually provides unambiguous identification of the eventual products of an ionizing event. This is clearly an advantage over the measurement of ionization efficiencies by the total ion current method [24,25], which cannot distinguish between such

processes as these:

$$AB + h\upsilon \rightarrow AB^+ + e^-$$

$$AB + h\upsilon \rightarrow A^+ + B + e^-$$

$$AB + h\upsilon \rightarrow A^+ + B^- .$$

Photoelectron spectroscopy [14,26,27] (PES, another photoionization technique) is also an excellent technique for the measurement of ionization potentials. Although PES and PIMS often provide similar information, there are significant differences between the two. These differences could be regarded either as advantages or disadvantages, depending on the information being sought.[1] For instance, PES can provide precise information on how much internal energy is deposited in the ion by the ionization process, which PIMS cannot. But PES cannot provide any information on how the ion eventually disposes of that energy--whether it fragments or not, and into what pieces, with what probability. Another major difference is that photoelectron spectra are rarely complicated (or enriched, depending on point of view) by autoionizing processes, while autoionization structure is frequently the most intense of the features in a PIE curve.

A tremendous number of ionization efficiency measurements have been made during the past fifty years by the technique of electron impact mass spectrometry [3,28] (EIMS), over which PIMS has a number of very significant advantages. The most important is the relative ease with which the energy and energy bandwidth of the photon beam can be controlled. Wavelength accuracy and bandwidth of even the older PIMS

---

[1]The two techniques are actually highly complementary, a fact which has prompted the development in recent years of combined photoion-photoelectron coincidence instruments [29-32].

instruments are typically better than 1 Å, which is equivalent to about 12.4 meV at 1000 Å. In fact, for more modern instruments, the wavelength accuracy is typically an order of magnitude better, and photon bandwidths as low as 0.035 Å (0.43 meV at 1000 Å) have been reported [33]. This precise control of ionizing energy is not only an advantage in ionization efficiency measurements, but also in the preparation of reactant ions in ion-molecule reaction studies. Reactant ions can often be prepared without simultaneously producing other, unwanted ions, and often with well-known distributions of internal energy [5].

In contrast, most EIMS measurements have used an electron beam with an energy spread of 1-2 eV. Furthermore, the actual energy of the electrons is influenced by stray fields and contact potentials so that the energy scale is not well characterized and must be calibrated with reference compounds. Since the contact potentials are likely to change with time, the calibration must be performed simultaneously with the experiment. Many of the procedures used to treat the data appear to have little theoretical justification [3,34], and the results of such measurements are typically a few tenths of an eV too high, but not predictably so [3]. In recent years, electron monochromators have been used to reduce the energy spread of the electron beam significantly (see the references in [3] and [34]), but even the best EIMS measurements are hard put to match the energy resolution and accuracy of even a very average PIMS instrument.

The only advantage of EIMS over PIMS is that much higher ion currents can be obtained, due to two factors. First, electron impact cross sections are larger than photoionization cross sections, by about

two orders of magnitude for 70 V electrons [34]. Second, the flux of ionizing particles is typically much higher in an electron beam than can be achieved with photons, perhaps by an order of magnitude even for undispersed radiation. However, much of the flux advantage is lost if an electron monochromator is used. Furthermore, the electron impact threshold law is not a step function, but rather an approximately linear function of excess energy (see the discussion in [3]). In contrast to the behavior of PIE curves, then, the EI ionization cross section will be several orders of magnitude smaller just above threshold than at higher energies, and it is not clear that EIMS has much of an intensity advantage in appearance potential measurements, provided that the two techniques are compared at comparable energy resolution. In addition, the photon beam introduces no space charge in the ionization region and causes no pyrolysis of the sample, which tend to be problems with electron beams and hot filaments.

D. Fundamental Experimental Difficulties

Although PIMS posesses numerous advantages, the price that must be paid to obtain those advantages is high, both in dollars and time. The photon energies needed to ionize and fragment most molecules correspond to wavelengths in the vacuum ultraviolet (VUV) (i.e. less than about 2000 Å). Most substances, including oxygen and nitrogen, absorb strongly in this region, and as a result the optical path in a photoionization mass spectrometer must be kept evacuated. This is made difficult by the fact that at wavelengths below the short wavelength cutoff of lithium fluoride (≈1050 Å, or 11.8 eV), there are no

satisfactory window materials which can be used to isolate lamp or sample gas from the rest of the instrument. The vacuum system must therefore be capable of maintaining an acceptably low pressure ($\approx 10^{-5}$ torr) in spite of intentional (and large!) leaks. Fortunately, the state of vacuum technology is such that this can be done, although the expense is significant. The book by Samson [7] provides an excellent discussion of the difficulties involved in working in the VUV spectral region and the techniques used to overcome them.

A more serious problem is the fact that, even with an excellent design and the best available equipment, ion signal intensities are often very low. Most experiments (with the possible exception of high-pressure ion-molecule reaction studies) must be performed with sample pressures of a few millitorr or less in order to avoid the collisional effects which can distort the PIE curves at higher pressure [35]. Thus, the ion signal cannot be increased by merely increasing the sample pressure. Instead, one must maximize the photon intensity and the ion collection efficiency of the mass analyzer. Unfortunately, the best avaliable light sources in this spectral region tend to have limited intensities (10^8 - 10^{10} photons sec^{-1} $Å^{-1}$, maximum) or high price tags (frequently more than $10,000) or both. In addition, the best avaliable optical materials have very low reflectivities (15-30% at 600 Å) so that every reflection to disperse or focus the light throws away a large fraction of whatever the light source is able to produce. Any decrease in the photon energy bandwidth to increase resolution also decreases the signal intensity, and further aggravates the problem.

Typically, when ion collection efficiencies approach 100%,

when the best available light source is used, and when the sample pressure and photon bandwidth have been increased as much as possible consistent with the goal of the experiment, one finds that many of the processes that might be of interest are still of extremely low intensity--perhaps only a few ions per second or worse. Use of ion counting techniques allows long enough data integration times that useable data can often be obtained even with such weak signals, but only at a cost of very long experiments. Data runs lasting several days have been reported [33], and they could conceivably last much longer. Given sufficient sample and patience, one could presumably obtain useful data at count rates of a few ions per minute, but at some point the time involved must become prohibitive.

E. Design Requirements

Each datum in the overall PIE curve must be measured with sufficient precision that all features of interest in the curve can be clearly discerned. In other words, the data must have a sufficiently high signal-to-noise ratio (S/N). If such features, although discernable, are distorted because of the non-ideal behavior of the instrumentation used in the measurement, then the high S/N may be of little use. Therefore, the primary goal in designing a photoionization mass spectrometer must be to create an instrument which can be used to acquire data with both precision and accuracy.

If precise and accurate data can be obtained, but only in experiments lasting for inordinate lengths of time, then the experiments will probably not be attempted at all. Thus, a secondary but highly

desirable goal is to design the instrument in such a way that the overall measurement process is as efficient as possible, so that the time necessary for a given series of experiments is minimized.

The triple goals of precision, accuracy and efficiency each impose certain requirements on the design of the instrument. These requirements are enumerated in the remainder of this section.

1. Precision of Data

A number of factors influence the S/N (and therefore the precision) of the measured photoionization efficiency. These are discussed in Chapter V, where it is shown that the limiting factor is almost always the S/N of the ion intensity measurement. In fact, in the usual case when ion counting techniques are employed, the S/N of a given PIE measurement is approximately equal to the square root of the total number of ions counted during the measurement. The precision of the measurement can therefore be increased either by increasing the number of ions formed or detected per unit time, or by increasing the measurement time, or both. Theoretically, any desired S/N could be achieved with even very low count rates, given sufficient time. Practically, however, instrumental instabilities usually impose some limit on the integration time. Thus it is important that the overall instrument design maximize the photon (and therefore ion) intensity, maximize the probability that an ion, once formed, will be detected, and also maximize the stability of the entire instrument, especially the data acquisition electronics. Furthermore, the experimental procedure used should ensure that every PIE measurement be at least long enough to attain the desired S/N.

2. Accuracy of Data

The accuracy with which the data are measured is also influenced by a variety of factors. Perhaps the most important of these is the accuracy of the data acquisition system(s). Ideally, the transfer function relating the recorded numbers to the photon and ion flux incident on the detectors should be linear. Although there may be some compromise involved (see Chapter IV), it is usually possible to achieve both adequate stability and linearity in these systems.

Even assuming ideal linearity in the data acquisition electronics, non-idealities of other sorts can adversely affect accuracy if not accounted for properly. For example, all of the most commonly used photon and ion detectors (see Chapter II, sections D and G) produce some background signal even in the absence of incident photons or ions, and these backgrounds are likely to change slowly with time. Unwanted backgrounds can be accounted for easily enough by occasionally closing a shutter between the light source and the sample region, measuring the background signal directly, and subtracting it from the other data. In fact, accuracy requires that such background measurements be made sufficiently often to "track" the change in background as a function of time, and the overall instrument design should allow this to be done.

The background-corrected photon and ion signals are still likely to drift with time for a number of reasons. For instance, the output of the light source and the grating reflectivity are certain to change with time, even at constant wavelength. However, changes in the photon or ion signals due to such causes will not affect the measurement of the PIE, since it is a ratio of ions to photons. However, if the photon detector efficiency deteriorates so that the measured photon

intensity decreases while the actual photon intensity does not, the accuracy of the measurement will suffer. Similarly, drifting sample pressure or a deteriorating ion multiplier, if not accounted for, can introduce error. Such drifts are unavoidable in real instruments, and although they are usually relatively slow, they can introduce artificial structure in those PIE curves which take a long time to measure.

The sample pressure can be monitored continuously, but about the only way to measure detector deterioration is to re-measure the PIE periodically at some"reference wavelength". Since the measured PIE at the reference wavelength is also affected by sample pressure, such reference measurements can be used to correct for pressure variation without having to make separate pressure measurements. In fact, reference measurements are sensitive to, and can be used to correct for, any sort of long term instabilities in the instrument. If the overall shape of the PIE curve is to be measured accurately, the instrument must be designed so that periodic reference measurements can be incorporated into its operating procedure. As with the background measurements, reference measurements must be made often enough to accurately sample the long term drifts that they are intended to correct.

Another source of inaccuracy is that the sensitivity of the photon detector may vary significantly with wavelength. This is an example of the kind of problem about which no information can be obtained during the experiment in which the PIE curve is measured. Instead, a separate experiment must be performed, comparing the response of the detector to that of a "standard" detector with a known wavelength response function. Post-experiment data analysis is then required to correct the PIE curve. A similar example is the variation

in ion detector sensitivity with ionic mass and composition. When it is important to know accurately the relative magnitudes of the PIE curves of different ions, correction factors must be measured in a separate experiment.

All real monochromators exhibit some degree of scattered light, which is another factor which must be taken into account. At any particular wavelength setting, the photons coming out of the exit slit will have not only the energies expected from the grating's dispersion and the slit widths, but also a (usually broad) distribution of other energies. The scattered light photons may cause ionization with a different probability than photons of the nominal energy to which the monochromator is set. The photon and ion detectors will measure such scattered photons and the ions they create along with the desired photons and ions. If the scattered light component of the measured ion and photon signals is not accounted for, it can grossly distort both the overall shape and the fine detail of the PIE curve. The possible artifacts, some of which have evidently been misunderstood in the past, are examined in detail in Appendix A.

Unfortunately, it is impossible to measure the actual scattered light distribution without employing a second monochromator, which is impractical in real PIMS instruments. One can, however, usually measure the photon intensity at one or two wavelengths that are not emitted by the particular photon source being used. The measured intensity at these wavelengths must be due entirely to scattered light, and these points can be used to estimate the amount of scattered light present at other wavelengths. Such estimated corrections will not usually be entirely accurate since at best they measure only "far scatter" and

cannot help estimate the "near scatter" to be expected at other wavelengths [36], but they may be good enough. Even if further manipulation is required to remove entirely the effects of scattered light (see Chapter V, section F), these measurements provide an excellent starting point, and the instrument should be designed to allow such scattered light measurements to be made.

3. Efficiency of Operation

Obtaining a high level of overall operating efficiency is especially important in photoionization mass spectrometry where the PIE curve for a weak fragment ion over a limited wavelength range can take literally days to acquire under the best of circumstances. As overall efficiency is increased, more experiments can be performed in a given time. Alternatively, better data can be obtained in that same time, so that processes which were too weak to be observed previously may be studied.

The instrument must produce as many photons of the desired energy as possible, and convey them to the sample region with an absolute minimum of loss. Any ions formed must have a high probability of being collected and focused into the mass analyzer, which should have a high transmission for ions of the desired mass. The photon and ion detectors must then be efficient in converting the incident particle flux into the electrical domain. Note that these are also requirements for good precision, as discussed above.

The extent to which the photon and ion signals are utilized can be as important as how efficiently they are produced. If intense signals are produced, but only a small fraction of the time can be spent

acquiring data, then most of the signal is wasted. Clearly, high efficiency demands that the percentage of time that the instrument is involved in actual data acquisition be maximized. The instrument should be designed to facilitate setting up the experiments so that the time spent doing so is minimized. Also, the data from one experiment often need to be reduced to a corrected PIE curve and plotted before the next experiment can be defined. Any time spent in doing so after the experiment is time that could be used performing the next experiment, and hence is wasted from the point of view of maximizing overall data acquisition time. In order to provide the user with the information necessary to make intelligent decisions about the type and sequence of succeeding experiments, without wasting potential experiment time, the ideal PIMS instrument would provide instantaneous display of fully corrected data. In practice, even partially corrected data may be sufficient, and the instrument should at least be designed to allow a partially corrected PIE curve to be displayed point by point as it is acquired (i.e., in "real time").

From the standpoint of total elapsed time, a PIE curve will be acquired most efficiently if each point is integrated for only a very short time. This conflicts with the requirement of long integration times for good precision, and some compromise must be reached. For any particular experiment, there will be some minimum acceptable signal-to-noise ratio. What the minimum is will depend on the system under study and the information that is desired, and must be defined by the investigator. Once defined, however, the goal of overall efficiency imposes the requirement that the integration time for each point be only long enough to reach the minimum desired S/N. Since the

ion intensity will vary with wavelength, the optimum integration time will also vary with wavelength. Best efficiency will be obtained if the instrument allows the integration time to be varied on a point by point basis so that all measured photoionization efficiencies are acquired with just the minimum acceptable signal-to-noise ratio.

Similarly, while accuracy requires that the correction measurements discussed above be made "often enough", efficiency requires that they not be made any more often than required for the minimum acceptable accuracy. Depending on the purpose of the experiment, this may mean that some or all of the correction measurements of which the instrument is capable should not be made at all. The instrument design should readily allow such changes in procedure. In fact, time spent acquiring data will be maximized if the instrument is designed to allow hardware or procedural modifications to be made quickly.

From the user's point of view, the overall efficiency of the study in progress will be markedly increased if the instrument does not require constant attention. If the instrument's operation can be automated, the user can spend time in other ways and will probably be more productive and certainly happier.

Finally, the instrument is not being fully utilized when shut down for repairs. It should therefore be designed to be as foolproof as possible, and ideally it should be able to take corrective or preventive action automatically in the event of an emergency or accident, especially if no operator is present.

A summary of the design requirements discussed in this section is presented in Table I-1.

TABLE I-1. Requirements Imposed by Design Goals

Goal	Requirements
Precision	High ion count rate Stable instrumentation Long integration times
Accuracy	Linear data acquisition electronics Post-experiment correction measurements (Photon detector sensitivity vs. wavelength) (Ion detector sensitivity vs. mass) During-experiment correction measurements (Background) (Pressure) ("Reference") (Scattered light)
Efficiency	High percentage of time doing data acquisition (Facilitate setup, use) (Real-time data reduction, display) Point-by-point optimization of integration time Flexibility for hardware or procedure changes Correct and automatic emergency action Constant operator attention unnecessary

F. Merits of Previous Designs

1. Basis of Comparison

Since no two photoionization mass spectrometers are alike, any attempt at classifying them is bound to lump together dissimilar instruments. This fact has not prevented classification attempts from being made, however, most of which have been based on the type of monochromator or mass analyzer used. While recognizing that differences in these important elements can have tremendous influence on the capabilities of the instrument, discussion of such differences is postponed to Chapter II. Here, however, an attempt is made to classify the various instruments in terms of the operating procedures used with them and their basic approach to data acquisition. At first glance, the

operating procedure might not seem to be a "part of the instrument", since it is, after all, only what the user decides to do with the instrument. However, it will be shown that the range of procedures from which the operator may choose is definitely limited by the hardware of the instrument, particularly the data acquisition system. Certain aspects of the experimental procedure can be designed into or out of an instrument, and therefore the operating procedures to be used are an important factor to consider in designing the instrument, and are a legitimate basis for comparison.

For the purpose of such a comparison, the various types of instruments discussed in the remainder of this chapter are assumed to have basically equal capabilities in other areas. Specifically, ion and photon signal intensities and instrument stability are assumed equal, as is the accuracy of the data acquisition electronics. The post-experiment correction measurements are assumed to be possible with all instruments, also.

2. Manual Operation

Nearly all of the early photoionization mass spectrometers and even some later ones are operated manually [19,37-42], and can be diagrammed as shown in Figure I-2. The user adjusts such parameters as the wavelength, mass, optical resolution and sample pressure via instrument controls which may be electronic or mechanical. Data acquisition consists of writing down photon and ion intensity data which are read on meters, digital counters or strip chart recorders. The operator can usually control the time constant or integration time of the data acquisition electronics to adjust the S/N of the data. There are also

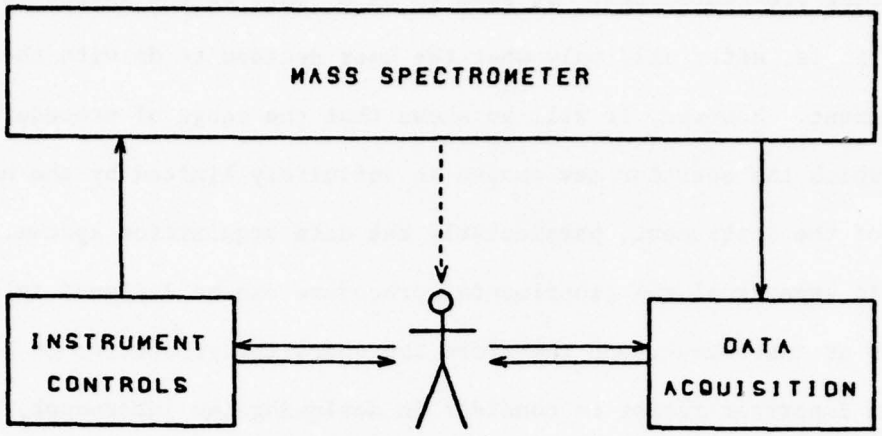


FIGURE I-2. A Manual Instrument.

other elements of data acquisition involved when the operator gains information by monitoring meters, knob positions, etc. on the instrument controls. The operator may also check the status of the mass spectrometer by reading vacuum gauges, checking positions of vacuum valve actuators, feeling or listening to the pumps, and so forth.

The manual approach has a number of advantages, and in fact meets most of the requirements outlined in the previous section. It is the quickest design to implement and, requiring an absolute minimum of data acquisition equipment, is the least expensive design from the standpoint of permanent equipment costs. It is also the most flexible design--changes in procedure are implemented literally as soon as the operator decides what to do. The user can make any of the necessary correction measurements, as often as necessary (including never).

Users of ion counting instruments will frequently allow the data to integrate until some relatively constant number of ions have been counted. As shown in Chapter V, this is very nearly the right procedure to use in order to acquire all points at a constant S/N in the

minimum necessary time. Data reduction and display can sometimes be accomplished as fast as the data are acquired, especially if very long integration times are used. For shorter integration times, manual plotting may take longer than the integration time, which slows down data acquisition. Compared to designs discussed later, a high percentage of the time is not spent acquiring data, but rather in plotting the last point or in adjusting the wavelength between points, etc.

One further advantage of the manual instrument is that if (correction: when) something goes wrong, the operator can take corrective action as soon as the problem is noticed. Unfortunately, the operator may not notice that there is a problem very quickly, and may have a slow response time or make an incorrect response even when the problem is noticed.

The major disadvantage of the manual approach, however, is that the presence of the operator is required continually. The instrument cannot be used continuously for more than several hours at a time, unless several people work shifts tending the instrument. Despite its initial low cost, the manual approach soon becomes expensive enough that one of the alternatives (to be discussed shortly) becomes economically competitive, if the operator is being paid something like a living wage.

A final drawback to manual data acquisition is not a necessary limitation of the approach, but is virtually always encountered in practice. As the operator's boredom increases, the "minimum acceptable S/N" seems to decline, as does the desired frequency of correction measurements. The S/N of manually acquired data seems to be always far less than the ultimate that the instrument could provide if only the

operator were more patient. Furthermore, data points are often taken at much wider wavelength intervals than optimum, so that some of the fine structure in the PIE curve may be distorted by undersampling or may be missed entirely.

3. Data Logging

In an attempt to overcome the limitations of manual operation, most recent designs have included provisions for some sort of automated data acquisition. One of the earliest approaches [43-45] is shown in Figure I-3. The basic equipment is the same as in the manual design, except that an electronic sequencer and some device to record digital data (e.g., a Teletype, paper tape punch, magnetic tape recorder, etc.) are added, and the wavelength is controlled with a stepping motor drive.

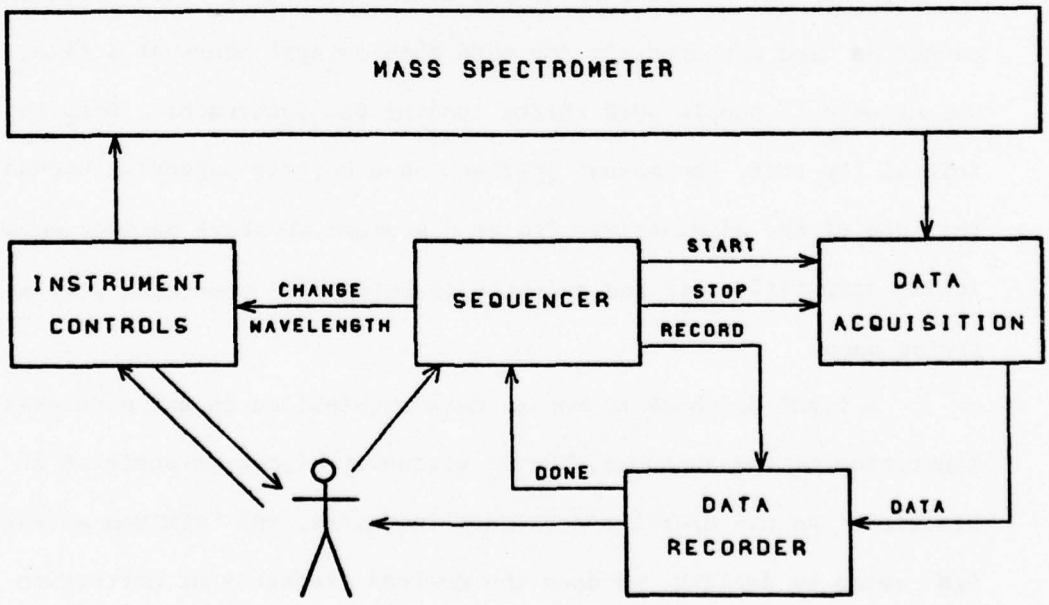


Figure I-3. A Simple Data Logging Instrument.

Setting up the experiment is done exactly as in the case of the manual instrument, with the user admitting the sample, adjusting wavelength resolution, mass setting and initial wavelength. In addition, an integration time and wavelength increment are set in the sequencer controls. When started, the sequencer integrates photon and ion signals for the preset time, causes the data to be stored, advances the monochromator the desired wavelength interval and begins the entire process over again. This type of operation with a simple sequencer and data recorder is frequently called "data logging".

The overwhelming advantage of this type of design is that the user need not be present. The instrument can run 24 hours a day, using long integration times and small wavelength intervals, without losing patience. The initial cost of the added equipment is soon repaid by savings in user's time and in the high quality of data that can be obtained.

A typical data logging system also gives up some of the advantages enjoyed by the manual system, however. There is often no operator present during much of an experiment and failures of vacuum equipment can cause severe damage before they are discovered. The system is no longer versatile at all--a change in procedure more drastic than changing the integration time demands a total re-design of the sequencer. Set up of the experiment is, if anything, more difficult than with a manual instrument, since the user must make very sure that the parameters specified to the sequencer are appropriate for the entire run before starting it.

The same integration time is used for every point in an experiment, no matter what the intensity may be. This means that the

tradeoff between integration time and signal-to-noise ratio must be made on a scan-by-scan basis, rather than the much more efficient point-by-point basis often used during manual operation. The correction measurements that should often be made during the experiment are usually not made with this sort of system, due to the extreme complexity that would be required in the sequencer design. If made at all, correction measurements must be made manually, and if they are required frequently, the advantage of not requiring the presence of an operator is eliminated. Hence, when such a data acquisition system is used, correction measurements are often made only at the beginning and end of a run, and do not necessarily give an accurate indication of drifts during long experiments.

Data reduction must be done after the experiment. If paper or magnetic tape is used to record the data, the post-experiment data reduction is easily performed by computer, but the user may have no way of telling how the experiment is progressing or whether the acquired data are actually of the desired quality until after such reduction is complete. It may take hours after the completion of a several-day experiment to discover that the entire run is wasted because of some factor overlooked during the setup or some problem which arose in the course of the experiment.

Another approach which has been used recently [46] attempts to provide at least a crude real-time PIE output, and also attempts to optimize data integration time on a point-by-point basis. In this "modified data logger" approach, the ion and photon signals are not integrated for a preset time, but rather until a preset number of photons have been counted. Thus in regions of low photon intensity (and

hence low ion intensity) the integration time will be longer. As shown in Chapter V, this approach is successful in optimizing the integration time, providing that the fluctuations in the ion intensity are caused by fluctuations in the incident photon intensity. This is often the case, but not always. If the PIE curve has sharp structure, or if the threshold region is being measured, then the ion intensity can vary radically in regions of relatively constant photon intensity, and this approach is no more valid than the constant integration time used in the simple data loggers.

The modified data logger has the further advantage that the number of ions recorded at each wavelength is normalized to a constant photon intensity, and therefore equivalent to the (uncorrected) PIE. If the data are printed out as they are acquired, it is possible to get at least some indication of the progress of the experiment without necessitating any further calculation.

In one design [47] which incorporates this modification, the sequencer varies the mass rather than the wavelength when the desired photon count has been reached. When all ions have been recorded, the user manually adjusts the wavelength and restarts the sequencer. This approach is claimed to provide "uniform precision with the maximum possible efficiency obtainable without complete computer control of the instrument" [47]. This claim can only be valid when (1) all fragment ions to be observed are created with equal or nearly equal probability at all wavelengths studied, and (2) the number of wavelengths at which data are desired is fewer than the number of ions to be studied. Except in very special cases, neither of these requirements is met. Different fragment ions from a given molecule typically have

intensities which differ by 2-3 orders of magnitude or more, even at those wavelengths where all ions are formed. The approach described in [47] will use the same integration time (at a given wavelength) for all ions, and the resulting PIEs will not be of comparable precision, although the precision for a given fragment may be roughly constant as the wavelength is varied. Furthermore, a typical PIE curve may contain data at hundreds or even thousands of wavelengths, though fewer than a dozen or so fragment ions will usually be of interest. The presence of the operator may be required often to change the wavelength so that this design, in spite of being "automated", should probably be regarded more as a slightly modified manual instrument than as an automated data logger. Either of the two data logger designs described previously will usually provide higher overall operating efficiency than this design, even though lacking "complete computer control".

The two basic data logger designs described earlier each introduce a number of problems, but the ability to collect data unattended over long periods of time can overcome the major disadvantage of the manual instruments. The fact that this one disadvantage is significant is demonstrated by the impressive quality of data that can be obtained with the automated instruments, despite their disadvantages.

G. The MSU Instrument

The photoionization mass spectrometer described in this thesis (Figure I-4) is also designed to permit unattended operation, but to simultaneously retain the advantages previously obtainable only by manual operation. It combines the best features of the designs

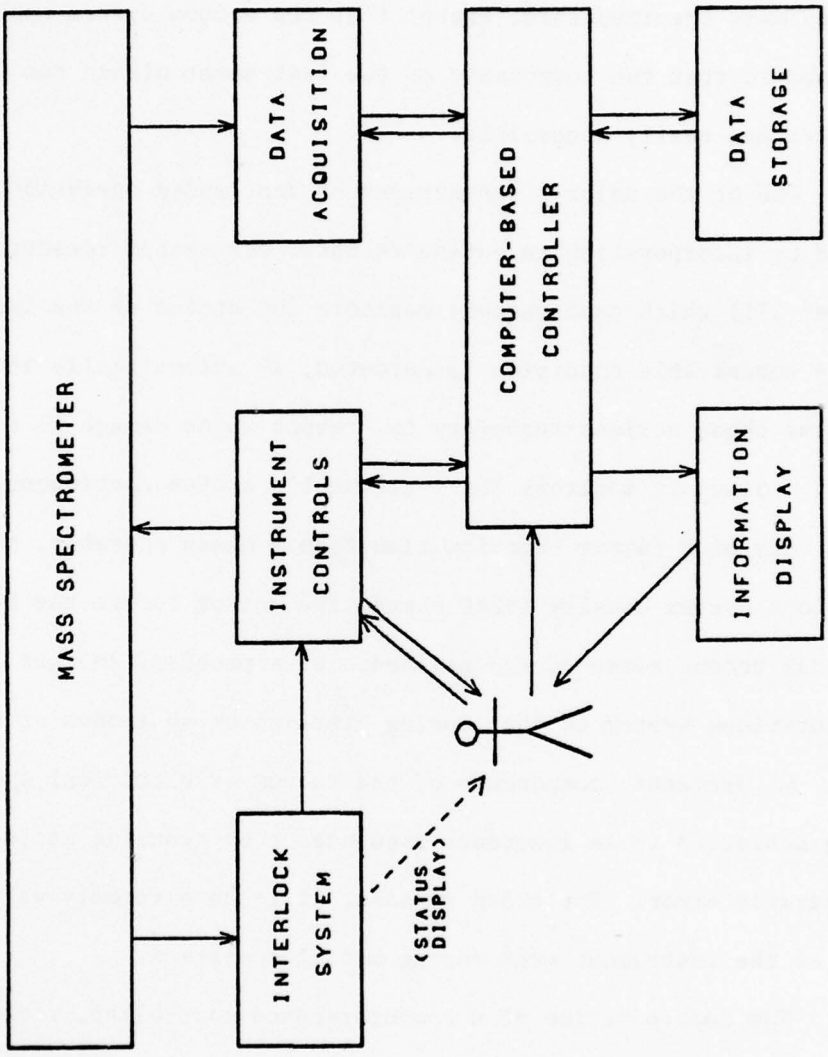


Figure I-4. The MSU PIMS Instrument.

discussed in the previous section, but also includes advantageous features not found in any previous design.

The basic elements of the instrument, described in detail in Chapter II, are fairly typical of those used in many other photoionization mass spectrometers, except that the vacuum system has been designed so that the components of the instrument within the vacuum chambers are easily accessible.

One of the major disadvantages of unattended operation is eliminated by incorporating an extensive interlock system (described in Chapter III) which continuously monitors the status of the instrument. If any undesirable condition is detected, it automatically and rapidly performs those actions necessary to prevent major damage to the instrument. Since it monitors the instrument's status continuously and has a very much faster reaction time than a human operator, the interlock system usually takes corrective action before the human operator has become aware of the existence of a problem. Another feature of the interlock system is that during start-up or shut-down of the instrument, it prevents components of the vacuum or electrical systems from being activated in an incorrect sequence, thus reducing accidents due to operator error. For these reasons, it is an extremely valuable part of the instrument even during manual operation.

The incorporation of a computer-based controller, rather than a simple sequencer, allows the other disadvantages of the data logging designs to be overcome. The computer presently controls a shutter in the photon beam, the wavelength drive, and the acquisition of photon and ion data. The interface and data acquisition circuits involved, including a novel high-speed, low cost circuit for photon or ion

counting, are described in Chapter IV.

The specific actions taken by the computer during an experiment are controlled by the programs (software) used, rather than by permanently wired electronic circuits. This is both the main disadvantage and the main advantage of computer-controlled instrumentation. The programs must be written and de-bugged before the instrument can be run. The software system is as important to the overall performance of the instrument as the hardware, and so designing the software becomes a task that must be performed in addition to designing the hardware of the instrument. However, the use of software to control the operations of the system results in a great deal of flexibility and versatility, since most changes in experimental procedure can be accomplished merely by running a different program, rather than by re-designing an electronic sequencer, and re-writing a program can usually be accomplished more quickly.

The computerized instrument is programmed to make the various necessary correction measurements that the simpler data logger instruments cannot perform automatically. The computer calculates and plots the PIE curve, at least approximately corrected for scattered light, background, etc., as each point is acquired and stored, so that the quality of the data can be judged at any time during the experiment. If it is not as high as necessary, the experiment is easily terminated and restarted with modified parameters withour wasting futher time. Also, the computer is programmed to integrate each point until a desired PIE (not photon) S/N is achieved, which results in nearly optimum efficiency of data acquisition.

Besides including all the advantages of other instruments, a computerized instrument can potentially provide even further advantages. For instance, any real instrument is certain to be incompletely automated (somebody has to at least find a sample!), so that certain tasks must be performed manually, especially during the initial stages of an experiment. The MSU instrument is designed to facilitate these manual tasks as far as possible, in order to reduce to a minimum the time spent in their performance. The computer is programmed to guard against common operator errors during the stage of the experiment in which data acquisition parameters are being specified. Post-data acquisition data reduction can be performed with the same computer so that the experiment can flow smoothly and quickly from setup to acquisition to analysis and back in a manner which can greatly increase the overall efficiency of the experiment.

Table I-2 summarizes the extent to which the basic designs (manual, data logger, modified data logger and the MSU computer-controlled design) meet the design requirements described earlier. It will be noted that the design reported here is (not surprisingly!) superior to the other designs in common use. It cannot be emphasized too strongly, however, that the major advantages attributed to the MSU design are <u>not</u> necessarily obtained as a result of adding a computer to an instrument. The potential advantages of computer-interfaced instrumentation are only potential advantages until realized by the software system to be used with the instrument. If the interactions between the instrument, computer and user are not carefully evaluated, it will not be possible to design an effective software system, and the result of merely "adding a computer" may be to create an instrument with

TABLE I-2. Comparison of Four Design Approaches[a]

Requirement	Manual	Data Logger	Modified Logger	MSU
Correction measurements made during experiment	?	-	-	✓
Provides real-time display of corrected data	✓	-	*	✓
Pointwise optimization of integration time	✓	-	*	✓
Operating procedures easily changed (flexible)	✓	-	-	✓
Prompt, correct emergency action taken	✓	-	-	✓
Long integration times, close point spacing possible .	?	✓	✓	✓
Operator's constant attention not required	-	✓	✓	✓
Design facilitates setup and use	-	-	-	✓

[a]Key:

- \- = does not meet requirement
- ✓ = meets requirement
- ? = can meet requirement, but usually does not in practice
- * = meets requirement under certain circumstances, or meets modified requirement

capabilities about the same as a data logger instrument, but which is more expensive and much more difficult to use.

Chapter V of this thesis discusses these concepts in more detail, both in relation to computerized instruments in general and photoionization mass spectrometers in particular. The specific operating procedures used with the MSU instrument and the important features of the PIMS software system are described, and data are presented which illustrate the specific advantages of the overall design approach.

CHAPTER II

THE MASS SPECTROMETER

A. Introduction

Any mass spectrometer can be described in terms of the basic elements shown in Figure II-1. The ion source comprises all components necessary to create ions from the sample. The ion optics guide the ions from the source to the detector and provide some way of discriminating against unwanted ions according to their mass-to-charge ratio. The ion detector, more accurately called a transducer, is responsible for converting the arrival rate of incident ions into an electrical signal proportional to that rate, which can then be processed by the data acquisition electronics. The maximum pressure at which each of these three components can function properly varies, but is always well

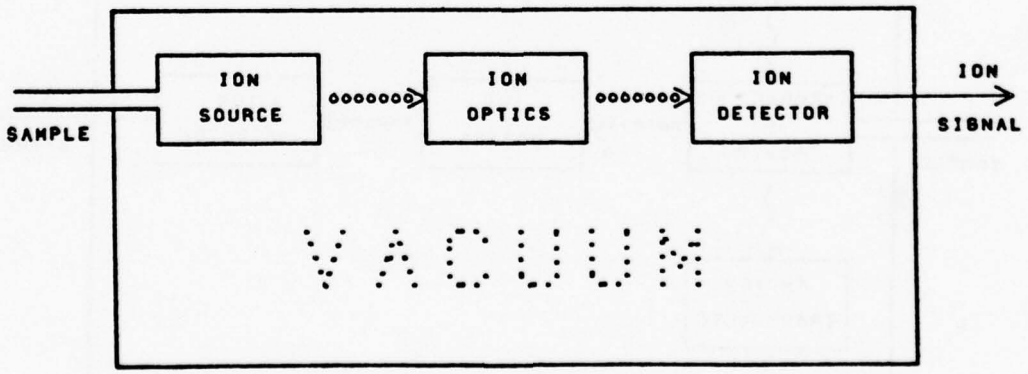


FIGURE II-1. The Basic Elements of a Mass Spectrometer.

below atmospheric pressure (e.g., about 10^{-5} torr for most ion optics). Therefore, a vacuum system capable of maintaining the necessary pressure must be included as the fourth basic element.

In the case of photoionization mass spectrometry, the ion source consists of a photon source, photon optics, an interaction region, and a photon transducer, as shown in Figure II-2. The photon source includes all the components necessary to create the photons, the photon optics guide the photons to the interaction region and discriminate against photons with unwanted energies, and the photon transducer converts the photon arrival rate to an electronic signal. Some photoionization mass spectrometers include no provision for photon energy

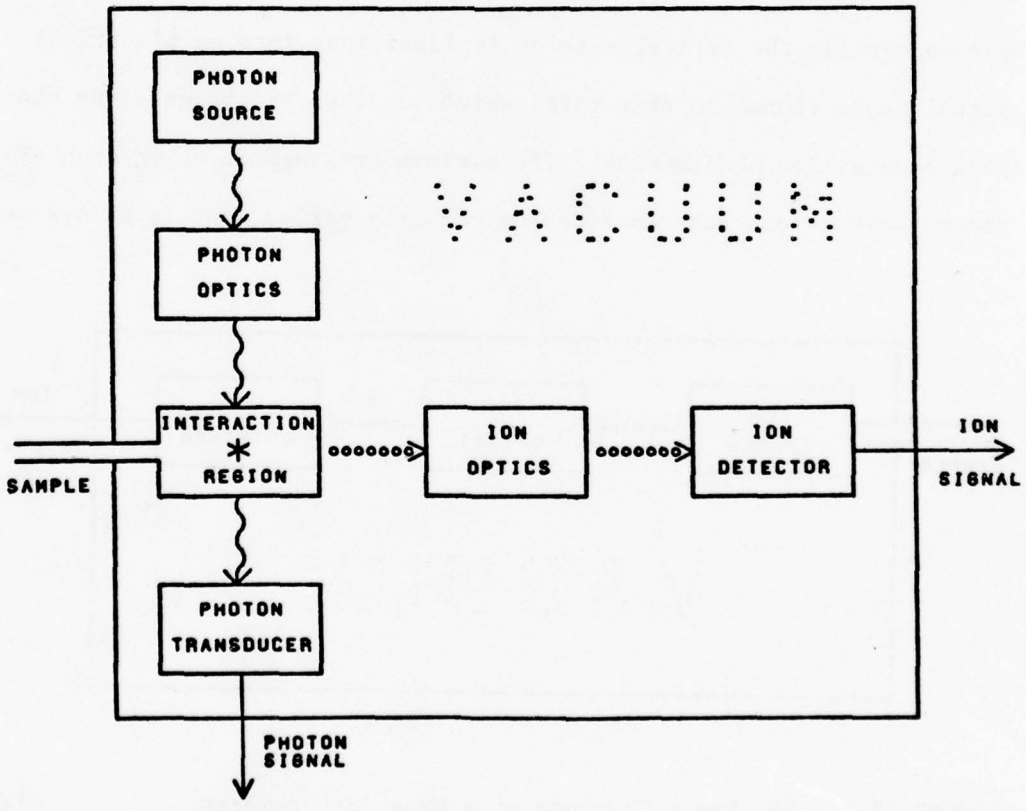


FIGURE II-2. The Basic Elements of a Photoionization Mass Spectrometer.

discrimination. This considerably simplifies the photon optics, but prevents the use of the instrument for determination of ionization efficiency curves, and such designs will not be considered further. The interaction region is simply some sort of sample molecule reservoir in which the ionization takes place. It is often referred to as the ion source, independent of photon source, optics, and transducer, a practice which is followed in the remainder of this thesis.

Each of the components in Figure II-2 can be implemented in a variety of ways. Each succeeding section of this chapter is devoted to one of the components shown in that figure, and includes both a brief discussion of the major alternatives and a description of the corresponding portion of the Michigan State University photoionization mass spectrometer.

B. Photon Sources

1. Overview

The ideal photon source for PIMS would continuously emit intense radiation with a wide and continuous energy distribution, preferably covering at least the range of 300-2000 Å. Ideally, it should also be compact and inexpensive. References [7] and [8] give an excellent introduction to the many different devices which have been used as photon sources in the vacuum ultraviolet, most of which fail to meet any of these requirements. Only three types of radiation sources come close enough to meeting these requirements to be useful in PIMS: synchrotron radiation, the rare gas discharges, and the molecular hydrogen emission spectrum.

From the standpoint of wide, continuous energy distribution, the radiation emitted as a result of the centripetal acceleration of electrons in synchrotron rings is easily the best of the available sources. The energy distribution of a synchrotron source depends on the size of the ring and the electron energy, but might typically rise to a peak at about 100-200 Å (124-62 eV) after an onset at lower wavelength, and then slowly decrease towards longer wavelength, retaining perhaps 20% of the peak intensity at 2000 Å (6.2 eV). Although actually a pulsed source, the synchrotron repetition rate is so rapid that the pulsed nature can usually be ignored. Although far from compact, its biggest drawback is its expense; few synchrotrons exist in the world, and most people simply do not have access to such a light source. Therefore, although synchrotron radiation has been used for PIMS [38,39], most workers in the field are forced to use other photon sources.

In 1930, J. J. Hopfield discovered that a high-power pulsed discharge in helium produced an emission continuum ranging from roughly 600 Å to 1100 Å [48-50]. This "Hopfield continuum" results when excited He_2 molecules undergo a transition to the steeply repulsive portion of the unstable ground state of the molecule (see Figure II-3). The mechanism includes the following steps:

$$2He + He^+ \rightarrow He_2^+ + He \qquad (a)$$

$$He_2^+ + e^- \rightarrow He_2^* \qquad (b)$$

$$He_2^* \rightarrow He_2 + h\nu \qquad (c)$$

$$He_2 \rightarrow He + He \qquad (d)$$

Since the recombination of He_2^+ ions and electrons (b) cannot occur efficiently under the conditions that exist during the discharge, the Hopfield continuum is emitted only as an afterglow, lasting typically

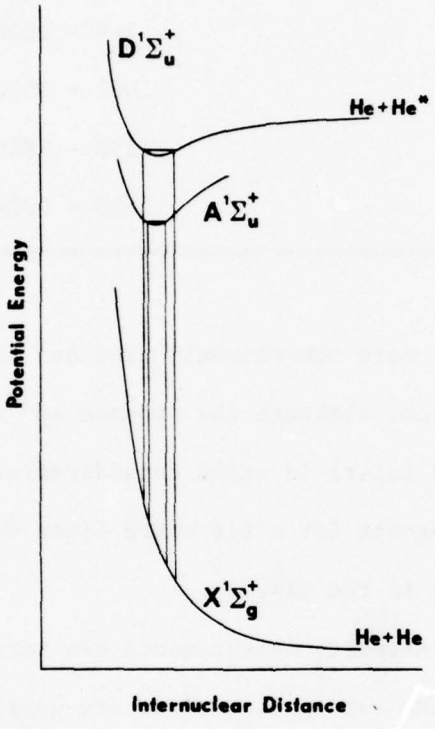


FIGURE II-3. Schematic Diagram of the Potential Energy Curves of He_2.

ten to twenty microseconds after the discharge, depending on pressure. If the discharges occur frequently enough and are short compared to the time between discharges, the emission becomes essentially continuous.

Similar continua have been discovered for all of the rare gases [51-55]. Their approximate wavelength limits are summarized in Table II-1. The major advantage of these sources is that they can be produced

Table II-1. Approximate Wavelength Limits of Rare Gas Continua.

Gas	Approximate Range, Å
He	580 - 1100
Ne	740 - 1000
Ar	1067 - 1550
Kr	1250 - 1800
Xe	1480 - 2000

in an apparatus which is more conveniently used and is much less expensive than a synchrotron, although the expense and size of the instrumentation (described later) is still considerable. The continua are relatively smooth, except for a few sharp lines due to atomic emission from impurities in the gases.

Since absolute intensity measurements are rare, comparisons are difficult to make, but the rare gas continua are usually less intense than the radiation from a synchrotron source. Their intensity depends strongly on the power supply used to cause the discharge, however, and the better rare gas lamps may actually exceed the intensity of some of the synchrotron sources, especially at longer wavelengths. Although it is inconvenient to have to change gases in order to cover the entire wavelength range, the most important disadvantage of these continua as radiation sources for PIMS is that none extend below 580 Å (21.4 eV). Furthermore, although the Hopfield continuum extends to 1100 Å, it is extremely weak above about 1000 Å (see Figure II-4).

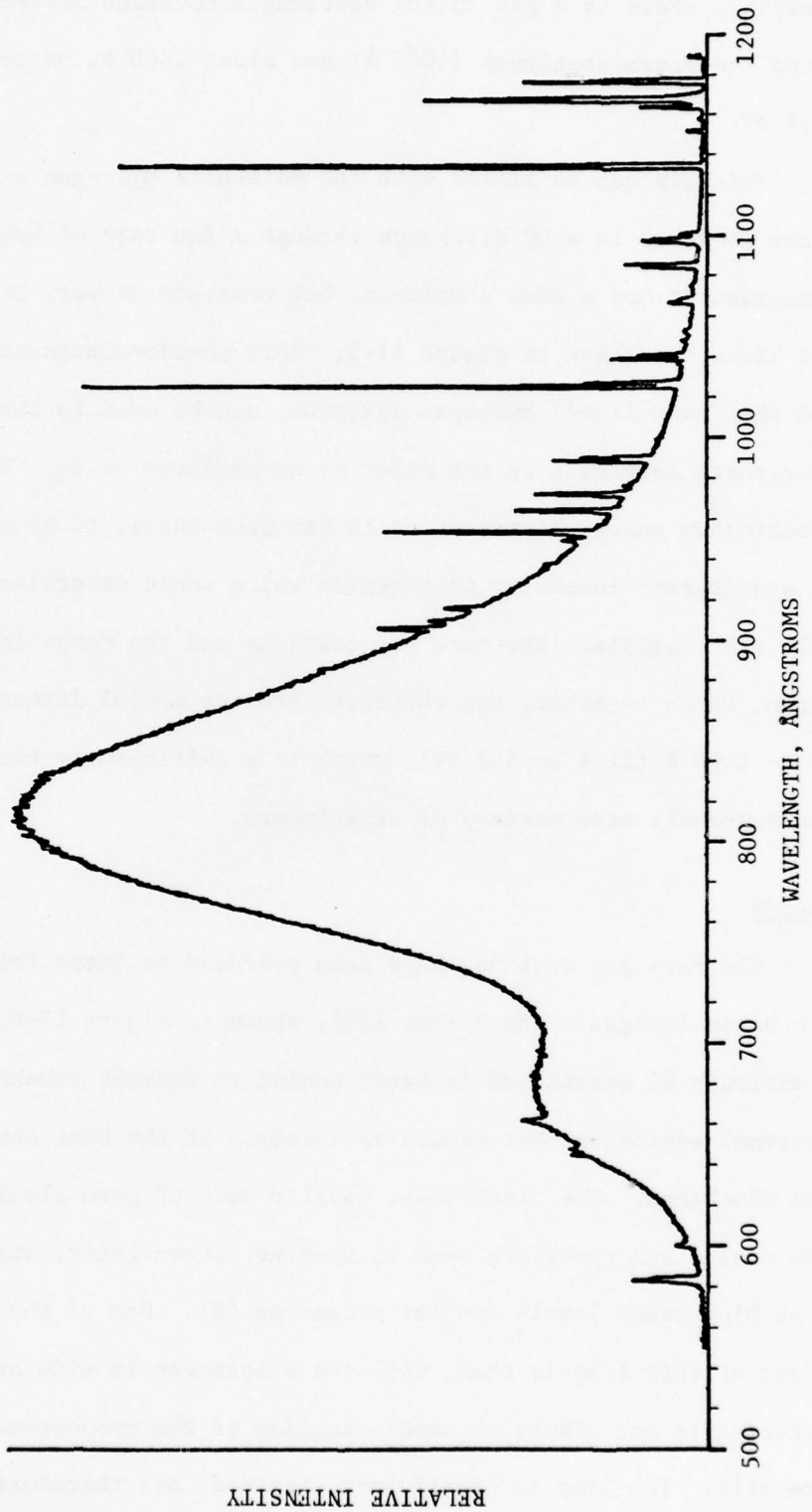


Figure II-4. The Helium Continuum.

In practice, there is a gap in the wavelength coverage between the onset of the argon continuum (1067 Å) and about 1000 Å, or about 11.6 to 12.4 eV.

This gap can be filled with the molecular hydrogen emission spectrum produced in a DC discharge through a few torr of hydrogen. The emission is not a true continuum, but consists of very closely spaced lines, as shown in Figure II-5. This pseudo-continuum, often called the "many-lined" hydrogen spectrum, can be used to obtain data at wavelength intervals on the order of an angstrom or so. While its non-continuous energy distribution is far from ideal, it at least produces significant intensity in a region which would otherwise be practically inaccessible. The rare gas continua and the many-lined hydrogen spectrum, taken together, can therefore provide useful intensity from 580 Å to 2000 Å (21.4 to 6.2 eV), which is a sufficiently broad range for an extremely wide variety of experiments.

2. Lamps

The rare gas continua have been produced in lamps following one of two basic designs. The Π lamp [56], shown in Figure II-6, is usually made entirely of quartz and is water cooled to prevent breakage from the thermal expansion that occurs as a result of the heat generated in the discharge. The electrodes, usually made of pure aluminum, cannot be cooled and therefore tend to sputter rather badly, and may even melt at high power levels and low pressures [6]. One of the main advantages of this lamp is that, with the electrodes in side arms, sputtered material is not likely to cause clogging of the monochromator entrance slit. The lamp is usually not shielded and therefore radiates

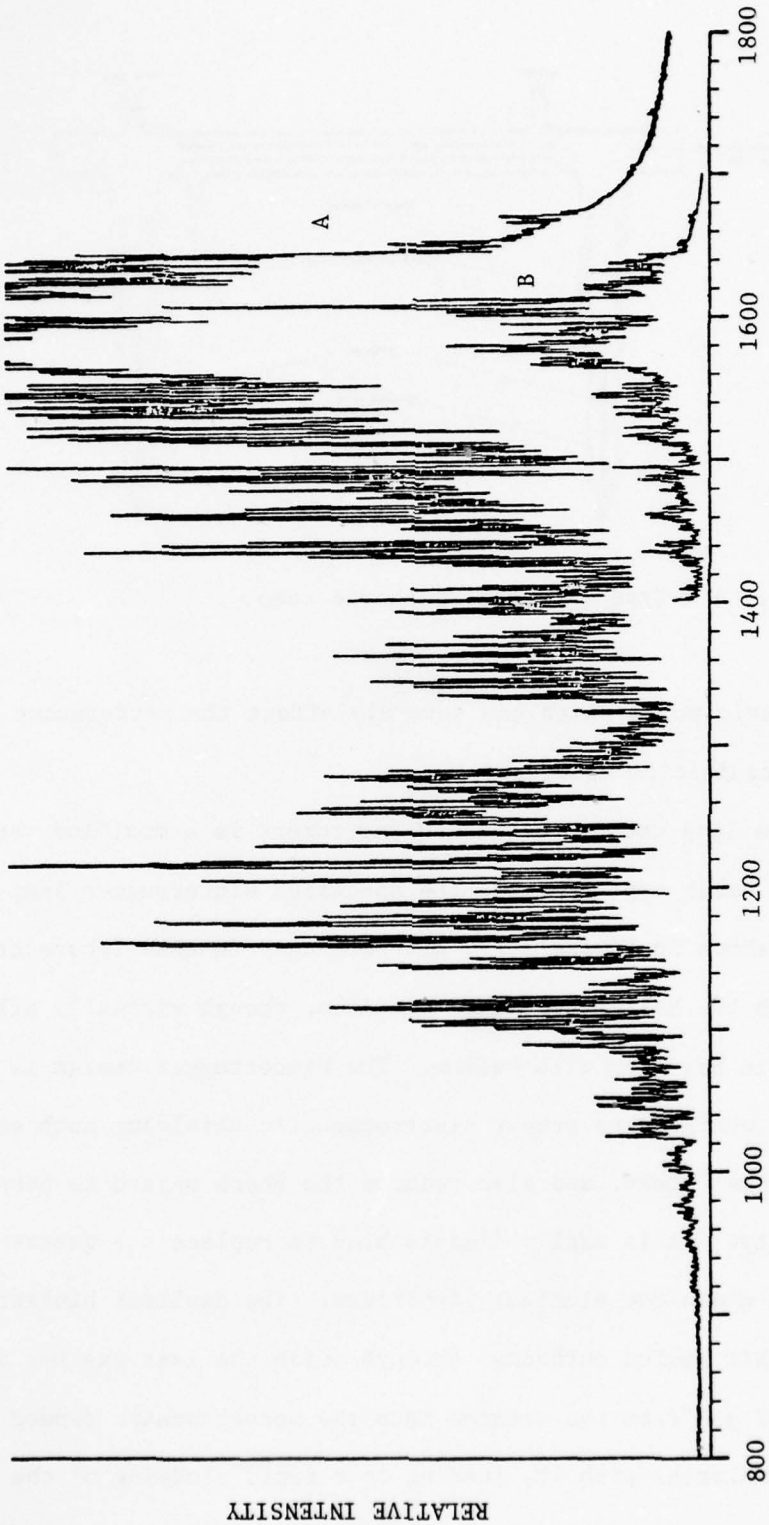


Figure II-5. The Hydrogen Many-Lined Spectrum. Curve B is reduced by about a factor of ten relative to curve A.

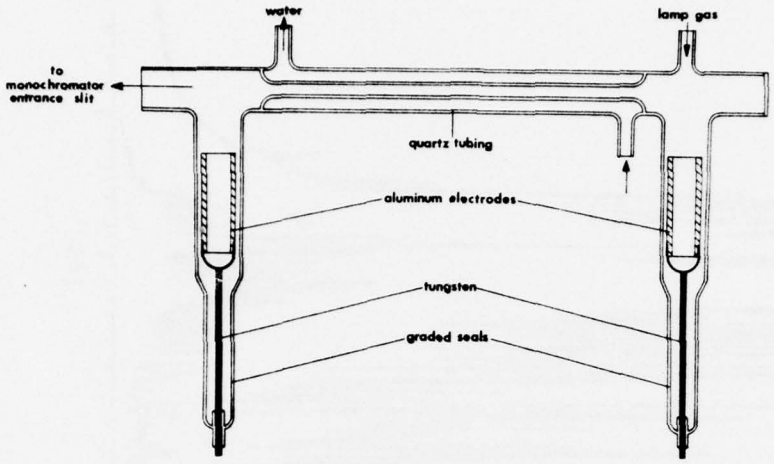


Figure II-6. A Π-Type Rare Gas Discharge Lamp.

electromagnetic noise which can severely affect the performance of sensitive data acquisition electronics.

The lamp used with the MSU instrument is a modified version of the second basic type of lamp, the so-called Hinterregger lamp [57]. The lamp, shown in Figure II-7, has been used in this laboratory to excite both the helium and argon continua, though virtually all work done to date has been with helium. The Hinterregger design is axially symmetric, which makes proper electromagnetic shielding much easier than with the Π lamp, and also reduces the shock hazard to people in the vicinity. It is easily disassembled to replace the quartz discharge tube or to clean the aluminum electrodes. The earliest Hinterregger lamps had air cooled cathodes, through which the lamp gas was admitted. The flow of gas from the cathode into the monochromator tended to carry sputtered material with it, leading to a rapid clogging of the entrance slit. The lamp shown here is based on a design first used in the

Figure II-7. The MSU Hinterregger Lamp.

a) monochromator entrance slit
b) plunger slit seal
c) insulating disc
d) one of three holes for gas inlet, pressure measurement and plunger control rod
e) anode cooling water
f) preslit
g) O-ring compression seal
h) quartz discharge tube
i) aluminum anode
j) shield and ground return
k) one of three cathode support rods
l) glass insulators
m) aluminum cathode
n) cathode cooling water
o) backpumping port
p) insulator (one of three)
q) alignment screw (one of three)

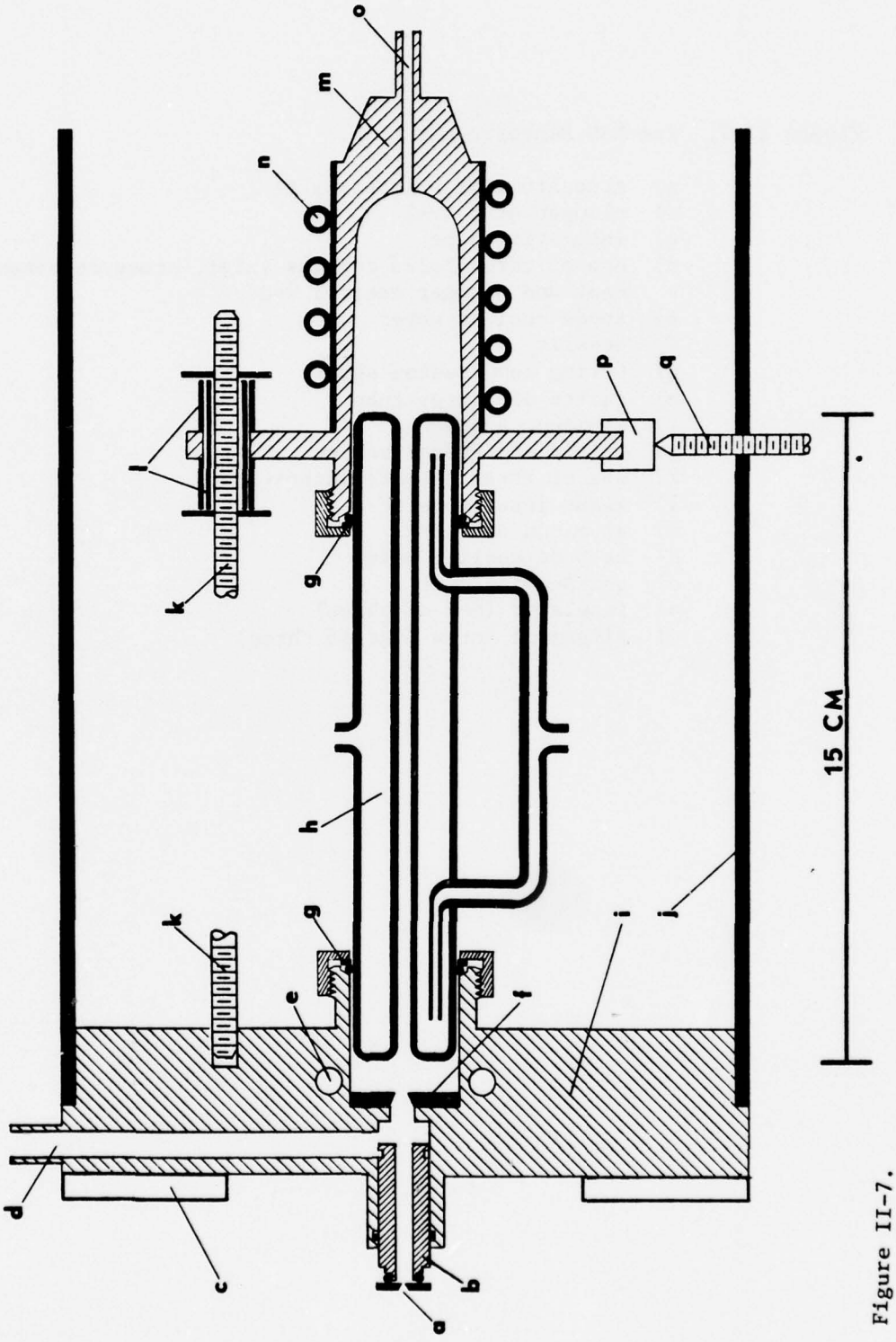


Figure II-7.

laboratories of W. A. Chupka and J. Berkowitz at Argonne National Laboratory (ANL), and incorporates a design modification first described by them [43] to reduce the slit clogging problem. The gas is admitted at the anode end of the lamp, and flows into the monochromator through the entrance slit. However, an auxiliary pump connected to the cathode also causes a gas flow from anode to cathode, which to a large extent prevents sputtered material from reaching the slits. Like most modern Hinterregger lamps, both cathode and anode are water cooled, as is the discharge tube, which allows operation at higher power without severe sputtering. The ANL design also incorporates a separate port at the anode for measuring the pressure of the gas in the lamp. This avoids errors that arise due to pressure gradients when the pressure is measured closer to the gas supply or backing pump.

The MSU lamp incorporates two minor modifications not present in the ANL design. One is the addition of alignment screws around the cathode. These were found to be necessary, as when longer lamps were incorporated to increase the output intensity, the weight of the cathode caused some droop in the main cathode support rods. This caused as much as a factor of two or three decrease in intensity compared with an aligned lamp. The second minor modification is the use of two "separate" water supplies, one for the anode and one for the cathode and discharge tube. The water is actually from the same supply, but the water flowing to and from the cathode passes through some fifty feet of plastic tubing (see Figure II-8). This long column of water has sufficiently high resistance to effectively insulate the cathode from the rest of the plumbing (at ground potential), and thus practically

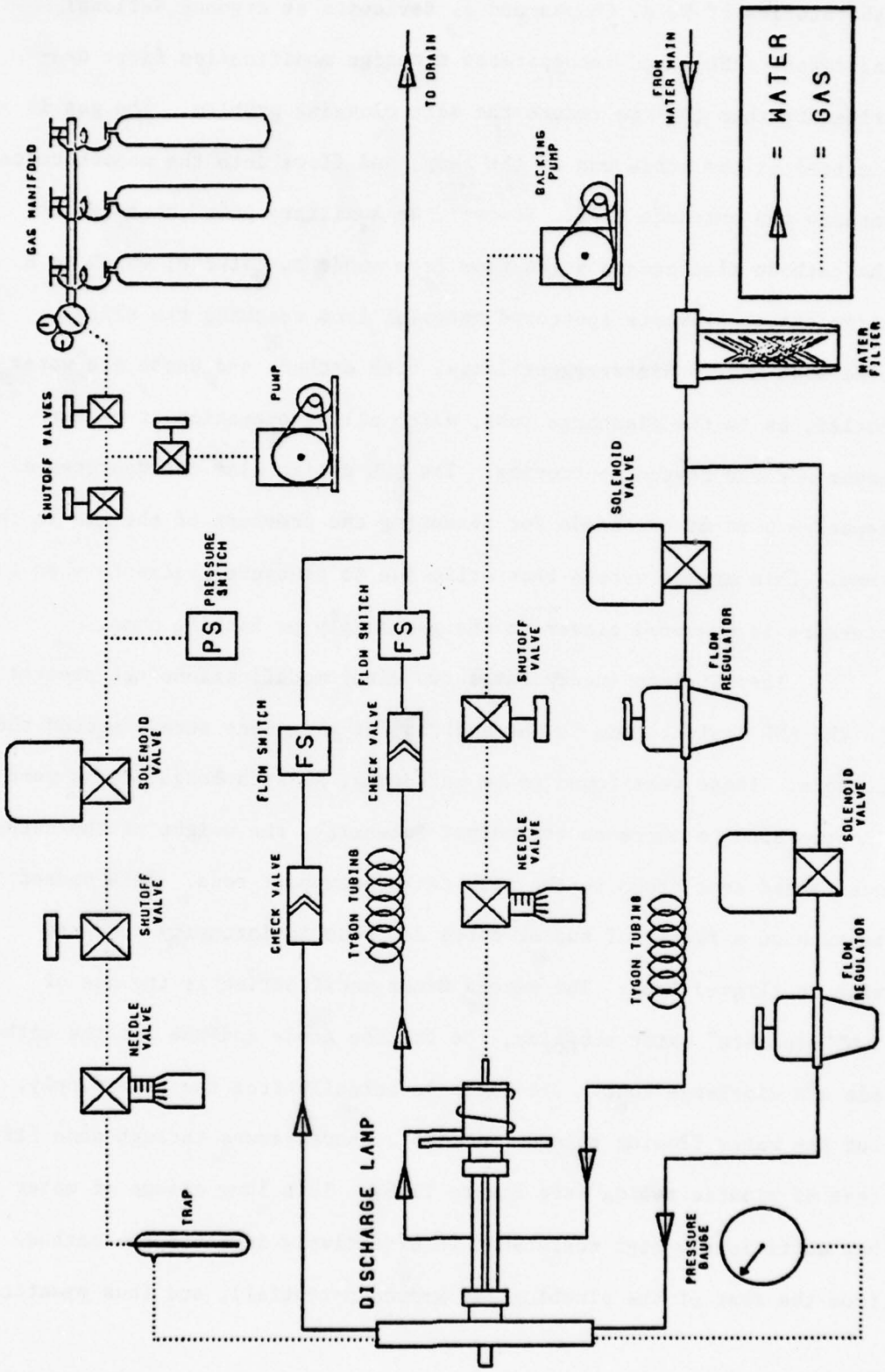


Figure II-8. Lamp Utilities.

eliminates the rather severe electrolysis of the water fittings that was observed when only a few feet of tubing were used between anode and cathode.

The lamp gas handling line is also shown in Figure II-8. The gas flow rate to the lamp and the amount of backpumping are controlled with micrometer-handled needle valves. A trap filled with molecular sieve can be cooled to liquid nitrogen temperature for purifying the helium used. This is found to reduce the intensity of the atomic emission lines superimposed on the continuum, but not to eliminate them. Since the reduced line emission is not accompanied by any measurable increase in the intensity of the continuum, and since the trap is fragile and inconvenient, it is often not used. The pressure switch, solenoid valves and water flow switches shown in Figure II-8 are all connected to the interlock system described in Chapter III.

The many-lined hydrogen spectrum can be produced in either of the two types of lamps described above, although an order of magnitude more intensity can be obtained by using a hot-filament cathode design [58]. So far, relatively little work has been done on the MSU instrument with the hydrogen source, and the Hinterregger lamp described here has been used for this purpose. This has the advantage that lamps do not have to be changed and realigned when changing sources. However, if much work is done in the future in the hydrogen lamp region, the increased intensity obtainable would certainly make construction of a hot cathode lamp for the purpose worthwhile.

. . . . . .

3. Power Supplies

The power supply circuit for the hydrogen lamp (Figure II-9) is very simple, consisting of a 20 KV, 1 A, unregulated DC power supply [59], the lamp, and a ballast resistor of a few thousand ohms. The voltage supplied by the DC supply is far in excess of that necessary to power the hydrogen lamp, but it is also used to supply the power

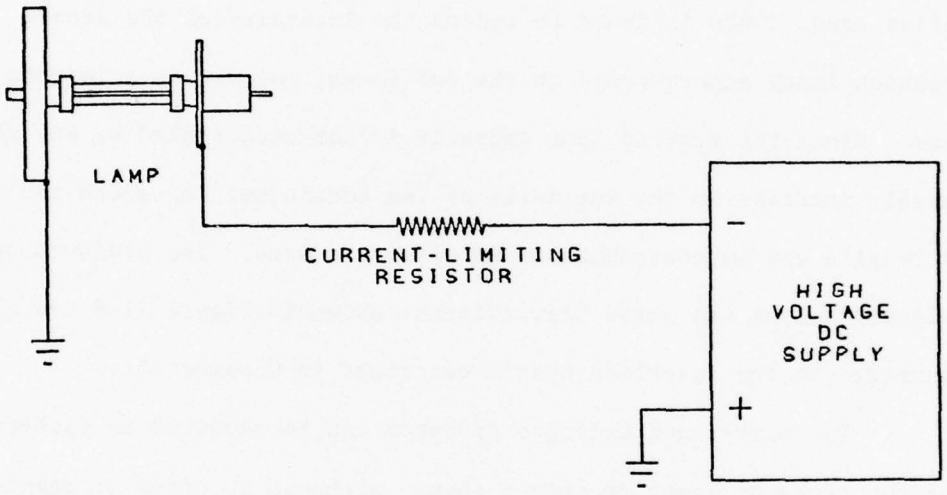


FIGURE II-9. DC Power Supply for the Hydrogen Lamp.

for the rare gas lamps, which require higher voltages. Typically, the voltage drop across the hydrogen lamp is only 1000 volts, with a 25 cm long x 4 mm id discharge tube at 2 torr and 300 mA.

The rare gas lamps must be pulsed, and so their power supplies are more complex than that for the hydrogen lamp. A variety of circuits have been used; one of the earliest is the simple spark gap circuit shown in Figure II-10. The DC supply charges the capacitor

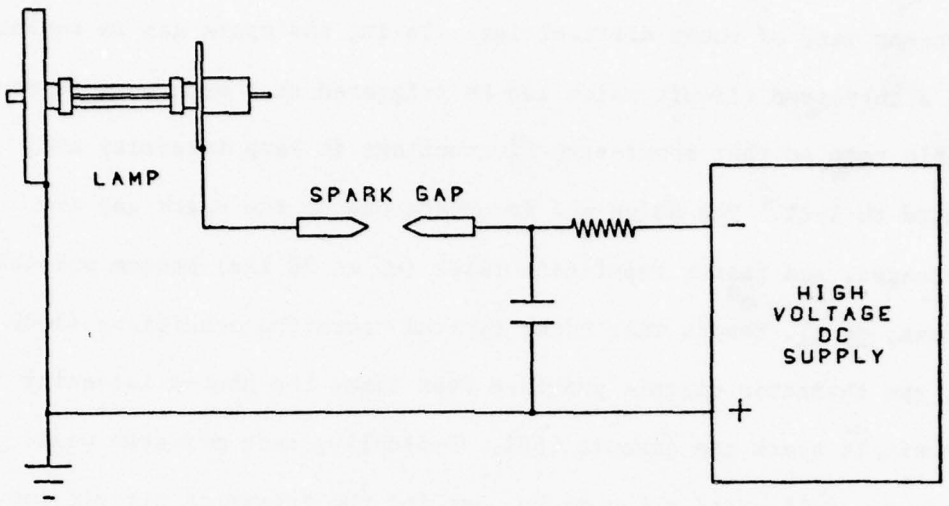


FIGURE II-10. Spark Gap Power Supply for the Rare Gas Lamps.

through the current limiting resistor until the breakdown potential of the gap (higher than that of the lamp) is reached. The capacitor then discharges through the lamp until the voltage left on it is less than the maintenance voltage of the spark gap and lamp, at which point the discharge ceases, the afterglow commences, and the cycle begins over again. The spark gap circuit is the simplest and cheapest circuit which can be used to produce the rare gas continua effectively, and these are its only advantages. Such circuits are extremely noisy (both electrically and acoustically), and have a limited repetition rate, which in turn limits the lamp intensity. Even "stabilized" spark gaps have somewhat unpredictable firing rates, resulting in about 4% random fluctuation in the average intensity of the lamp [60]. The spark gap electrodes also need to be adjusted and replaced rather frequently.

A power supply circuit first described by Huffman, et al. [60] overcomes many of these difficulties. In it, the spark gap is replaced with a thyratron circuit which can be triggered at a much more reproducible rate so that short-term fluctuations in lamp intensity are reduced to 1-2%. The noise and inconvenience of the spark gap are eliminated, and faster repetition rates (up to 20 KHz) become possible. Huffman, et al. report that under typical operating conditions (5000 Hz), the thyratron circuit provides four times the photon intensity of a simple spark gap circuit [60]. Typically, such a system would occupy two full-sized relay racks, one for the thyratron circuit and one for the high voltage DC supply. The cost of a commercially produced system would be in the range of about $4000 for the DC supply and $8000 - $10,000 for the thyratron trigger circuit, although presumably either could be "home-made" for considerably less money.

One disadvantage with both the thyratron and spark gap circuits is that the discharge, once initiated, continues until the capacitor is more or less completely discharged. More recently, power supplies have been built which employ vacuum (rather than gas-filled) tubes in the final stage. These have the advantage that they can be turned off as fast as they can be turned on. The sharper pulse termination allows afterglow production to get underway sooner. Optimum repetition rates with such supplies tend to be in the range of 50-100 KHz, and much higher intensities can be obtained as a result.

The power supply used at Argonne National Laboratory is evidently the most powerful currently in use with rare gas lamps, but it has been described only briefly [33]. It is capable of generating 10 KV pulses

as short as 150 nsec (FWHM, 60 nsec rise time) at rates up to 100 KHz. Although the tubes in the final stage of the supply are capable of providing peak pulse currents of 120 A, in practice it is found that the lamp draws peak currents of only 20-30 A. No direct comparison has been made with the previously used thyratron circuit, but the ANL supply is estimated to provide at least an order of magnitude more intensity. It is only slightly more bulky than the thyratron supply, and costs about twice as much.

The power supply used for most of the work reported in this thesis is a Cober model 605P high power pulse generator [61]. It is much less powerful than the ANL power supply, but also smaller (15 x 20 x 22 inches) and less expensive ($5500). It is capable of delivering 2200 volt pulses with a 1.5% duty factor at repetition rates up to 1 MHz. The maximum current output is 11 A, and the rise time is usually adjusted to match the fall time of 35 nsec. Dr. W. A. Chupka kindly provided an opportunity to compare the Cober directly with the ANL power supply. Both power supplies were used in turn to power a 10 cm helium lamp. Gas pressure, pulse width, and repetition rate were adjusted to find the maximum intensity that each supply was capable of providing; the results are indicated in Table II-2. The relatively low voltage available from the Cober prevents pressures higher than about 80 torr from being used, and limits the length of the discharge tube to about 15 cm (which can be used only at lower pressures). The relatively low current available from the Cober also limits the intensity obtained at a given length and pressure. The two effects combined to produce an ANL : Cober intensity ratio of 3.4 : 1 with a 10 cm helium lamp. The ANL supply has been used with 50

Table II-2. Comparison of the Cober and ANL Power Supplies.

Optimum Conditions (10 cm lamp)	Power Supply	
	Cober	ANL
Peak Voltage, KV	2.2	8-9
Peak Current, A	12	30
Pulse Width (FWHM), μsec	0.1	0.15
Repetition Rate, KHz	130	100
Lamp pressure, torr	70	130
Relative Intensity	1.00	3.4

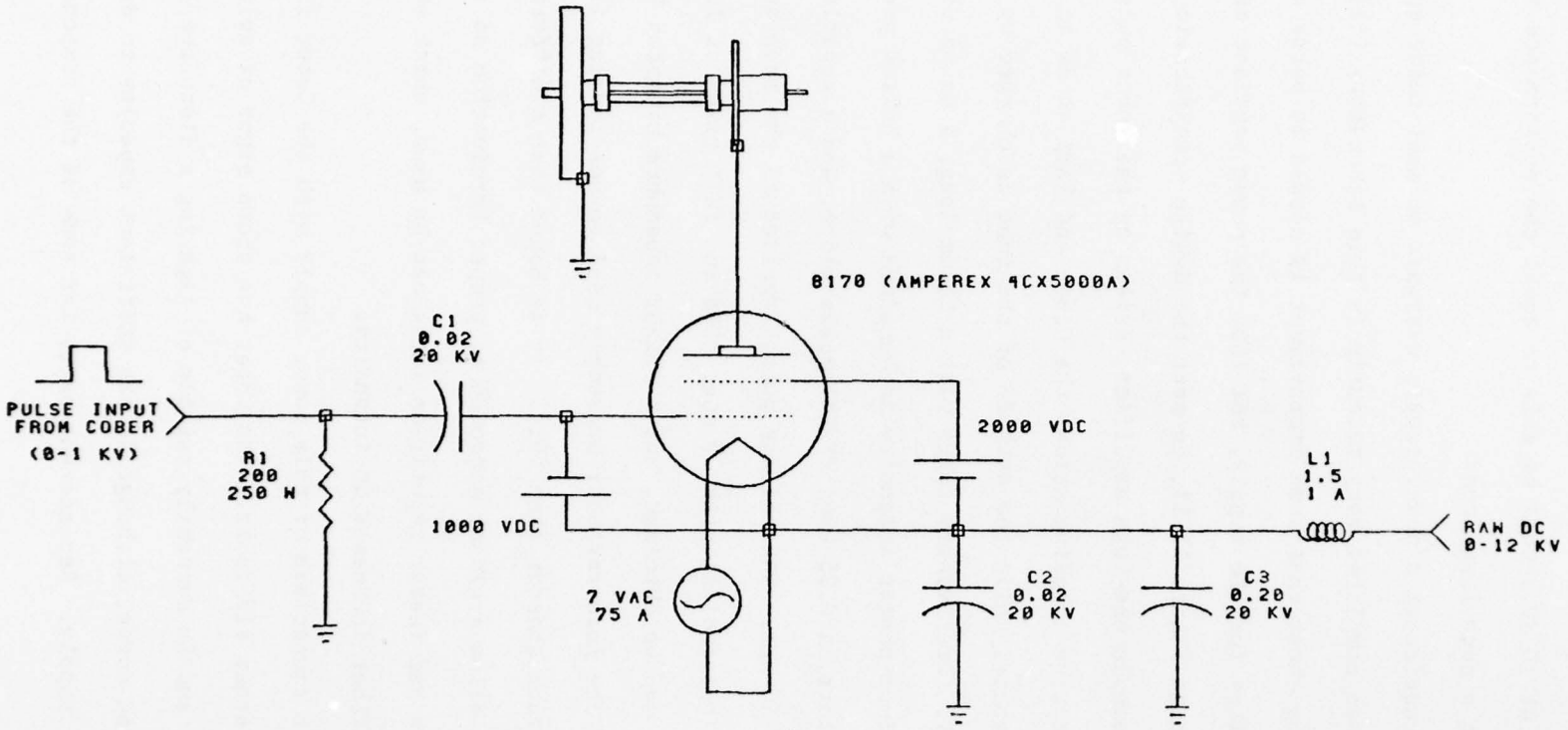
cm discharge tubes, and the photon intensity was found to increase linearly with the length of the discharge tube [33]. Therefore, the Cober is estimated to provide only about 1/17 of the intensity that can be obtained with the ANL power supply.

Fortunately, this is sufficient intensity for a large number of experiments. The Cober has been used intensively for three years, and has been found to be very dependable. It provides a very stable lamp output, and as long as a complete electrostatic shield is maintained around the lamp and the leads from the Cober to the lamp, no difficulty is experienced with radiated electrical noise. It's only drawback is that it provides significantly less than "state-of-the-art" intensity. On the other hand, the ANL supply is clearly (though intentionally) overdesigned. A power supply capable of generating 20-30

ampere pulses at 10 KV should be able to equal the performance of the ANL supply, but at a much lower cost.

Construction of a power supply designed to meet these specifications has been completed very recently in this laboratory [62]. Initial testing shows that some improvement is needed in parts of the control circuitry for the supply, but that the power portions of the circuit, shown in Figure II-11, do meet the design specifications. The circuit is a simple one-tube amplifier, driven by the Cober pulse generator. Capacitive coupling allows the Cober and lamp anode to remain at ground potential while the cathode of the tube is charged up to as much as -10 KV. Preliminary tests with a 25 cm long, 4 mm id discharge tube show maximum photon intensity is obtained with a helium pressure of about 140 torr, a 0.25 μsec (FWHM) pulse width, and a repetition rate of about 60 KHz. The voltage pulses applied to the lamp are approximately trapezoidal with 70 nsec rise and fall times at 10 KV. Sharper edges can be obtained, but a slight impedance mismatch between the Cober and the load resistor presently used causes ringing if the rise time is much shorter than this. It is hoped that a different load resistor will allow a closer approach to proper termination so that sharper pulses and faster repetition rates can be used, which should yield even further increases in intensity.

Direct comparison of this power supply with the Cober is unfortunately rather difficult. The Cober has shown signs of aging in recent weeks, and is currently capable of lighting a discharge lamp only at reduced power, although it has sufficient capacity to drive the new power supply. Replacement parts for some of the components



NOTE: RESISTANCE IN OHMS, CAPACITANCE IN MICROFARADS, INDUCTANCE IN MILLIHENRIES
R1 MUST BE NON-INDUCTIVE (E.G., DALE NH250-200).
C1, C2 MUST ALSO BE LOW INDUCTANCE (E.G., PLASTICS CAPACITORS HC200-203).

Figure II-11. Vacuum Tube Power Supply for the Rare Gas Lamps.

suspected of causing the problem will not arrive in time for a direct comparison between the two power supplies to be included in this thesis. An estimate based on intensity measurements made several months ago is that the new power supply provides about seven times the intensity that the Cober did at its best. Use of longer discharge tubes should make an additional factor of two or three possible. A more exact comparison and further tests of the new power supply will have to be reported elsewhere once completed.

C. Photon Optics

Any optical elements of the instrument which are intended for use below 1050 Å must be reflective components, since no known material transmits well enough to be used as lenses or prisms. Unfortunately, even osmium - which seems to hold the current reflectivity record - only reflects about 30% of the radiation that hits it (normal incidence, 600 Å [63]). More commonly used coatings such as platinum, gold and aluminum are even worse [7], and thus the number of reflections must be kept to an absolute minimum. This can be accomplished by mounting the lamp and ion source directly on the entrance and exit slits of the monochromator and using a concave diffraction grating, which both diffracts and focuses the radiation with one reflection. The monochromator will therefore consist of one concave grating and two slits. Many different monochromator designs using these three elements exist [7], but most require that one of the slits be moved as the wavelength is scanned in order to maintain proper focus. The bulk of the equipment that must be located at the entrance and exit slits of a PIMS monochromator

virtually requires fixed slit positions, however, and only two types of monochromators have found wide use in the field.

One of these is the Seya-Namioka monochromator [64-66], in which the entrance and exit slits subtend an angle of 70°30' at the grating. The wavelength is scanned by a simple rotation of the grating. The major advantages of the Seya-Namioka design are its simplicity and the fact that the entrance and exit slits are far apart, leaving plenty of room for coupling to the light source and the rest of the mass spectrometer. However, although reflectivity is better at this angle than at normal incidence, only relatively small gratings can be used, and optimum, stigmatic focusing is compromised for the simplicity of design. The image of the entrance slit at the exit slit is both enlarged vertically and curved, so that both resolution and intensity suffer.

These disadvantages are largely overcome by the near-normal incidence designs, in which the slits subtend a very small angle (ideally, but impractically, 0°), dramatically reducing astigmatism. The wavelength scanning mechanism in most near-normal incidence designs simultaneously rotates and translates the grating in such a way as to maintain correct focus. These differences, combined with the use of larger gratings, yield both increased resolution and intensity. (Resolution may be increased by a factor of five for instruments of comparable focal length and dispersion, and for comparable focal length and resolution, the intensity gain may be as much as a factor of ten [5].) Aside from the more complicated scanning mechanism, the main disadvantage of the near-normal incidence design is the close proximity of the entrance

and exit slits.

The McPherson 225 [67], a one-meter near-normal incidence monochromator, is probably the most widely used monochromator in photoionization mass spectrometry, and is also used in the MSU instrument. Our monochromator was modified by the manufacturer to allow the exit slit assembly to protrude four inches into the vacuum chamber of the mass spectrometer. The entrance and exit slits, subtending an angle of 15° at the grating, are separated by about 27 cm, which is sufficient, though not ample, room for both the lamp and the mass spectrometer chambers. Any one of four positions on a round slit table may be selected at the entrance slit position without breaking vacuum. Three positions hold fixed-width slits, and the fourth is a blank position used for sealing the entrance slit hole. The exit slit table is linear and one of four positions may be chosen with a rack-and-pinion gearing system which is in turn connected to a rotary vacuum feedthru on the mass spectrometer chamber via a chain-and-sprocket mechanism, so that any one of four exit slits may also be chosen without breaking vacuum. A small flap valve just behind the exit slit table serves both as an optical shutter and as a valve to seal the exit slit side of the monochromator. The monochromator can thus be kept evacuated even when the lamp is removed and the mass spectrometer chambers are at atmospheric pressure. The monochromator also features an extra-long wavelength drive screw shaft, which protrudes through a rotary seal in the side of the monochrmator so that a stepping motor can be directly coupled to it.

Although other materials have better reflectivities below

1000 Å, aluminum is the best of the commonly available coatings above that limit [7]. The only grating used in this instrument to date is an aluminum coated grating with magnesium fluoride overcoating to prevent oxidation. It is ruled with 1200 lines/mm, blazed at 1200 Å. When equipped with this grating, the monochromator has a reciprocal linear dispersion of 8.3 Å/mm, and a range of 0-3000 Å. The best resolution obtainable with the smallest slits currently mounted (10 microns) in first order is approximately 0.12 Å FWHM, as illustrated in Figure II-12 for the atomic nitrogen emission triplet at 1134 Å.

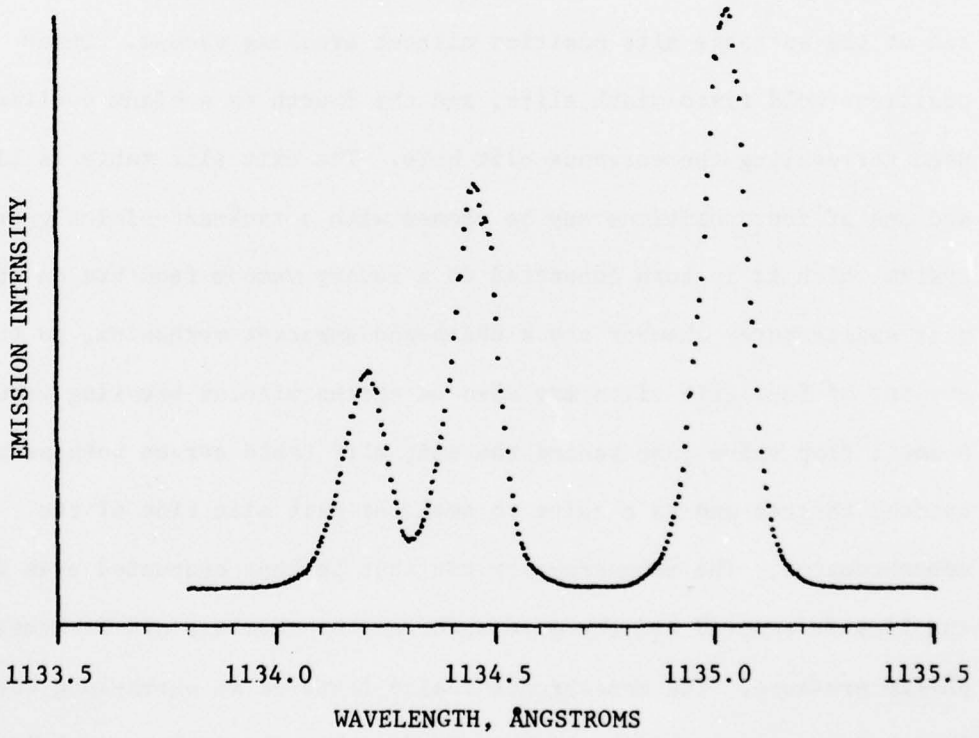


FIGURE II-12. Atomic Nitrogen Emission Lines at 1134 Å. These are three of the nitrogen impurity lines in the emission from the helium lamp.

D. Photon Transducers

There are four basic types of photon transducers which have been found suitable for use in the regions of the vacuum ultraviolet that are accessible to PIMS. Some of their important characteristics are summarized in Table II-3.

Solar blind photomultiplier tubes (PMTs) can be used down to $\simeq$1050 Å, if equipped with lithium fluoride windows. Such multipliers have high work function photocathode materials which are insensitive to visible wavelengths. They also exhibit much lower dark current than typical UV/visible photomultipliers, since thermal emission from the photocathode is very low. The low dark noise, combined with the high gain of the electron multiplier structure in the tube, means that such a transducer can be used to measure very low photon intensities, especially if photon counting techniques are used. The detection limit in Table II-3 was calculated assuming a quantum efficiency of 0.10, a gain of 10^6, and DC current measurement techniques, with the dark current setting the detection limit. The sensitivity is entirely adequate for even the weakest photon intensities expected. The lithium fluoride window is subject to gradual deterioration when exposed to high energy photons, however, and the photomultiplier tube will show a gradual loss of sensitivity with time. The only other major disadvantage of this type of transducer is that it cannot be used at wavelengths below the lithium fluoride cutoff.

If, however, the window is removed entirely, the electron multiplier structure itself can be used as a VUV detector below about 1400 Å,

TABLE II-3. Comparison of Common Vacuum Ultraviolet Photon Transducers

Characteristic	Transducer			
	Solar Blind[a] PMT	Electron Multiplier	Photodiode	Sodium[b] Salycilate
Dark Current (A)	3×10^{-12}	$\approx 10^{-12}$	0	3×10^{-10}
Detection Limit (Photons/sec)	200	60	6×10^{7}	10^{4}
Wavelength Range (Å)	>1050	200-1400	200-1400	>200
Sensitivity vs. Wavelength	varies	varies	varies	constant
Rate of Aging	slow	medium[c]	slowest	fastest [c]

[a] EMR 510G-08-13 with CsI photocathode and LiF window [68]
[b] RCA 8850, K-Cs-Sb photocathode, cooled to ≈-20°C
[c] Depends on cleanliness of vacuum and corrosiveness of sample

since photons in this region have more than enough energy to cause ejection of electrons from the metal surface of the first dynode. The ejected electrons are amplified by the remaining dynodes exactly as electrons from a photocathode would be. A wide variety of electron multiplier structures are commercially available for use in such fashion. Most common dynode materials have an even higher work function than the photocathode of the solar blind PMT, and thus a "bare" electron multiplier (or EMT) has an even lower dark current. The dynodes, which are all exposed to whatever ambient atmosphere exists in the vacuum chamber, will eventually acquire a thin coating of pump oil, and may be poisoned even sooner by reaction with certain sample vapors. This causes a loss in gain of the entire EMT, so that the sensitivity of the electron multiplier transducer will decrease at a rate which depends on the cleanliness of the vacuum and the reactivity of the dynode material to the sample being studied.

The simplest of the four transducers is the photodiode, consisting of a plate of clean, polished metal and an electrode which collects the photoelectrons emitted from the plate. It is essentially an electron multiplier with no stages of gain; because it has fewer surfaces to become poisoned or oil-coated, its sensitivity is much more stable than that of the electron multiplier. In addition, the photodiode can be made of a metal which is more resistant to chemical attack than commonly used electron multiplier dynode materials. Its major disadvantage is its lack of sensitivity. The detection limit shown for this transducer in Table II-3 is calculated assuming a photoelectron yield of 0.10 and a minimum detectable current of 10^{-12} amperes,

although use of a vibrating reed electrometer could reduce this limit by two orders of magnitude. Considering that a very intense photon source may be expected to provide 10^{10} photons sec^{-1} $Å^{-1}$ at the peak of the helium continuum, the sensitivity of this transducer is seen to be marginal for studies with narrow slits in the weaker portions of the continuum.

All three of the transducers discussed so far share one disadvantage: their photoelectron yield or quantum yield varies with the wavelength of the incident radiation, often quite dramatically. For instance, the photoelectric yield of copper-beryllium, one of the most commonly used dynode materials, peaks at about 700 Å and has lost 75% of its sensitivity by about 1000 Å [70]. The fourth type of transducer is commonly used to avoid, or at least correct for, this problem. It consists basically of a thin layer of sodium salycilate deposited on the outer surface of a typical UV/visible PMT. VUV photons striking the sodium salycilate layer cause it to fluoresce (the peak of the emission spectrum is about 4200 Å) and the fluorescent emission is measured with the photomultiplier. The advantage of this transducer is that the fluorescent yield of sodium salycilate is at least approximately independent of excitation wavelength over a wide range [7]. Freshly prepared coatings have a constant efficiency from 200 Å to 1200 Å, and exhibit a small rise above this wavelength. Unfortunately, sodium salicylate which is contaminated with pump oil or poisoned by reactions with any of a number of chemicals no longer has a constant response, but exhibits a drop in sensitivity between 1200 and 900 Å. The ease with which a thin sodium salycilate layer can become

contaminated is one of the major disadvantages of this transducer, but a fresh layer of sodium salycilate can at least be used to calibrate the wavelength response of the other types of detectors discussed above. In addition to the ease with which it can be contaminated, the sodium salycilate transducer has two other disadvantages. The photomultiplier used typically has a much higher dark current than any of the other transducers mentioned, so that its overall sensitivity is not as high, although it is usually adequate. Also, the photomultiplier is sensitive to visible light, and care must be taken to prevent light leaks into the chamber.

The first photon transducer used with the MSU instrument was a simple photodiode. At the time it was used, however, the lamp intensity was so low that the photodiode could not be used to measure it. The photodiode was replaced with an electron multiplier and has never been tried again, although photon intensities are now at least three orders of magnitude greater than during the first attempts at lighting the lamp. We have generally used electron multiplier transducers since then. Currently in use is an EMR 510W-00-16 multiplier with 16 Cu-Be dynodes [68].

We have also used a sodium salycilate detector system occasionally, in wavelength regions where the response of the electron multiplier is very small, or in order to calibrate the electron multiplier. An RCA 8850 photomultiplier [69] in a thermoelectrically cooled housing [71] is optically coupled with a highly polished plexiglass rod to a quartz disc [72] upon which the sodium salycilate layer is deposited.

Figure II-13 shows the Hopfield continuum recorded with the

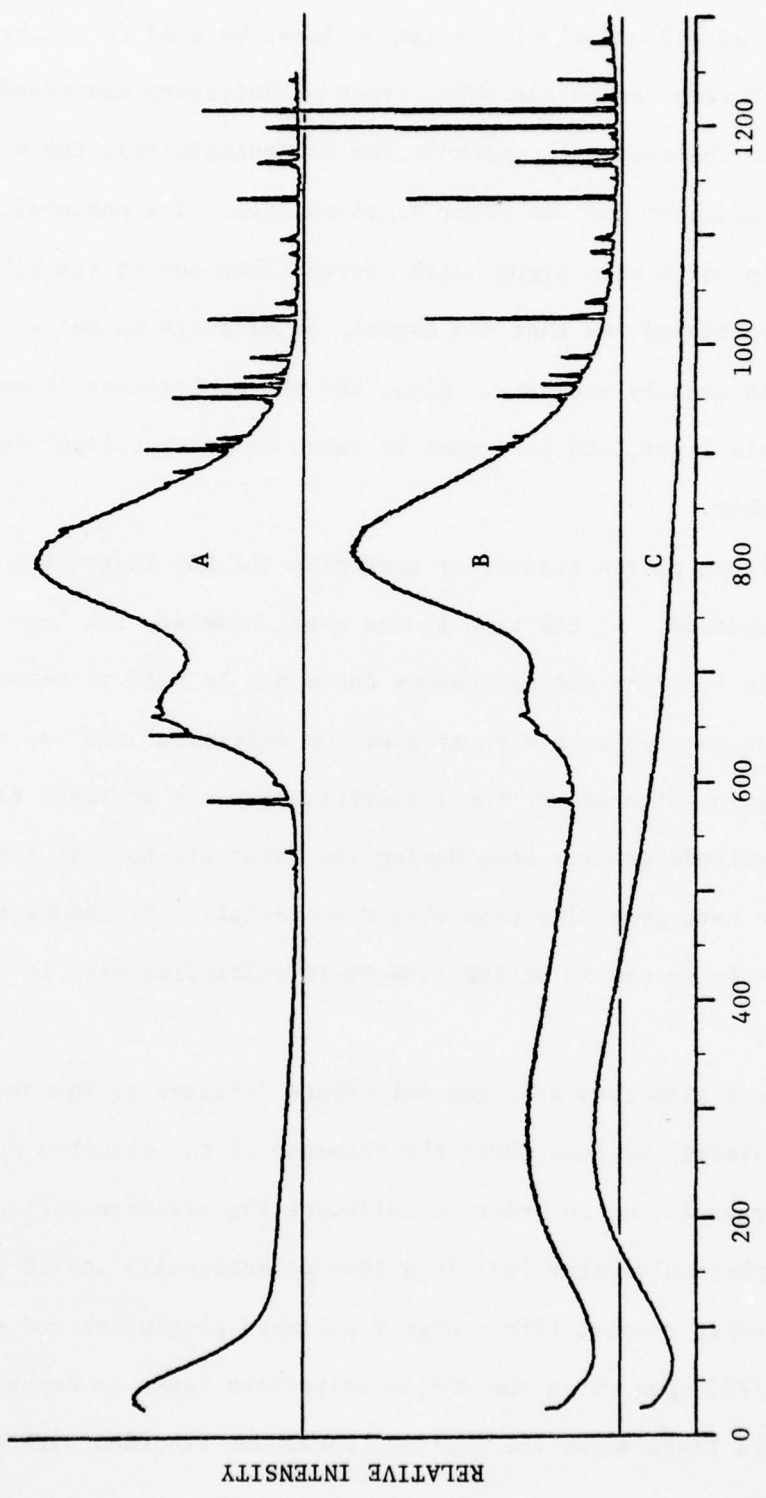


Figure II-13. The Helium Continuum and Scattered Light Recorded with Different Photon Transducers. Curve A - copper-beryllium electron multiplier; curve B - sodium salycilate over an RCA 8850 photomultiplier; curve C - blank quartz filter over an RCA 8850.

electron multiplier (a) and sodium salycilate (b) transducers. The dropoff in sensitivity of the electron multiplier at wavelengths above 900 Å is demonstrated by the decreased intensity of both the continuum and the atomic lines in (a) relative to (b). Also of interest is the scattered light distribution, all of the light below 500 Å being attributed to scattered light since the source does not emit radiation shorter than about 550 Å. The helium lamp produces a great deal of near UV and visible radiation as well as the Hopfield continuum. The electron multiplier is very insensitive to radiation above 1500 Å, while the RCA 8850 is sensitive to wavelengths longer than about 2000 Å. It is this sensitivity to long-wavelength scattered light that causes the difference seen below 500 Å in Figure II-13. The fact that most of the radiation detected between 0 and 500 Å with the RCA multiplier is not vacuum ultraviolet radiation is supported by Figure II-13c, which shows the results obtained when a blank (instead of sodium salycilate coated) quartz disc is used as a 2000 Å high-pass filter in front of the RCA multiplier.

The sodium salycilate transducer detects so much scattered light when used with the Hopfield continuum that the effects of the scattered light are difficult to correct for (see Appendix A). This transducer is therefore used in this region only to calibrate the electron multiplier. The scattered light problem is much less bothersome when the hydrogen lamp is used, since it emits less visible and UV radiation, and since the many-lined spectrum doesn't begin until wavelengths greater than 800 Å, i.e., in a region where the scattered light distribution has fallen off considerably.

E. Ion Source

The most commonly used type of ion source in photoionization mass spectrometry [5] is simply a small box with holes for photon entrance and exit, and another hole for ion extraction. It incorporates a repeller plate to establish a field that pushes the ions towards the exit hole (see Figure II-14). The holes must be small enough that an adequate

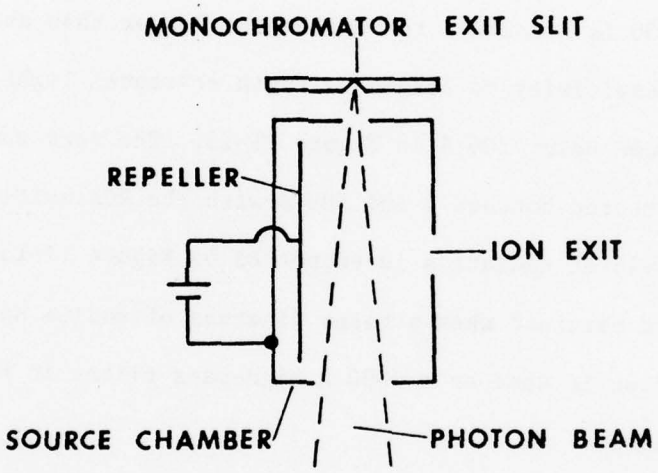


Figure II-14. A Simple Ion Source.

sample pressure can be maintained inside the source without placing an inordinate burden on the vacuum pumps which must keep the region outside the source at a lower pressure. If the photon exit hole is smaller than the cross section of the photon beam when it reaches the far wall, some provision must be made to collect the photoelectrons

emitted from the wall so that they are not accelerated into other regions of the instrument where they could potentially cause electron impact ionization.

The interpretation of appearance potentials is simplified if the sample gas can be cooled below room temperature to eliminate (or at least reduce) the effects caused by the internal energy spread of the molecules [10,12,73,74]. Several ion sources designed to accomplish this have been described in the literature [33,43,73]. All basically work by cooling the walls of the ion source and allowing the sample vapor to come into thermal equilibrium by making several contacts with the walls before actually entering the ionization region. Although much valuable work has been done this way, the approach is limited by the fact that many molecules condense before reaching very low temperatures, and the amount of cooling that can be accomplished for them is fairly small.

Sample cooling can also be accomplished using a radically different approach [38,75]. The ion source box is eliminated and instead photoions are created in a high intensity "supersonic" molecular beam [76]. In such a beam, most of the rotational energy of the molecules has been converted into translational energy during expansion from the nozzle, and rotational temperatures as low as a few degrees Kelvin can be obtained, even with easily condensed molecules. The main disadvantage of this approach is that the supersonic beam source introduces much greater complexity and requires much greater pumping capacity. The increased resolution obtained by the elimination of thermal broadening can be well worth the effort, however. A striking example of this

is the photoionization efficiency curve for NO^+ (from NO) near threshold - compare Figure 1 of Reference [77], obtained at 150 °K, to Figure 3 of Reference [75], obtained with a nozzle beam source.

A supersonic nozzle beam source has been designed for the MSU instrument, but is still under construction. The ion source currently in use is described in more detail elsewhere [78], but is basically a simple, ambient temperature box-type source. Intended for use with low sample pressures, it has fairly large exit holes (the ion exit hole is 0.25 inches dia., the photon exit hole is 0.140" x 0.350"). The sample is admitted via and all-metal vacuum manifold, which incorporates a variable leak to control the flow rate and therefore the sample pressure. A separate port on the ion source is connected to a capacitance manometer [79] which is used to measure the sample pressure.

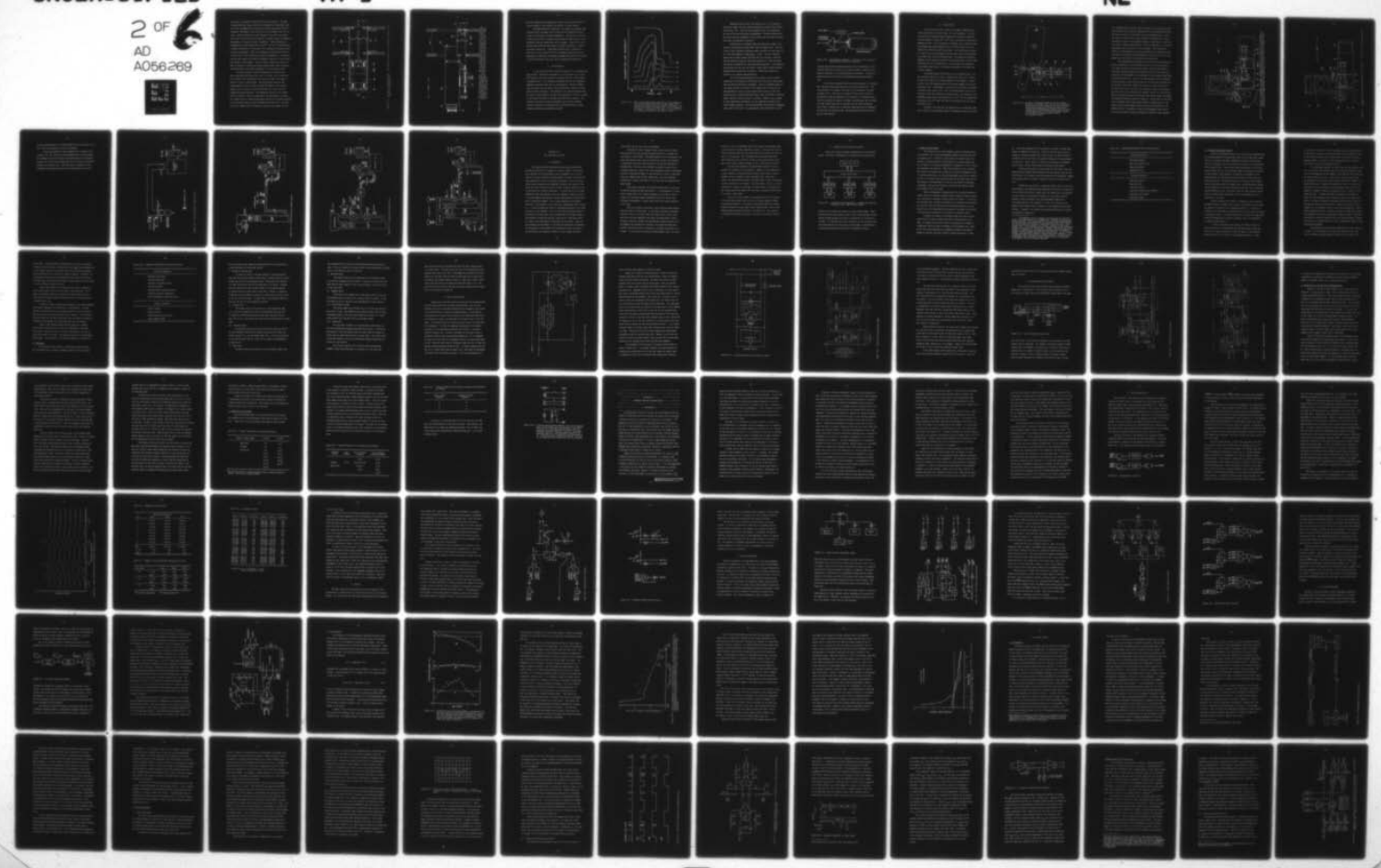
F. Ion Optics

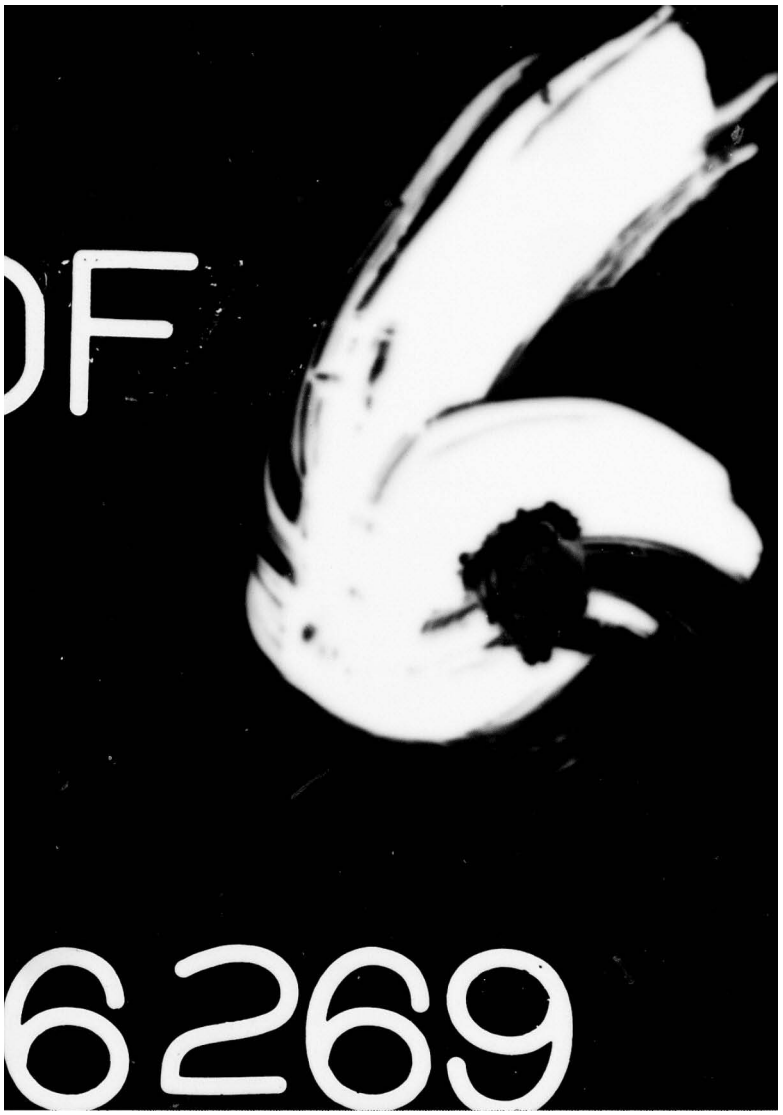
Most photoionization mass spectrometers have used time-of-flight, magnetic sector or quadrupole mass analyzers [5]. The pulsed operation of the time-of-flight mass spectrometer is advantageous in coincidence studies, but is otherwise a liability, both because the rare gas lamps do not emit pulses of light that are short enough and because discontinuous production of ions is an inefficient use of experimental time.

Magnetic sector [80] and quadrupole [81] instruments both allow continuous production and detection of ions, and can attain very high ion collection and transmission efficiencies. The magnetic sector instruments require that the ions be accelerated by a potential of several kilovolts before entering the sector region, and usually the

AD-A056 269 MICHIGAN STATE UNIV EAST LANSING DEPT OF CHEMISTRY F/G 14/2
THE DESIGN AND OPERATION OF AN AUTOMATED, HIGH-EFFICIENCY PHOTO--ETC(U)
FEB 78 E J DARLAND, G E LEROI N00014-76-C-0434
UNCLASSIFIED TR-1 NL

2 OF 6
AD
A056269




OF
6269

ion source is operated at several kilovolts above ground. The high voltages and extra lenses required to accomplish the acceleration make the sector instruments more complicated and less convenient than the quadrupole instruments, which work best at ions energies less than 100 volts. Another difference is that, because of the lower ion energy, the transit time from source to detector is usually longer in quadrupole instruments, by perhaps an order of magnitude. "Slow" unimolecular decompositions (rate constant less than 10^5 - 10^6 sec^{-1}) therefore have a greater probability of occurring in the quadrupole instruments before the ions are analyzed. This is an advantage in reducing the amount of "kinetic shift" [11] in appearance potential measurements. Quadrupoles are also more compact than sector instruments, needing no long acceleration region or bulky magnet. They also have a linear mass scale, and make it possible to choose the optimum balance between mass resolution and sensitivity by the simple adjustment of a front panel control.

The mass analyzer in the MSU instrument is an Extranuclear 324-9 quadrupole mass filter [82], with 1.9 cm dia. x 22 cm long rods. It is powered by an Extranuclear 311-type power supply with either a model E or model 13 high-Q head. The electrostatic aperture lens system supplied with the filter, modified by removal of the electron impact source, is used to focus ions from the ion source into the quadrupole entrance aperture. The quadrupole (as well as the lenses and ion transducer, which are connected to the quadrupole) is mounted on a support which is easily moved several inches in a direction parallel to the quadrupole axis, as shown in Figures II-15 and II-16. The push bar can be clamped (with set screws not shown in the figures) so as to

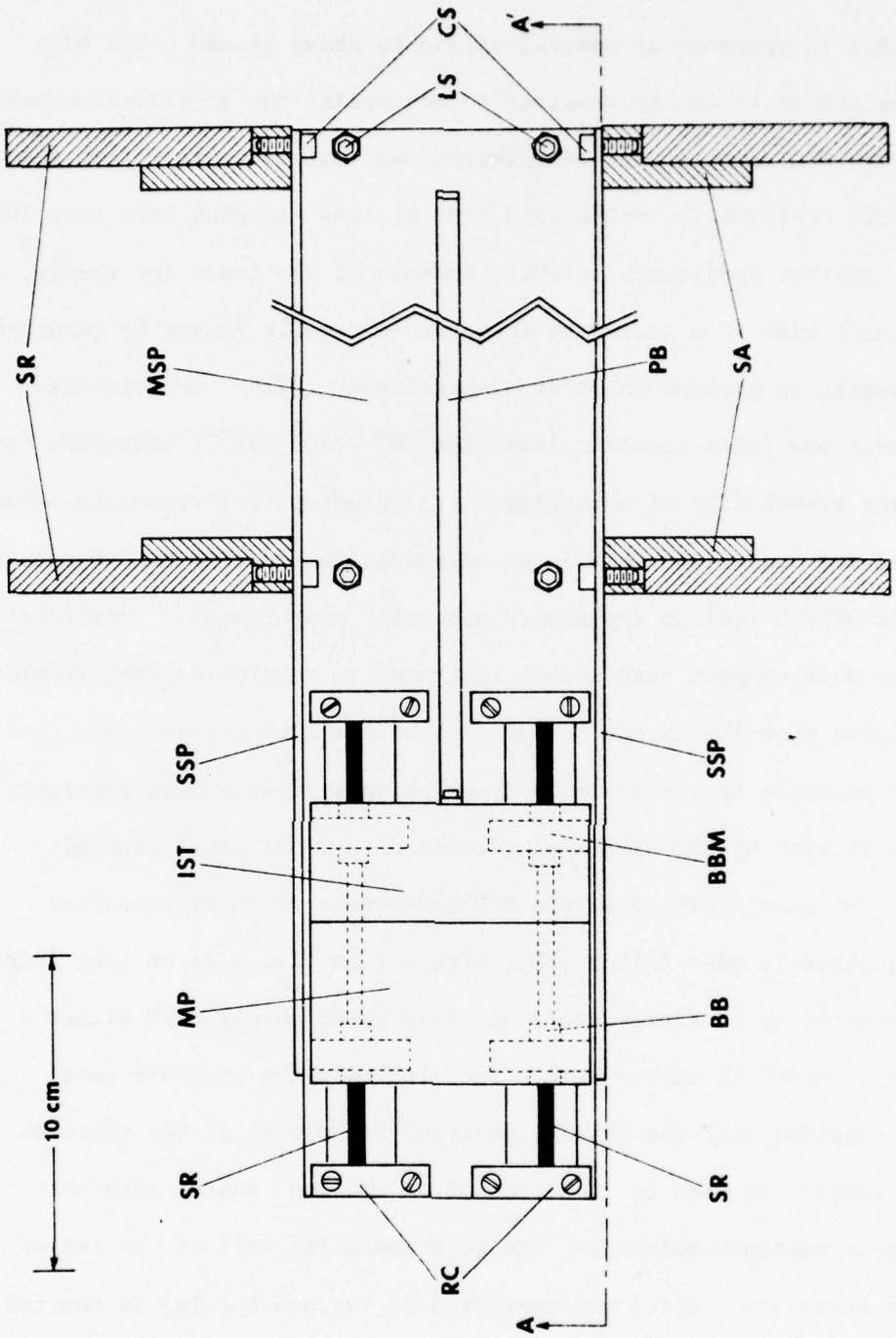


Figure II-15. Top View of Quadrupole Mount. The labels are defined in the caption to Figure II-16, which is a view along A-A'.

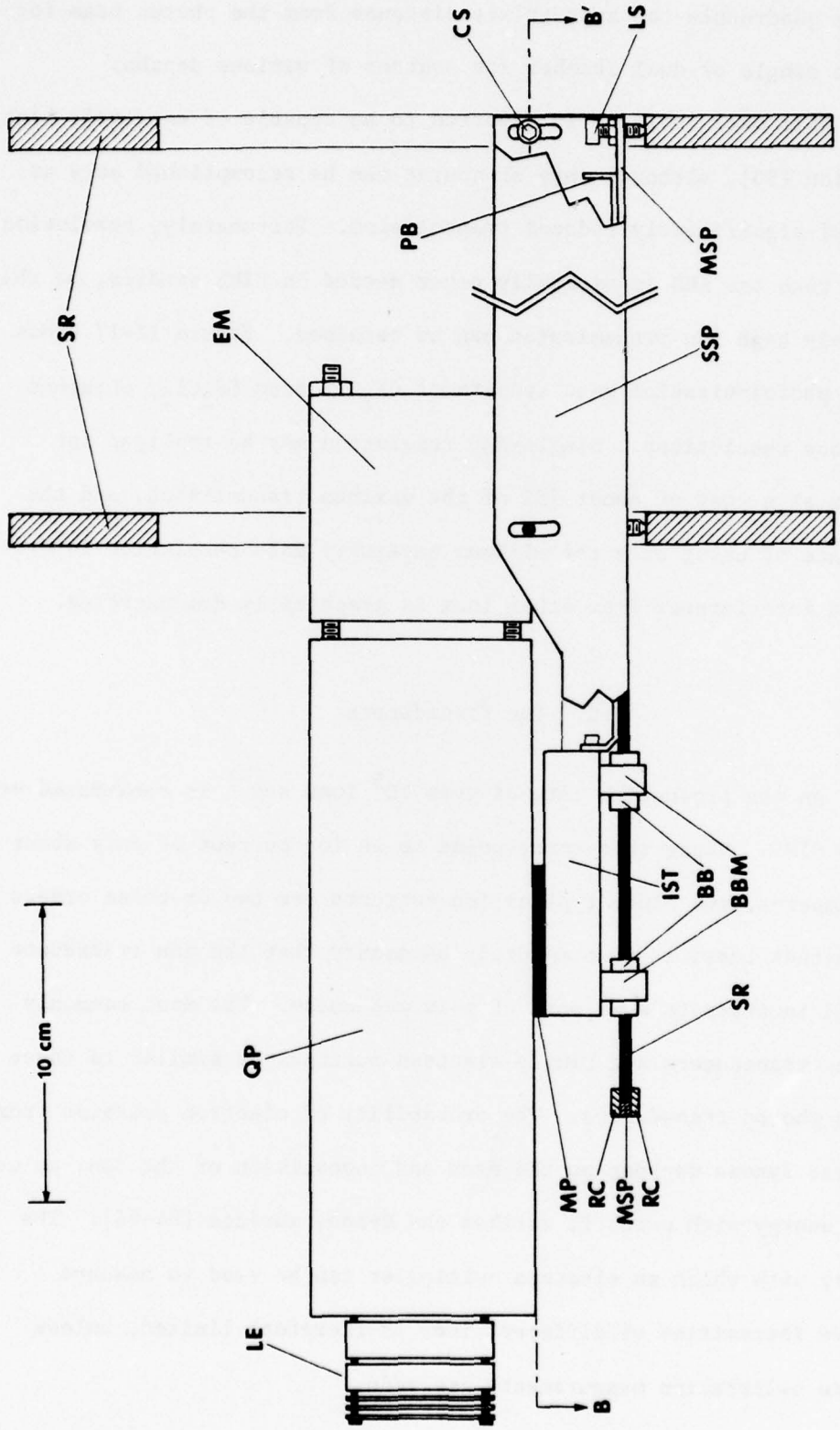


Figure II-16. Side View of Quadrupole Mount. BB-ball bushing; BBM-ball bushing mount; CS-clamping screw; EM-electron multiplier; IST-insulated support table; LE-lens; LS-locking screw; MP-mounting plate; MSP-main support plate; PB-push bar; QP-quadrupole; RC-rod clamp; SA-support adapter; SR-support ring; SR'-support rod; SSP-side support plate. Figure II-15 is a view along B-B'.

hold the quadrupole the appropriate distance from the photon beam for use with single or dual chamber ion sources of various depths.

This mass analyzer is reported to be capable of extremely high resolution [83], although this of course can be accomplished only at a cost of significantly reduced transmission. Fortunately, resolution of more than one AMU is virtually never needed in PIMS studies, so that relatively high ion transmission can be retained. Figure II-17 shows partial photoionization mass spectra of CF_2Cl^+ from CF_2Cl_2, obtained at various resolutions. Single-AMU resolution may be realized for this ion at a cost of about 75% of the maximum transmission, and the importance of using only the minimum necessary mass resolution in order to avoid interference from other ions is graphically demonstrated.

G. Ion Transducers

An ion production rate of even 10^5 ions sec^{-1} is considered very high in PIMS. Since this corresponds to an ion current of only about 10^{-14} amperes, and since typical ion currents are two or three orders of magnitude less, it is absolutely necessary that the ion transducer employed incorporate some sort of gain mechanism. The most commonly used ion transducers are simply electron multipliers similar to those used as photon transducers. The probability of electron emission from the first dynode depends on the mass and composition of the ion, as well as the energy with which it strikes the dynode surface [84-86]. The accuracy with which an electron multiplier can be used to measure relative intensities of different ions is therefore limited, unless separate calibration measurements are made.

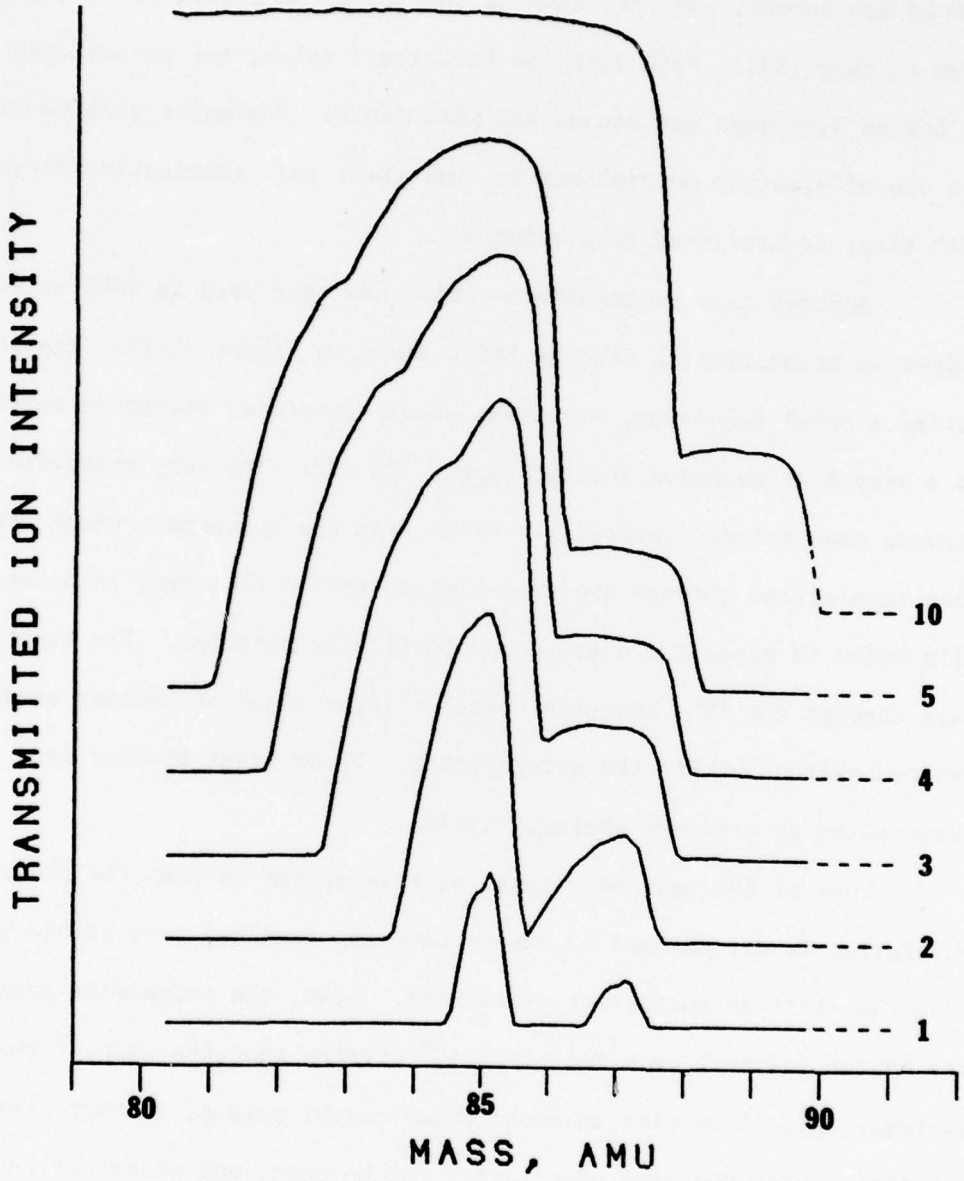


Figure II-17. Effect of Increasing Mass Resolution on Ion Transmission. These partial mass spectra show the mass region which includes the various isotopes of CF_2Cl^+ from CF_2Cl_2. The spectra are plotted to the same scale, but are displaced for clarity. The number at the right of each curve gives the approximate mass filter resolution, in AMU.

Background count rates on the order of 0.1 to 1.0 counts per second are common, and very careful shielding can reduce these figures even further [87]. With such low background rates, ion intensities as low as 0.01 ions per second are measurable. The major problem with the use of electron multipliers is that their gain inevitably decreases with time, as mentioned in Section D.

Another type of transducer which has been used in PIMS is the Daly-type scintillation counter [88], shown in Figure II-18. The ions strike a metal (aluminum, stainless steel) converter electrode which is at a very high negative voltage (e.g., -25 KV). The very energetic impacts each release several electrons from the converter, which are then accelerated through the same high potential to a very thin metal film which is deposited over some scintillator material. The electrons pass through the film and each causes a light flash of perhaps several hundred photons within the scintillator. These light flashes are detected by an ordinary photomultiplier.

One of the main advantages of this system is that the photomultiplier is not exposed to the vacuum, and thus has more stable gain than the electron multiplier transducer. Also, the tremendous gain of the system (as much as a factor of 10^3 greater than the gain of the photomultiplier) results in much larger output pulses, so that less sensitive pulse counting electronics can be used, and pickup of environmental electrical noise is less of a problem. However, such a system is more complicated and difficult to use, especially because of the high voltages necessary. One such system [89] has attained a background count rate of 0.02 sec^{-1}, but reducing the count rate below 0.4 sec^{-1}

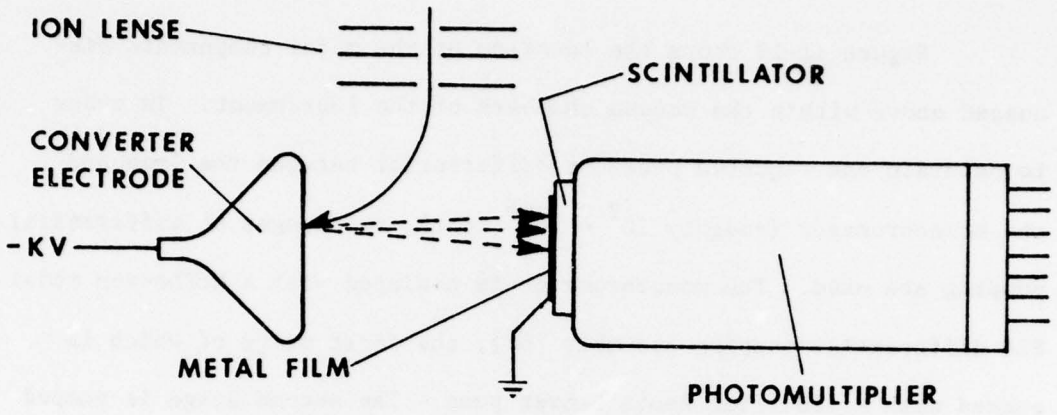


Figure II-18. Daly-Type Ion Transducer. Solid arrow: ion trajectory; dashed arrows: electron trajectories.

required repeated high temperature bakeout and ion bombardment of the converter electrode, as well as very careful optical, electrical and magnetic shielding of the photomultiplier and converter. This type of system has been used on only one photoionization mass spectrometer [90].

The electron multiplier used in the MSU instrument is a Johnston MM1, 20-stage focused mesh multiplier with Cu-Be dynodes [91]. This "ion multiplier" is mounted on the axis of the quadrupole, as shown in Figure II-15. Since the ion counting circuits used in the data acquisition system (see Chapter IV) are sensitive to frequencies well above the quadrupole frequency (2-3 MHz), the multiplier and its signal and high voltage leads must be shielded from the nearby quadrupole power leads. Evidently any rf radiation emanating from the quadrupole ion exit hole is relatively weak, and shielding mesh across this hole has not been required.

H. Vacuum System

Figure II-19 shows the location of the major components discussed above within the vacuum chambers of the instrument. In order to maintain the required pressure differential between the lamp and the monochromator (roughly 10^{2} - 10^{-5} torr), two stages of differential pumping are used. The monochromator is equipped with a McPherson model 820 differential pumping assembly [67], the first stage of which is pumped with a 300 l/sec Roots blower pump. The second stage is pumped by a 300 l/sec, four-inch diffusion ejector pump, and the monochromator by an 1800 l/sec, six-inch diffusion pump. The sample and quadrupole chambers are also pumped by six-inch oil diffusion pumps, rated at 2400 l/sec and 1500 l/sec, respectively. A baffle around the quadrupole also provides some measure of differential pumping of the sample gas in these chambers.

The pumping speeds quoted above are for untrapped pumps. All four diffusion pumps are, however, equipped with freon-cooled baffles to reduce the amount of oil backstreaming into the chambers. Because of this, the actual pumping speed at the various chambers will be significantly lower. Nevertheless, these pumps are sufficient to maintain a pressure on the order of 10^{-5} torr in the monochromator with 80 torr of helium in the lamp (100 micron entrance slits). The pressure in the quadrupole region can be maintained below 2×10^{-5} torr for sample pressures below $1\text{-}2 \times 10^{-3}$ torr, even with the relatively open ion source currently in use.

Because of the noise and heat generated by the mechanical pumps used to back the four diffusion pumps, the mechanical pumps are located

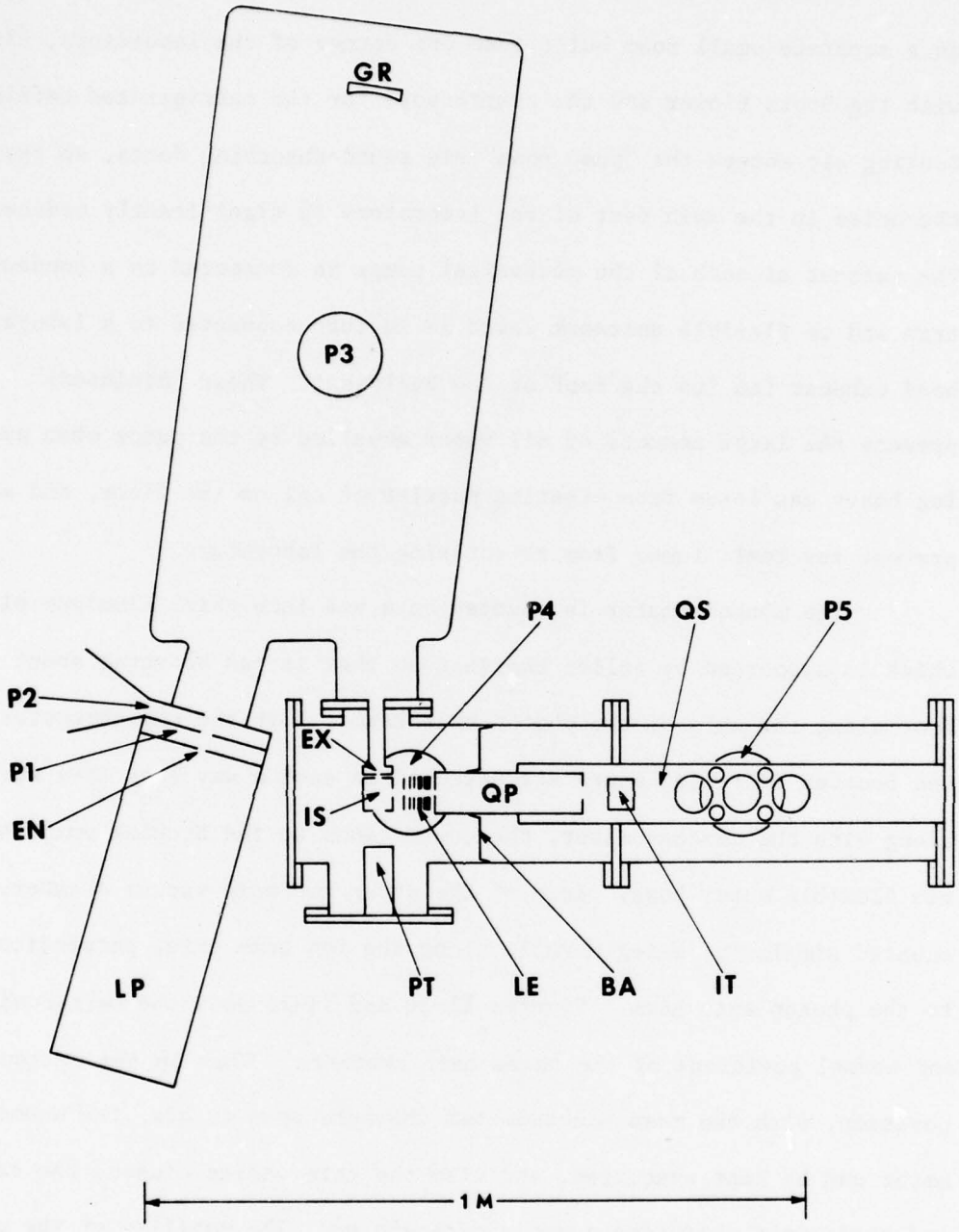


Figure II-19. Location of Components Within the Vacuum Chambers. BA-baffle; EN-entrance slit; EX-exit slit; GR-grating; IS-ion source; IT-ion transducer; LP-lamp; P1-first differential pumping port; P2-second differential pumping port; P3-monochromator pumping port; P4-sample chamber pumping port; P5-quadrupole chamber pumping port; PT-photon transducer; QP-quadrupole; QS-quadrupole support.

in a separate small room built into one corner of the laboratory, along with the Roots blower and the compressors for the refrigerated baffles. Cooling air enters the "pump room" via sound-absorbing ducts, so that the noise in the main part of the laboratory is significantly reduced. The exhaust of each of the mechanical pumps is connected to a condensate trap and to flexible ductwork which is in turn connected to a laboratory hood exhaust fan (on the roof of the building). These "minihoods" prevent the large amounts of oil vapor expelled by the pumps when pumping heavy gas loads from creating puddles of oil on the floor, and also prevent any toxic fumes from re-entering the laboratory.

The monochromator is mounted on a one inch thick aluminum plate which is supported by roller bearings so that it can be moved about a foot along the axis of the photon exit beam. Both the monochromator and booster diffusion pumps are attached in such a way that they move along with the monochromator, the connections to the backing pumps being via flexible metal hose. Each of the other two main vacuum chambers is mounted similarly, being movable along the ion beam axis, perpendicular to the photon exit beam. Figures II-20 and II-21 show the retracted and normal positions of the three main chambers. When in the retracted position, with the mass spectrometer chambers open to air, the monochromator can be kept evacuated, and with the gate valves closed, the sample and quadrupole diffusion pumps can remain on. The mobility of the chambers is extremely useful when making repairs or modifications to components in the vacuum chambers, which are fairly inaccessible in the normal position. The ability to keep the monochromator under vacuum and the other pumps hot greatly decreases the amount of time necessary

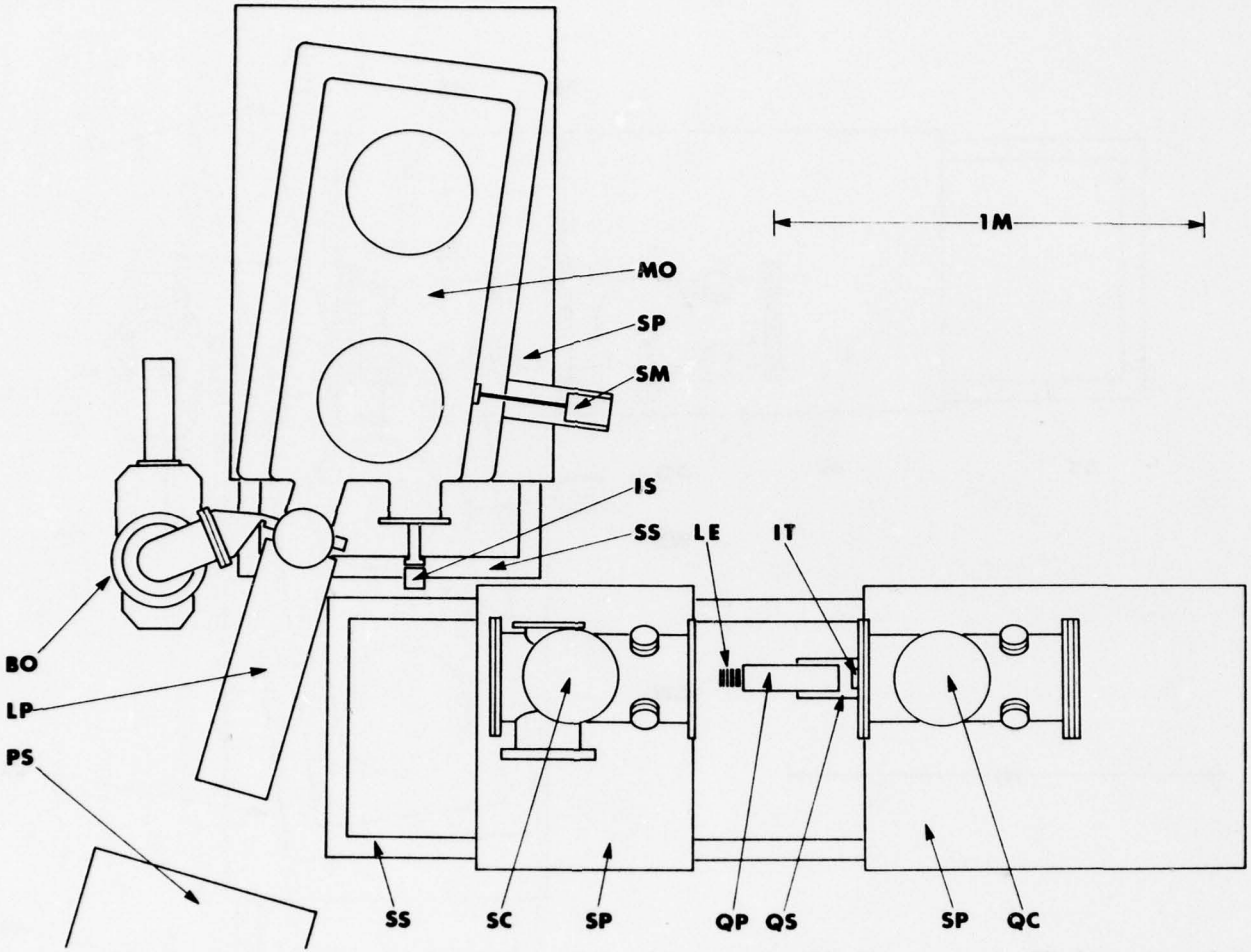


Figure II-20. Top View of Instrument, Retracted. BO-booster pump; IS-ion source; IT-ion transducer; LE-lens; LP-lamp; MO-monochromator; PS-lamp power supply; QC-quadrupole chamber; QS-quadrupole support; SC-sample chamber; SM-stepping motor; SP-support plate; SS-support stand.

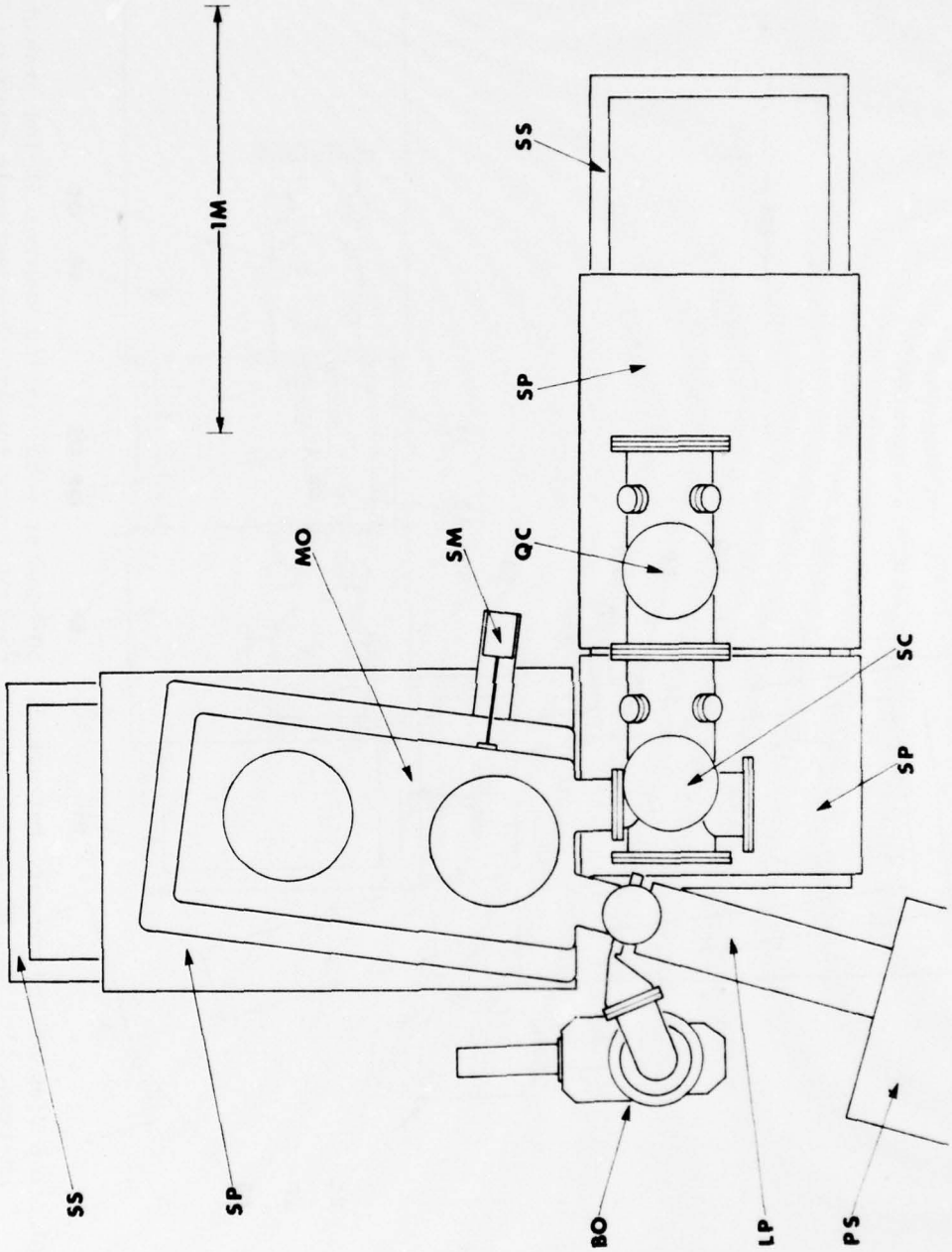


Figure II-21. Top View of Instrument, Normal Position. All labels are defined in the caption for Figure II-20.

to pump the system down to a working pressure after it has been "up to air", and also increases the life of the grating.

The vacuum plumbing is shown schematically in Figures II-22 through II-25. All valves are electropneumatically actuated (except the roughing and foreline valves of the monochromator and quadrupole systems) and can be closed automatically by the interlock system when necessary (see Chapter III). Note that water, compressed air and refrigerant lines have been omitted from these figures for clarity.

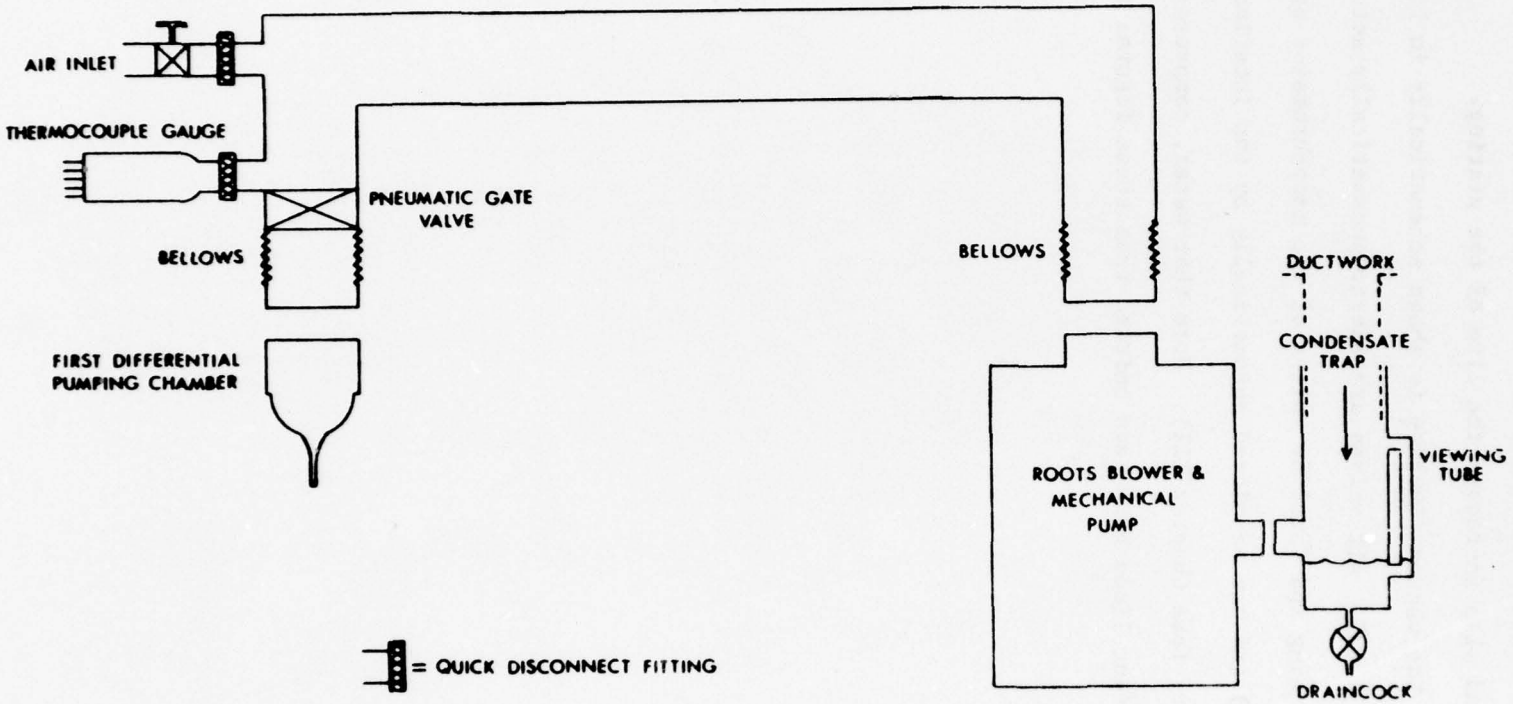


Figure II-22. First Differential Pumping System.

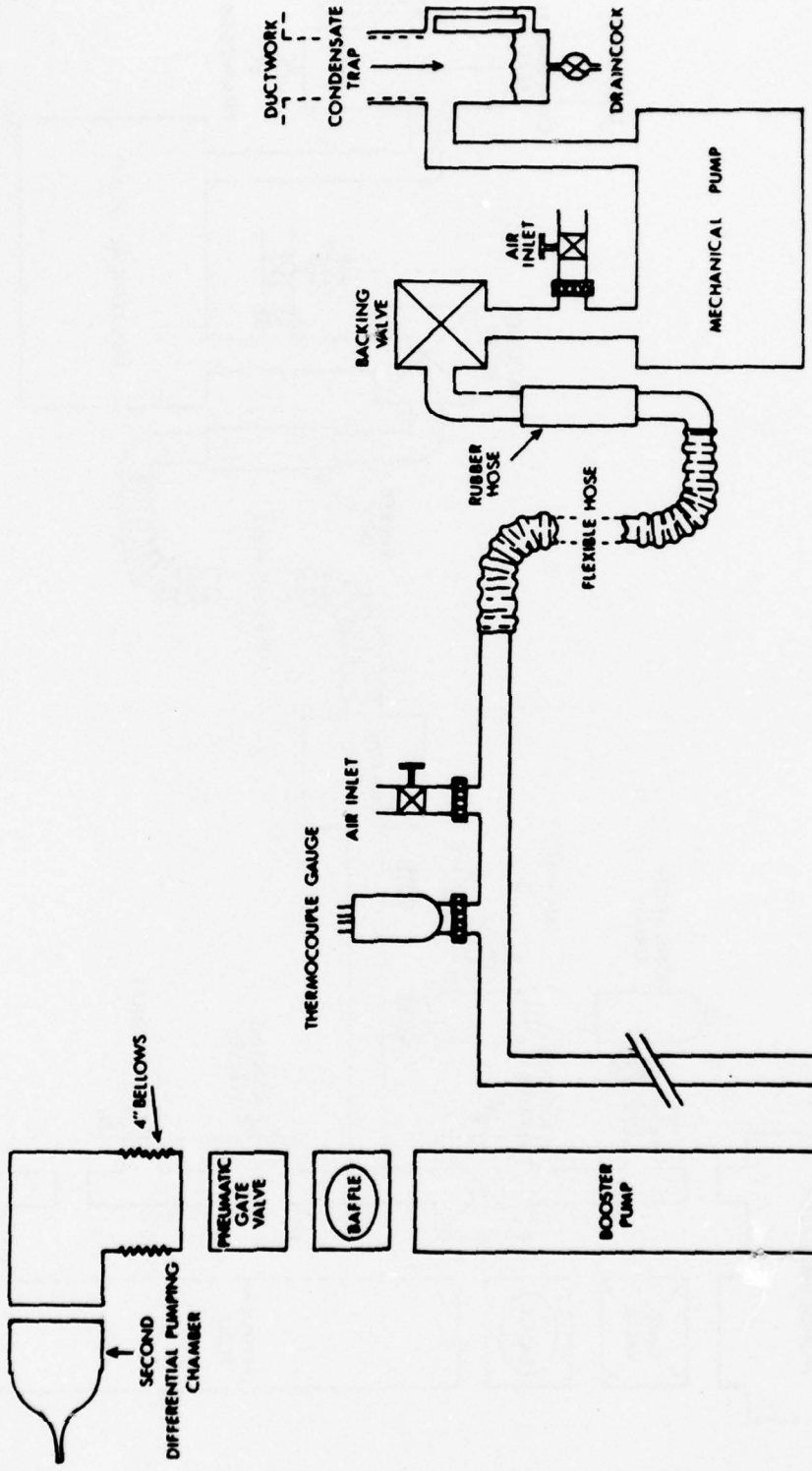


Figure II-23. Second Differential Pumping System.

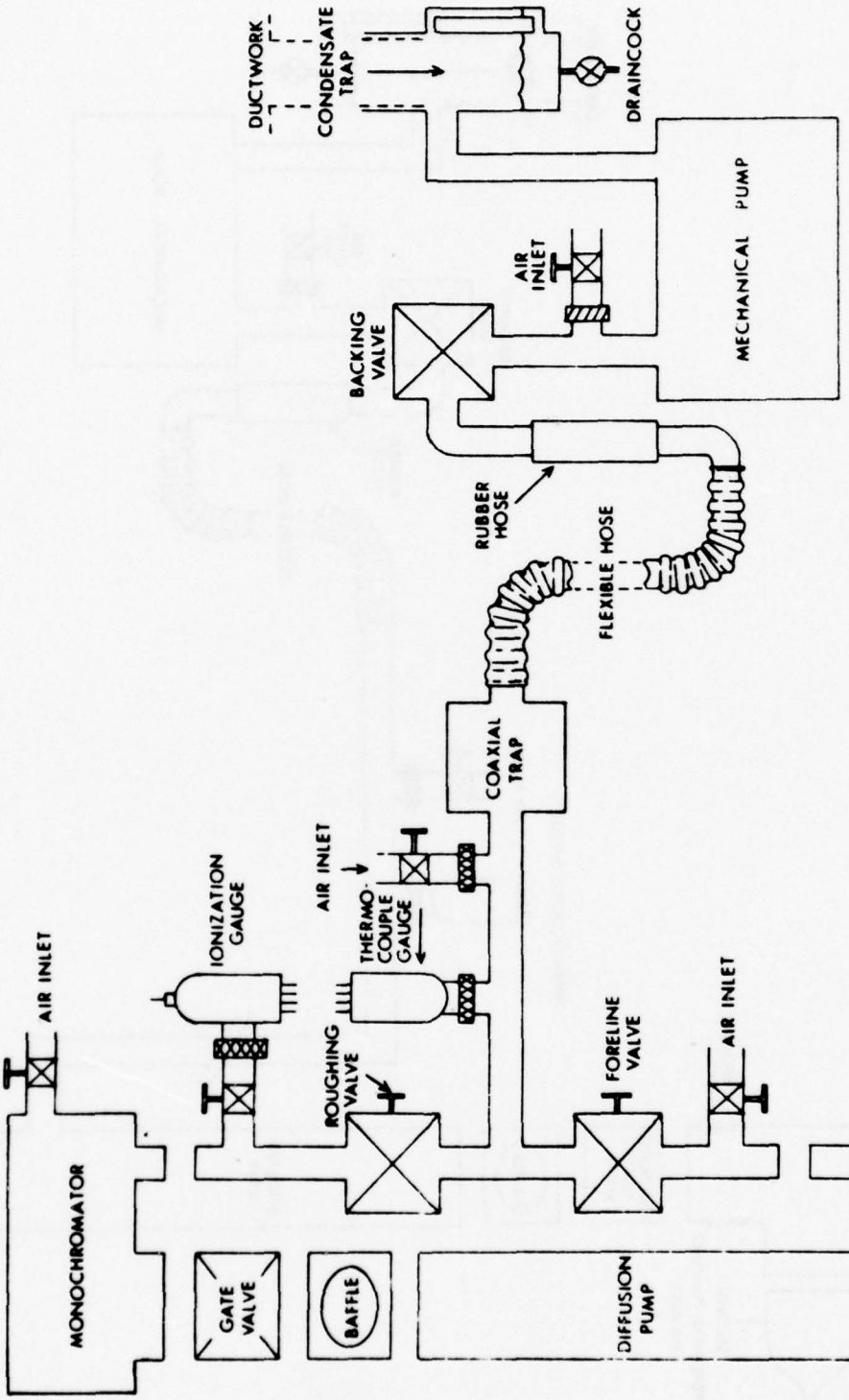


Figure II-24. Monochromator Pumping System.

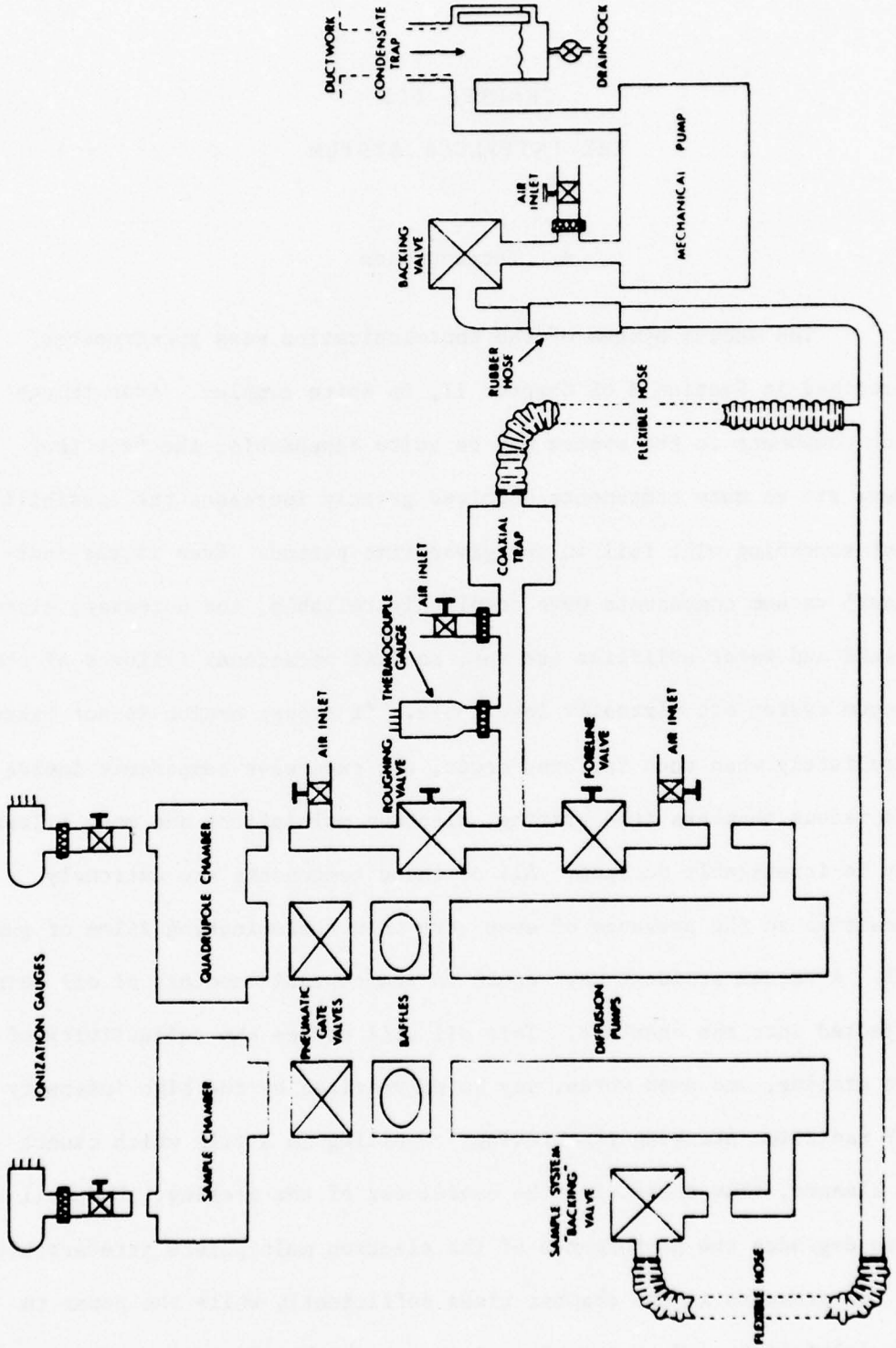


Figure II-25. Sample and Quadrupole Pumping Systems.

CHAPTER III

THE INTERLOCK SYSTEM

A. Introduction

The vacuum system of the photoionization mass spectrometer, described in Section H of Chapter II, is quite complex. Even though each component in the system may be quite dependable, the fact that there are so many components involved greatly increases the possibility that something will fail in any given time period. Even if the individual vacuum components were completely reliable, the necessary electrical and water utilities are not, so that occasional failures of the vacuum system are virtually inevitable. If proper action is not taken immediately when such failures occur, the expensive components inside the vacuum chambers (the grating, electron multipliers and mass filter) may be irreparably damaged. All of these components are extremely sensitive to the presence of even very thin contaminating films of pump oil. A vacuum accident may result in unacceptable amounts of oil being injected into the chambers. This oil will reduce the reflectivity of the grating, and even worse, may be polymerized by the high intensity VUV radiation striking the grating, resulting in a film which cannot be cleaned, thus destroying the usefulness of the grating. Pump oil also degrades the performance of the electron multipliers irreversibly. If the pressure in the chamber rises sufficiently while the power to the multipliers and quadrupole remains on, high voltage arcing may

occur which can ruin both types of components.

Although the risk of damage is most severe during an experiment when both the lamp and high voltage devices are on, damage can also result at other times. Unattended operation of the instrument thus poses considerable risk, since an accident may require the investment of significant amounts of time and money to return the instrument to working order. The risk can be avoided by leaving the gate valves closed and pumps off, which is of course impossible during an experiment, and which increases the amount of time necessary to start an experiment since the chambers must be first pumped down. The only reasonable alternative to taking such risks is to use some sort of automated safeguard system.

This chapter describes the interlock system which is used with the MSU photoionization mass spectrometer. It is designed as a "stand alone" system which is not computer operated; it can thus be used to protect the instrument between experiments as well as during them, allowing the instrument to remain safely under full vacuum conditions at all times.

Most of the devices controlled by the interlock system require either 115 VAC or 230 VAC power. At the time the system was designed and built (1973), solid state relays with logic level control inputs were still much more expensive than simple electromechanical relays. Although a much more flexible and sophisticated interlock system could be designed using standard TTL circuitry, the system described here uses RRL (relay-relay logic!) exclusively, providing considerable cost savings. If the interlock system were being designed today, the recent

decrease in price of dependable solid state relays would probably make an all-solid state design competitive in price. The parts cost for the entire interlock system was less than $1400, only a little more than the cost of a new grating. This investment has been repaid many times over during the past four years, as none of the vacuum failures which have occurred have caused any damage at all to the protected devices.

The interlock system is not sophisticated enough to totally automate the pumpdown of the instrument. However, it does mandate the correct sequence of operations during startup, which greatly reduces operator errors, although it cannot eliminate them. When used to protect the unattended instrument, the action that it takes on detecting an error condition is very simple: any device which, if left on, could conceivably be harmed or cause harm to another device, is deactivated. The vacuum system then remains shut down until an operator decides that it is safe to start again.

Section B of this chapter is a discussion of the capabilities of the interlock system, which is built in several separate, though interconnected modules -- one master control module (MCM) and several basically identical vacuum system control modules (VCM), one for each pumping system described in Section H of Chapter II. The circuitry of the MCM is described in Section C, and that of the VCMs in Section D.

B. Capabilities and General Description

Figure III-1 shows the general organization of the interlock system. Each VCM is responsible for monitoring and controlling the

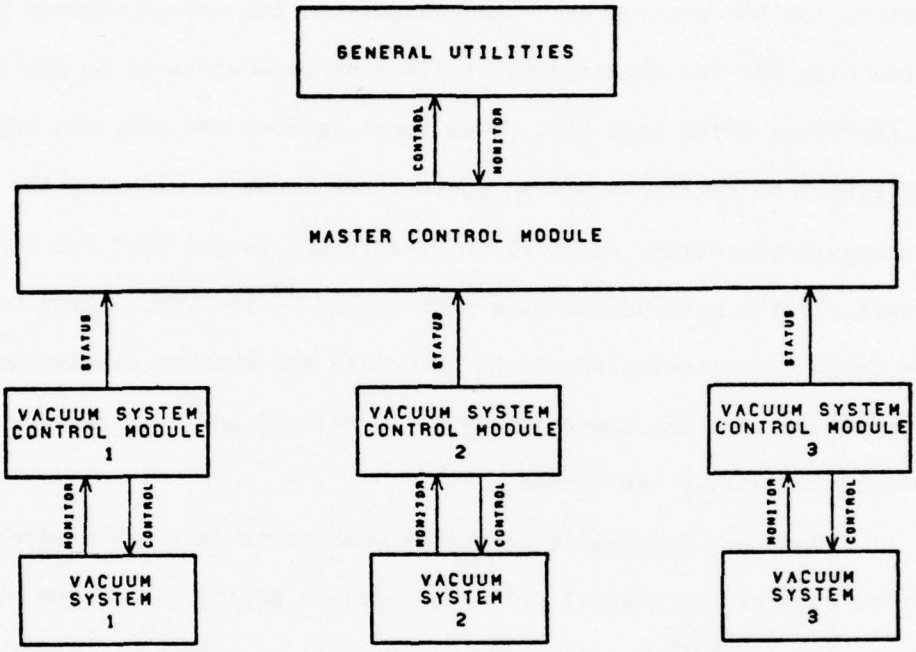


Figure III-1. Interlock System Organization. Although five VCMs are currently in use, only three are shown.

operation of the pumps and valves of a single vacuum system. Those devices which are not strictly a part of any of the individual vacuum systems (termed "general utilities") are monitored or controlled by the MCM. If a VCM detects an error condition, it not only shuts down that vacuum system, but also sends a status signal to the MCM which can then take appropriate action with the general utilities.

1. Master Control Module

The pressure in the vacuum chambers cannot be measured during an experiment, due to the high background signals that arise when the ion gauges are on. Whenever an error signal is received from a VCM, however, the MCM assumes that the pressure in the vacuum chamber may be too high for the electron multipliers or quadrupole to be run safely, and therefore turns them off. When these devices are off, the experiment cannot be continued and so there is no point in allowing the lamp to continue operating, or to allow further sample gas into the chambers. In fact, if the gate valves have been closed by the VCMs, there may be some danger in allowing sample to flow into the chamber continuously. Accordingly, the lamp power supply is turned off and lamp and sample gas solenoid valves are closed.

There are frequently occasions when it is safe and desirable to operate some of the general utilities without having all vacuum systems fully operational, especially during start-up or testing. To allow for such possibilities, the MCM is provided with a separate override switch for each VCM. When the switch is in the override position, an error signal from the corresponding VCM is ignored by the MCM, thus allowing for some operator discretion in the amount of automated control.

A simple flow switch in each water return line from the lamp (Figure II-8) is used to monitor the flow of cooling water to the lamp. If adequate flow does not exist, the lamp may be in danger of overheating, which may lead to breakage of the discharge tube. Water driven into the monochromator by atmospheric pressure could easily damage the grating, and would certainly require much effort to clean

up. Thus, when inadequate flow is detected by the MCM, the lamp power supply is immediately turned off. Since the low flow may in fact be caused by a broken discharge tube or water line, the solenoid valve in the water line is also closed to minimize flooding of the monochromator or laboratory. Again, there is no point in continuing the experiment with no light, and the other general utilities are deactivated.

The lamp power supply is also turned off by the MCM if the lamp pressure switch (Figure II-8) indicates that the lamp gas reservoir has fallen below a set pressure, since the grating can be permanently damaged if the power supply is allowed to remain on after the lamp gas has run out.[2]

The MCM can also monitor a blade-type airflow switch in the duct-work leading to the mechanical pump minihoods (see Section H, Chapter II). If the airflow falls below a preset limit for longer than a few seconds, and one or more of the mechanical pumps is on, an audible alarm is sounded to warn the operator that the pump exhaust fumes may be circulating back into the laboratory. So far, this feature has remained largely unused, since no noxious or toxic samples have yet been studied. A summary of the control and monitoring functions of the MCM is presented in Table III-1.

---

[2]An example of such an accident occurred during the term that I spent in the laboratory of W. A. Chupka and J. Berkowitz at Argonne National Laboratory. The helium supply for the one-meter PIMS instrument [43,92,93], which uses a thyratron type lamp power supply [60], ran out, but the discharge was observed to continue for several minutes, with changed color. The mechanism of the altered discharge is not understood, though it was found to be reproducible. However, the grating was ruined beyond the capability of a cleaning and recoating repair, presumably because of surface damage from sputtered lamp material. It is not known whether lamps powered by different types of high power supplies, or even if different lamps would behave in a similar fashion. We have been unenthusiastic about studying the matter further since the experiments, if successful, would be extremely expensive.

Table III-1. Summarized MCM Monitor and Control Functions.

Conditions Monitored
VCM status signals
Lamp cooling water flow
Lamp gas pressure
Minihad air flow
Devices Controlled
Lamp power supply
Lamp gas valve
Lamp water valves
Electron multiplier power supplies
Quadrupole power supply
Sample gas valves

2. Vacuum System Control Modules

Each of the pumping systems in the overall vacuum system include an electropneumatically operated gate valve, but the other main vacuum valves in the system (backing, roughing and foreline) may be either manual or automated, and in fact may not be present at all (see Figures II-22 through II-25). Some of the vacuum pumps require 115 VAC power, others require 230 VAC. The individual VCMs are nonetheless identical in basic design, being adapted to the specific requirements of the pumping system with which they are used by means of jumper wires on their back panels. The discussion here and in Section D will assume that all four main valves are present (e.g., the monochromator pumping system, Figure II-24) and are controlled via the VCM. With certain exceptions mentioned later, those units which use fewer automatic valves follow the same general guidelines, so that the discussion will be applicable to all units.

The main purpose of each VCM is to maintain a clean vacuum environment within the chamber, and to protect the chamber from the pumping system if the latter is not operating correctly. It does so by refusing to allow the gate or roughing valves of the system to be opened if anything is amiss. A secondary purpose is to protect the pumps themselves from damage due to improper operation, which is accomplished by simply turning them off.

In order to accomplish these goals, the VCM must be able to monitor the power to the mechanical and diffusion pumps to make sure they are on, and must be able to control the power to the diffusion pump so that it can be turned off if anything goes wrong. It must

of course have control of at least the gate valve, and preferably all of the valves, to ensure that they are opened only at appropriate times in the start-up sequence (and to ensure that they cannot be closed at improper times!). The details of the sequencing that is allowed by the interlock system are discussed in Part 3.

It is extremely important to monitor the foreline pressure, since if it is too high, the diffusion pump will exhibit an excessively high rate of backstreaming into the chamber, even though all other conditions for proper operation are met. Variations in foreline pressure once the experiment is started are usually small, unless some element in the vacuum system fails. Examples of things which could cause significant increases in foreline pressure include sudden and large leaks in the chambers, accidental closing of the backing valve, or failure of the mechanical pump. A sudden leak might be caused by the breakage of either the lamp discharge tube or some glass part in the sample inlet system. The VCM will prevent the backing valve from being closed via the control panel when the gate valve is open, but if the valve is unplugged or if air pressure is lost it will close nonetheless. The mechanical pump may fail for a variety of reasons, a common source being the breakage of the V-belts connecting the pump and motor. While such occurrences as these are hopefully rare, all have been known to happen, and the amount of damage that can be done is substantial enough to make precautions worthwhile.

The pneumatic gate valves need compressed air both to open and to close. If air pressure is lost while the valves are open, they will be "stranded" and the VCM will be unable to close them if the

need arises. Since the smaller backing valves only need air pressure to open, and are closed by a spring return, they will close automatically if air pressure fails, thus creating one of the situations, described above, which leads to an increase in foreline pressure. Therefore, the compressed air pressure is also monitored so that the gate valves can be closed after the pressure drops below a certain limit, but while there is still sufficient pressure to do so.

Since cooling water is also necessary for correct operation of the diffusion pumps, the flow of the water is also monitored. If it fails, the pumping system is shut down and a water solenoid valve is also closed to prevent possible flooding in case the failure was due to a ruptured water line.

In order to obtain the desired cleanliness in the vacuum chambers, the diffusion pumps must be baffled with a cooled baffle. The VCMs monitor the compressors for the refrigerant used to cool the baffles to make sure they are on before the gate valve is opened. If the compressors are turned off, the gate valves will close to prevent any material condensed on the baffles from being evaporated into the chambers.

Finally, some diffusion pumps have provision for a thermal switch used to indicate that the outer wall temperature of the pump is too high. This may be due to a loss of cooling water, but also to a low fluid level in the pump. The VCMs make provisions for monitoring such sensors. The functions of the VCMs are summarized in Table III-2.

3. Sequencing

The discussion here refers to a completely automated system. The requirements for a partially automated system are the same except

Table III-2. Summarized VCM Monitor and Control Functions.

Conditions Monitored
Mechanical pump power
Diffusion pump power
Position of automated valves
Foreline pressure
Diffusion pump cooling water flow
Diffusion pump wall temperature
Baffle refrigerant compressor status
Devices Controlled
Power to pumps
Power to valves
Coolant water solenoid valves
Status signal to MCM

that the operator must assume the responsibility for following the required procedures for the manual devices.

i. Mechanical backing pump:

To ensure the safety of persons working in the pump room far away from the interlock system control panel, a safety switch is located within easy reach of each mechanical pump. This switch will override all other switches and turn off the pump when it is thrown. Assuming that the safety switch has not been thrown, the mechanical pump can be started from the control panel at any time. However, it cannot be turned off while the diffusion pump is on, except with the safety switch or in case of power failure. If power fails, the mechanical pump will shut off and stay off until manually restarted.

ii. Backing Valve:

The backing valve can be opened only if the mechanical pump is on, and will automatically close if the mechanical pump goes off. It cannot be closed from the control panel while the gate valve is open, but can be at any other time, and will close automatically if power fails.

iii. Diffusion Pump:

The diffusion pump can be turned on and will remain on only if its wall tempeature and foreline pressure are below safe values, the baffle cooling is on, and the backing pump is on. It can be turned off at any time the gate valve is closed, and is turned off automatically if power fails.

iv. Gate Valve

The gate valve can be opened only if the diffusion pump is on,

the roughing valve is closed and the backing and foreline valves are open. It can be closed at any time, and will close automatically if power fails or the diffusion pump is turned off.

v. Foreline Valve:

The foreline valve can be opened only if the mechanical pump is on and the roughing valve is closed. It cannot be closed while the gate valve is open, except in case of power failure, but may be closed at any other time.

vi. Roughing Valve:

This valve can be opened only if the backing valve is open and the foreline valve is closed (i.e., the gate valve is closed). It may be closed at any time and will close automatically on power failure.

vii. Status Signal to MCM:

The status signal will indicate that all is well only when the gate valve is open. Any condition that causes the gate valve to close (including closing it via the control panel) will result in a "fault" status signal until the gate valve is once again opened.

viii. Exceptions:

The only major exception to the guidelines outlined above is the first differential pumping system (the Roots blower). The VCM for this system is very much simpler than the others since the system includes only two pumps and one valve, the gate valve. This VCM is built on the same chassis as the second differential pumping system VCM for reasons of space economy.

The circuitry supplied with the Roots blower-backing pump assembly allows the backing pump to be turned on at any time, and

then turns the blower on automatically when the inlet pressure drops to a preset value. The blower will also turn off automatically if the pressure rises above this limit. Both pumps can be turned off by the operator at any time, and will shut off and remain off if power fails. The VCM for this system consists solely of a gate valve control, which allows the gate valve to be opened only when the blower is on. The gate valve can be closed at any time, and closes automatically if power fails or the blower is turned off.

C. Master Control Module

Figure III-2 shows the circuitry involved in the airflow monitor and hood alarm portion of the master control module. The air flow switches, which are closed when sufficient flow is present, are located in the ductwork above the mechanical pump minihoods. The mechanical pump switches are actually relay contacts in the individual VCMs which are connected as shown, via connectors on the master control unit rear panel. The alarm operates on 115 VAC power and is thus on unless relay K2 is energized. To allow for momentary fluctuation of the airflow switches, K2 is a time-delay-on-release type of relay. Its proper operation demands that it receive continuous 115 VAC power, since it otherwise could not keep from releasing immediately. K2 is triggered by relay K1 so that when K1 is energized, then K2 is also and the alarm is off. This will occur when all mechanical pumps are off, or when both airflow switches indicate sufficient flow. If these conditions are not met (i.e., airflow fails when any pump is on), then after the adjustable time delay of K2, the alarm will sound. If K2 is re-energized by K1

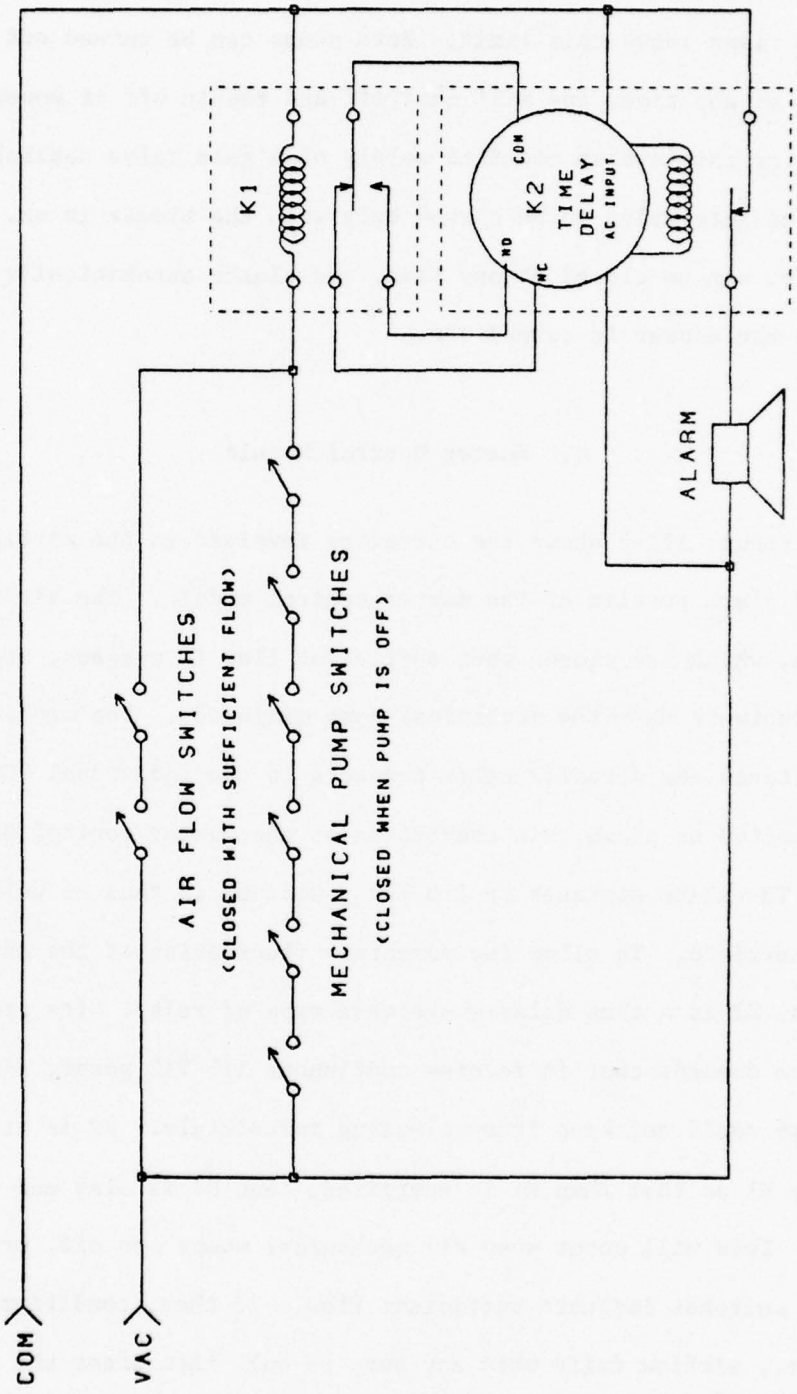


Figure III-2. Hood Alarm Circuit (MCM).

before the time delay expires, no action is taken.

Figure III-3 shows the circuitry which is used to control the diffusion pump water flow for each vacuum system. There is a similar circuit for each water-cooled pump. The water flow switch and water solenoid valve are located near the vacuum pump. When the override switch is closed, power is applied to the water solenoid valve, initiating water flow. Assuming the flow rate is sufficient, the flow switch will close, activating relay K3 and in turn time delay relay K4, and the override switch can be released. The second set of contacts on K4 is used to signal the appropriate VCM through one of its safety switch inputs (see Section D) that the water flow is sufficient. The time delay action of K4 ensures that air bubbles in the water line or other similar brief interruptions in water flow do not shut off the solenoid valve. If the flow interruption lasts longer than the delay of the relay (adjustable, 1-180 sec), then the water solenoid valve is shut, and the VCM is signalled by way of the open circuit to its safety switch input that water flow has ceased, and will take appropriate action. L1 is a small indicator light on the front panel which indicates that the flow switch is closed. These water flow circuits are perhaps more appropriately considered as part of the individual VCMs. However, the circuits are actually located in the MCM chassis, since the need for the time delay feature was not realized until after the VCMs were assembled.

The remainder of the circuitry in the main control module is shown in Figure III-4. It includes circuitry for monitoring and controlling the cooling water flow to the lamp cathode and anode, which is analogous to that for the diffusion pump cooling water discussed

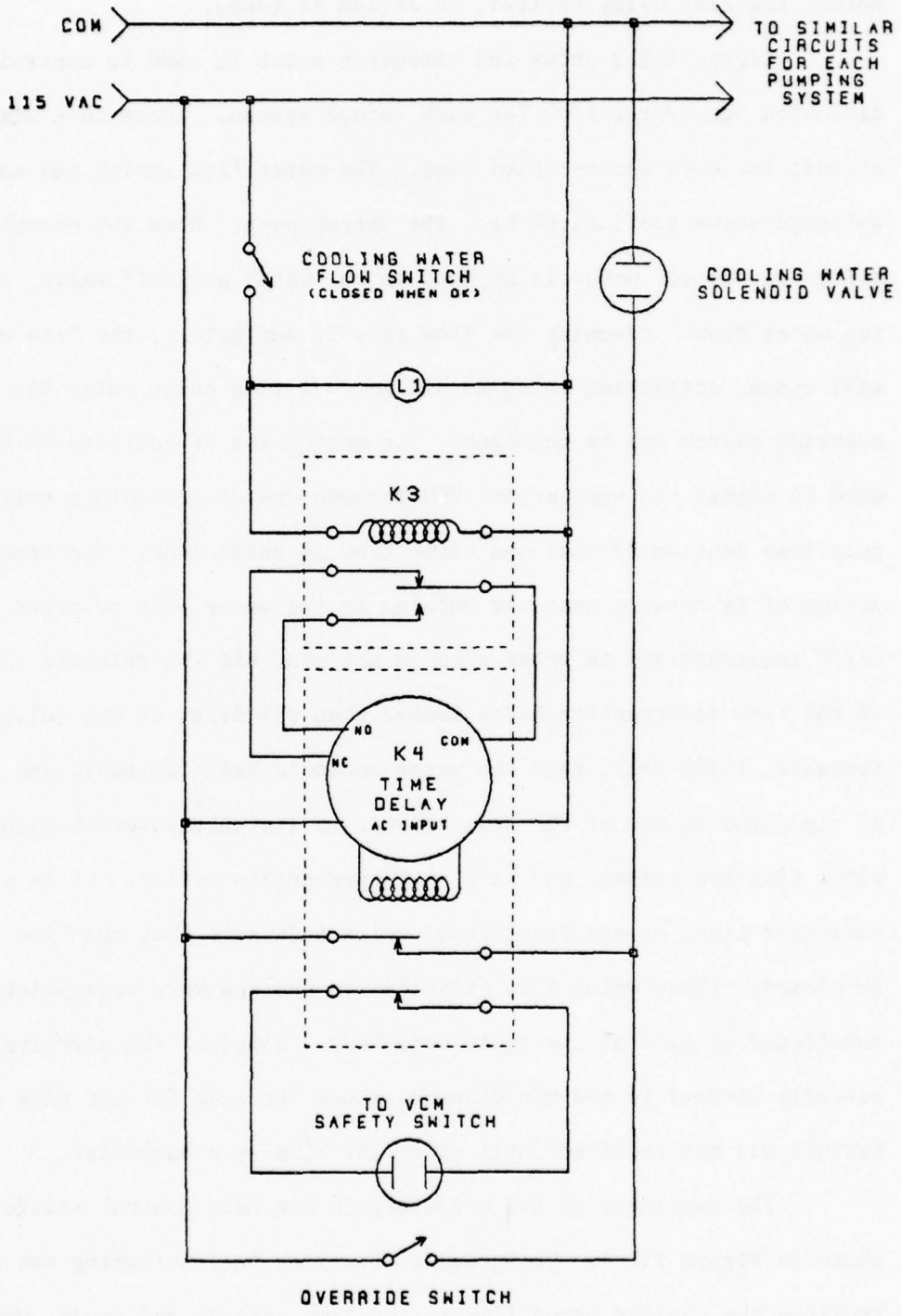


Figure III-3. Diffusion Pump Water Flow Interlock (MCM).

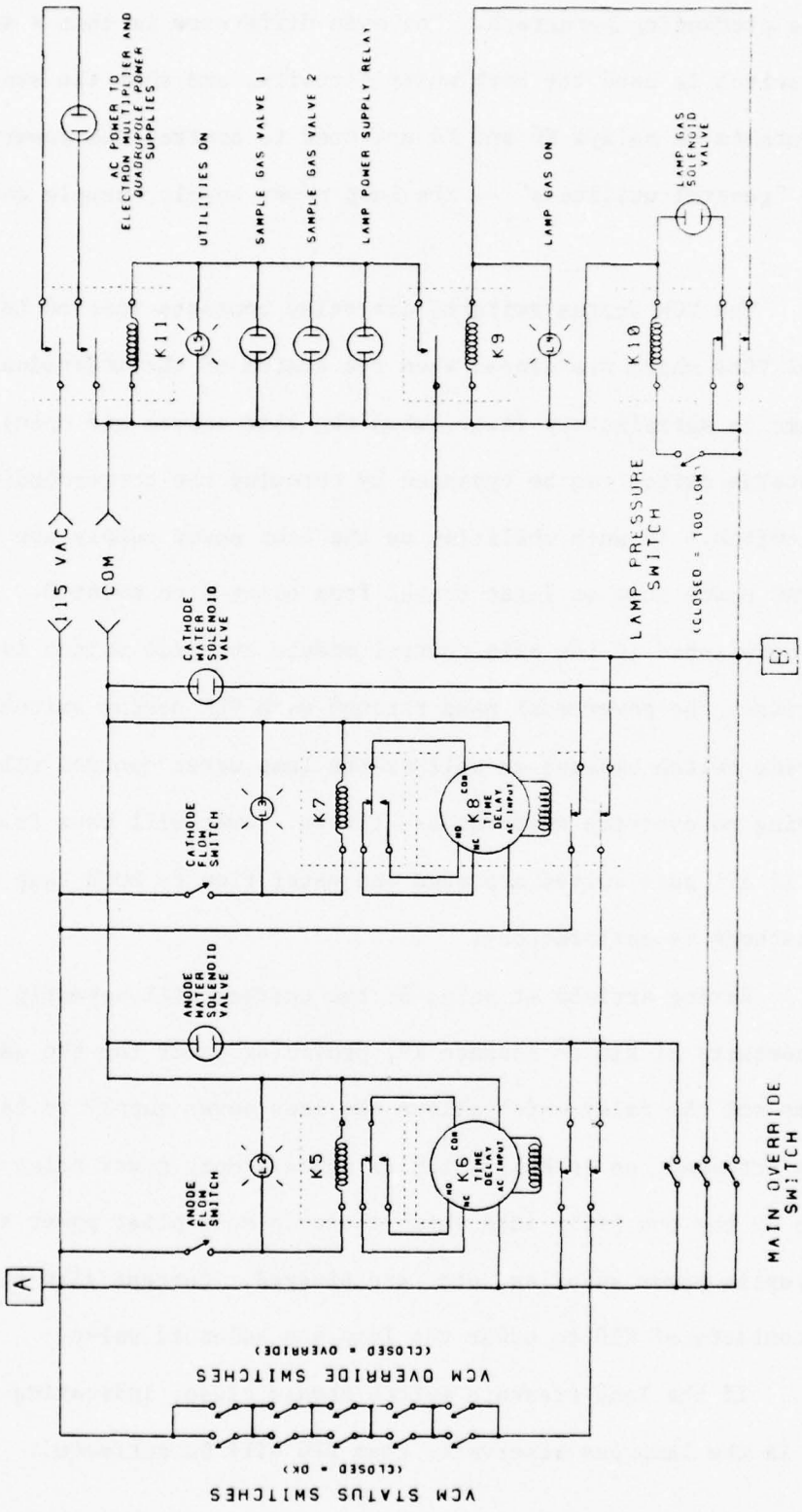


Figure III-4. General Utilities Interlock (MCM).

in the preceeding paragraph. The main difference is that a single override switch is used for botn water circuits, and that the second set of contacts on relays K6 and K8 are used to control the power to the other "general utilities" -- the lamp power supply, sample gas solenoids, etc.

The VCM status switches are relay contacts located in the individual VCMs which are closed when the status of the individual vacuum systems is satisfactory (i.e., when the gate valves are open). Any VCM status switch can be bypassed by throwing the corresponding override switch. If such utilities as the lamp power supply are to be on, 115 VAC power must at least travel from point A to point B. This can be accomplished if the main control module override switch is thrown. Otherwise, the power must pass through each VCM status switch (or its override switch bypass) as well as the lamp water control relays. Thus, assuming no override switches are thrown, power will pass from A to B only if all gate valves are open and water flow to both lamp anode and cathode is satisfactory.

Having arrived at point B, the current will normally flow through the contacts of K10 to actuate K9, providing power for the sample gas valves and the relay which allows the lamp power supply to be on. When K9 is actuated, so is K11, which is a heavy-duty power relay which turns on the bus strip into which electron multiplier power supplies, quadrupole power supplies, etc. are plugged. Current also flows through the contacts of K10 to power the lamp gas solenoid valve.

If the lamp pressure switch should close, indicating a low pressure in the lamp gas reservoir, then K10 will be activated. This will

de-activate K9 and K11 and all of the devices which are powered through these two relays.

D. Vacuum System Control Module

The circuits for the vacuum system control modules are shown in Figures III-5 through III-7. The circuitry shown in Figure III-5 is all located in a small box near the mechanical backing pump in the pump

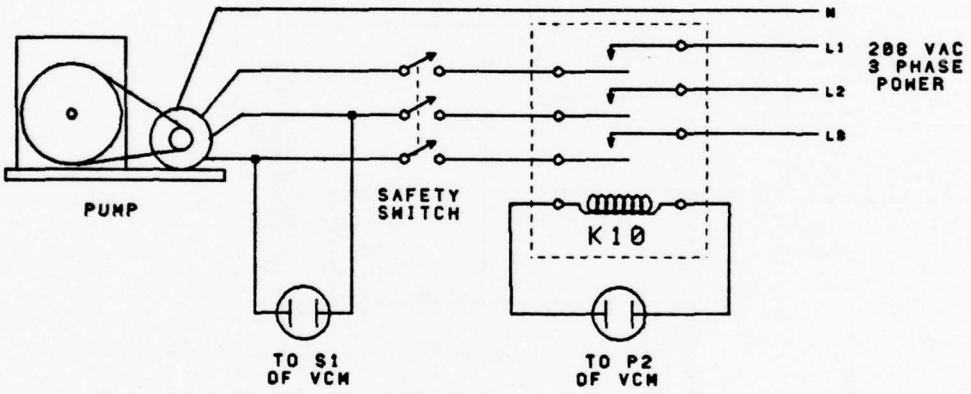


FIGURE III-5. "Local" Mechanical Pump Circuit.

room, while that in the other two schematics is all mounted in the VCM chassis near the instrument. The numbers in the small squares in these figures refer to terminals on the rear panel of the unit, which can be interconnected in a number of different ways to allow operation from different voltages or with a different number of automatic valves. They are shown connected for a complete (four-valve) system, and Part

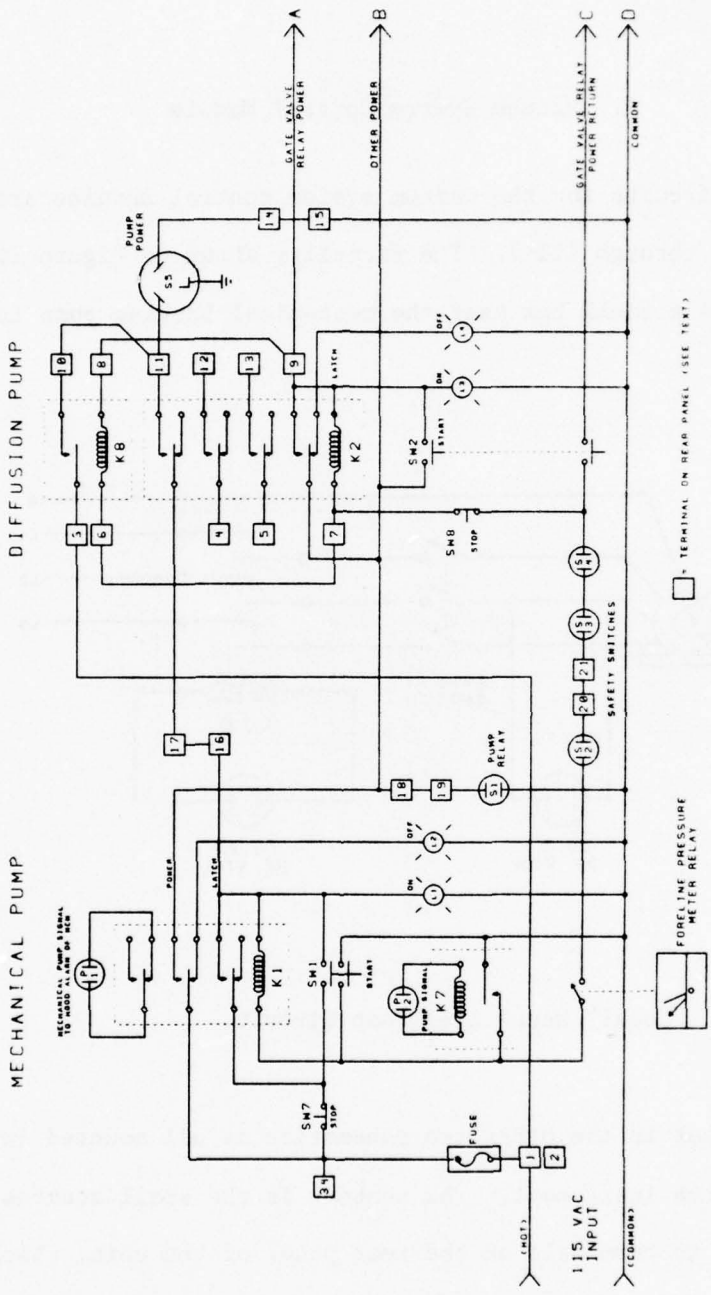


Figure III-6. Pump Control Circuit (VCM).

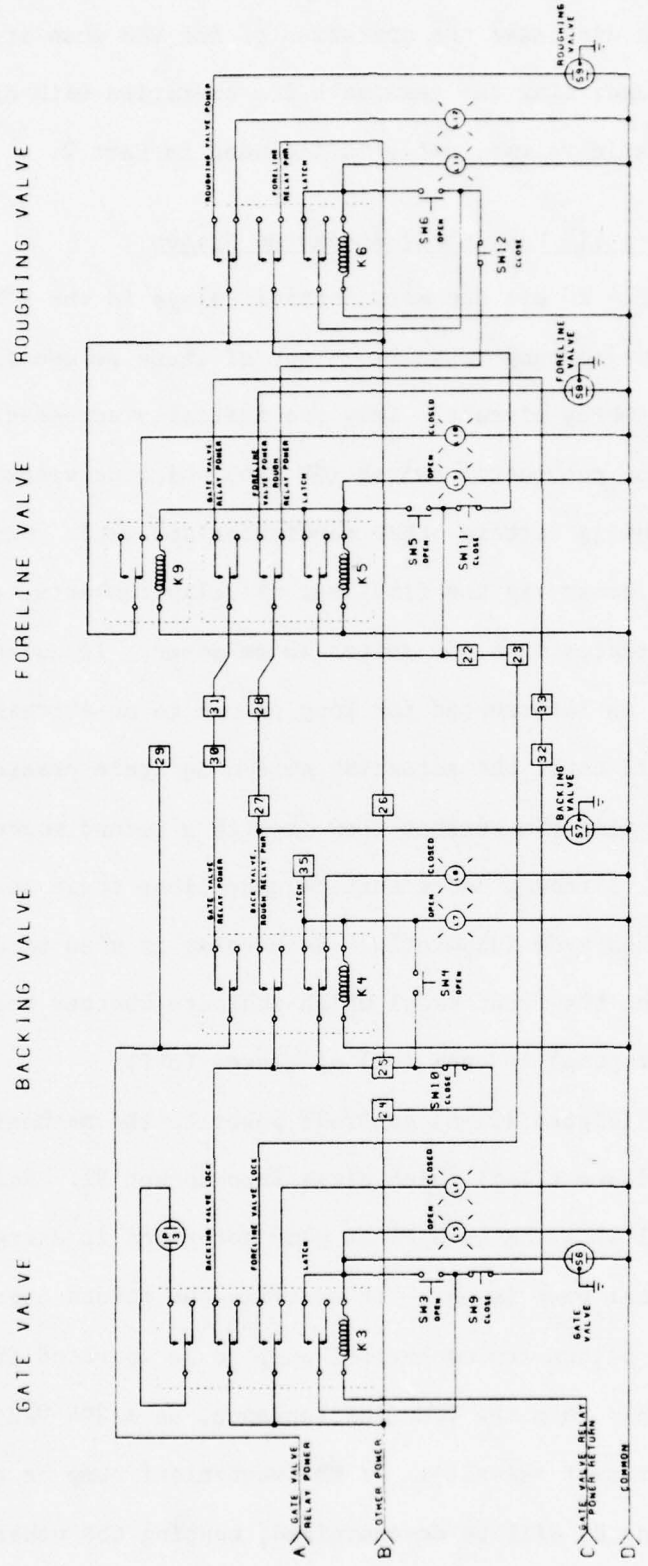


Figure III-7. Valve Control Circuit (VCM).

1 of this section discusses the operation of the VCM when it is so wired. Information on connecting the terminals for operation with different numbers of automatic valves, etc., is included in Part 2.

1. Operation of a 115 VAC, Fully Automated System

Relays K1 - K6 are the main control relays in the VCM; each is dedicated to a single pump or valve. Each of these relays is wired in a simple self-latching circuit. They are initially actuated by pressing a momentary action pushbutton switch (SW 1-6) which provides power to their coils (assuming certain other conditions are met). Once actuated, the coils obtain power via the first set of relay contacts, so that the relay remains actuated when the switch is released. If current flow through the coil is interrupted for long enough to de-energize the relay, it will remain off until the actuating switch is again pressed. One means of interrupting the current flow is with a second momentary switch (SW 7-12), although under certain conditions these switches may be shorted and thus made inoperable. Each relay is also wired to two indicator lamps on the front panel which indicate whether the corresponding valve (or pump) is open (on) or closed (off).

Relay K1 (Figure III-6) controls power to the mechanical pump via relay K10 (Figure III-5) which plugs into socket S1. Relay K7 is wired in parallel with the mechanical pump motor and is energized whenever the mechanical pump is on -- it controls the return current from K1. This system allows the mechanical pump to be operated from a different power supply than the VCM (for instance, on a 208 VAC three phase line as in the present example). If the mechanical pump or the VCM power fails, K7 or K1 will be de-energized, causing the other to also

be de-energized, and the entire system will be turned off until started again manually. Note that the safety switch (Figure III-5) will turn off the mechanical pump and de-energize both K1 and K7 regardless of their previous status.

SW1 provides current to energize K1 and also provides a bypass around K7 which is needed until the motor starts and K7 closes. All other control relays draw their power from B (Figure III-6) via contacts on K1. Thus if K1 is de-energized for any reason, the entire pumping system will shut down immediately. SW7 can be used to turn the mechanical pump off, except when the diffusion pump is on, in which case current to the relay coil is available through terminal 16 as well as through SW7, so that pushing SW7 has no effect. Thus, the mechanical pump cannot be accidentally turned off (from the control panel) while the diffusion pump is on.

Relay K2 (Figure III-6) controls power to the diffusion pump through its own contacts when a 230 VAC pump is used. However, it cannot handle the higher current required by our 115 VAC pumps. Relay K8 has a very high current handling capacity, and is added in parallel to K2 for this reason. The diffusion pump relays are energized by SW2 (providing the mechanical pump is on to provide a current path to SW2) and de-energized by SW8. The return current from these relays must pass through sockets S2-S4 as well as the switch contacts of a meter relay used to monitor the foreline pressure. Any sort of safety switch which is closed when the condition it monitors is within acceptable limits can be connected to S2-S4. One of these sockets is used for the water flow signal from the MCM, others may be used for diffusion pump

thermal switches or compressed air pressure switch. If any of these switches open, K2 and K8 will be immediately de-energized, turning off the diffusion pump.

The power for the gate valve must come through point A, and thus both the mechanical and diffusion pumps must be on for it to open. Note that this does not mean that the diffusion pump must be warmed up, only that it must be on. The operator is responsible for making sure that adequate warm-up time is allowed. K3 (Figure III-7) controls power to the gate valve. Since its return current passes through the same safety switches as the current from K2, the gate valve will shut whenever any of these switches are opened. SW9 will close the gate valve at any time. In order to open the gate valve, not only must SW3 be closed, but power must find a complete path from point A to SW3 through the contacts of K4 and K5. It will be able to do so only when both backing and foreline valves are open. When the gate valve is open, K3 provides another path for power to K4 and K5 so that the normal "close" switches for the backing and foreline valves have no effect.

The normally closed part of SW2 is in the circuit to prevent the gate valve from opening whenever the diffusion pump is started. If it were not included, power coming through SW2 and relay K2 can return to common not only through the safety switches, but also through the coil of K3 and the gate valve solenoid. This devious path was discovered only after the VCMs were completed, at which time the second half of SW2 was wired into the circuit as shown to prevent the problem. This solution works, but has the drawback that if the gate valve is open (and diffusion pump on) pushing the diffusion pump on button again, which

should have no effect, closes the gate valve! In retrospect, a better solution would be to draw power for the gate valve from the contact which provides the foreline valve lock.

Power for K6 comes via a contact on K5 which is closed when K5 is deenergized, and power for K5 comes from a contact on K6 which is closed only when K6 is deenergized. This ensures that the roughing and foreline valves cannot be open at the same time.

2. Wiring for other options

When the diffusion pump of the system requires 230 VAC power, the terminals must be wired differently than shown in Figure III-6 and III-7. Table III-3 lists the terminal connections for both options.

Table III-3. Terminal Connections for Main Power Options.

Diffusion Pump Voltage	115 VAC	230 VAC
Rear Panel	1-3	1-4
Terminal	6-7	2-5
Connections	8-9	11-12
	10-11	13-14
	14-15	16-17[a]
	16-17[a]	18-19[a]
	18-19[a]	20-21[a]
	20-21[a]	

[a]Must be modified when a single mechanical pump is shared between two systems. See text for further details.

Table III-4 lists the terminal connections to be used when different numbers of automatic valves are used. In addition, the VCMs were designed so that two diffusion pumps could share a backing pump (as in the quadrupole/sample chamber pumping systems), with the two VCMs being simply interconnected via the terminal strips. Table III-5 gives the connections to be made for such a system. In this situation the sample system interlock utilizes the thermal and baffle switches corresponding to the sample system diffusion pump, but also involves the same foreline pressure switch as the quadrupole interlock system. The dual-role mechanical pump is latched on if either diffusion pump is on, providing another path for power through terminal 16 (though the power to the two diffusion pumps must be in phase). The power for the control relays in the sample interlock system comes through K2 of the quadrupole system, and both systems will shut down upon failure of the mechanical pump.

Table III-4. Terminal Connections for Automatic Valve Options.

Automatic Valves	Gate, Backing	Gate, Foreline, Roughing	Gate, Backing, Foreline Roughing
		22-23	22-23
Terminal	30-32	24-25-26-27-28	25-26
Connections		29-30-31	27-28
		32-33	30-31
			32-33

Table III-5. Terminal Connections for Sharing a Mechanical Pump Between Two Systems.

Sample System Terminal	Quadrupole System Terminal
17	16
18	18
21	20

Note that it is important that the 115 VAC power for the VCMs which are interconnected in this way be in phase. Unfortunately, the power used for our sample and quadrupole systems is not in phase, and a more complicated interconnection scheme has been used. It is shown in Figure III-8.

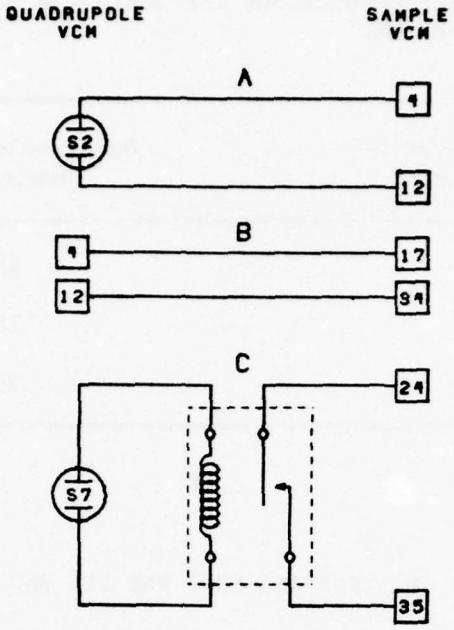


Figure III-8. Alternate Interconnection Method. The (shared) backing valve and mechanical pump are connected to the Sample VCM as usual. Connection group A ensures that the quadrupole diffusion pump will turn off if the sample diffusion pump does. Connection group B latches the mechanical pump on if the quadrupole diffusion pump is on. Connection group C latches the backing valve open if the quadrupole VCM backing valve relay is energized.

CHAPTER IV

CONTROL AND DATA ACQUISITION

A. Introduction

The instrument controller, in this case a minicomputer, must be capable of interacting with the instrument in several ways if efficient automated acquisition of accurate PIE curves is to be possible. The computer must be able to acquire integrated photon and ion intensity data and, if data acquisition is to be efficient, must be able to control the data integration time. The computer must also change the wavelength setting of the monochromator and, if periodic reference measurements or scattered light measurements are to be possible, the wavelength control must be bidirectional. In order to make background measurements, the computer must be able to prevent photons and photoions from reaching the corresponding transducers, perhaps by interposing a shutter in the photon beam before it enters the ion source.

These are the absolute minimum requirements, but there are other capabilities which may also be very desirable. For instance, when electron multipliers are used for both ion and photon detection, their background signals will be similar and very small. It is then appropriate to make photon and ion background correction measurements at similar and infrequent intervals. However, if a sodium salicylate photon transducer is used (see Chapter II, Section D), it will exhibit a much

THIS PAGE IS BEST QUALITY PRACTICABLE
FROM COPY FURNISHED TO DDC

higher and more unstable background than the ion electron multiplier, so that its background should be measured much more frequently. In the limit of a very weak signal, as much as half of the total photon measurement time should be devoted to measuring the photon background for optimum efficiency [94], but devoting such a fraction of the time to measurement of ion background would be very inefficient. It may therefore be desirable to include a second shutter between the ion source and photon detector which can be used to measure photon backgrounds without interrupting the integration of the ion signal.

The mass to be transmitted by the mass analyzer is usually set at the beginning of an experiment and left unchanged until the beginning of the next, so that the computer need have no control over it. However, as seen in Chapter II, Section F, it is important to use only the minimum necessary mass resolution in order to maximize the ion signal intensity. The setup of the experiment can be facilitated if the computer can be used to acquire partial mass spectra in the mass region of interest at various resolutions, and thus computer control of mass may be desirable.

It might also be useful for the computer to control the voltages applied to other elements of the ion optics. In general, the optimum focusing conditions will differ from ion to ion, depending on mass as well as the necessary resolution. If the computer were programmed to optimize these parameters, for instance by the use of some sort of SIMPLEX procedure [95], the amount of time the operator must spend in setting up each experiment could be greatly reduced. Furthermore, ion-molecule reaction studies in which the translational energy of the reactant ion is varied could then be easily automated.

Whenever a reference measurement is made, the time necessary to move to and from the reference wavelength as well as the actual reference data acquisition time are wasted as far as the acquisition of PIE data is concerned, and thus such reference measurements should be made as infrequently as possible. If the sample pressure fluctuates faster than any of the other system variables which are accounted for by such measurements, it would be more efficient to measure the pressure separately (and simultaneously with photon and ion data) so that reference measurements (to correct for the remaining variables) can be made less frequently. Simultaneous measurement of pressure, photon and ion data requires the use of a pressure transducer which does not itself create ions (e.g., the ionization gauge). The capacitance manometer is most often used in such cases, and has the additional advantage that its response is independent of the nature of the sample; furthermore it can be easily interfaced to the computer. The major disadvantage of the capacitance manometer is that, on its most sensitive pressure scales, it is extremely sensitive to temperature variations, which cause rather large zero drifts (as much as 1-3% of the reading per °C). This requires that the computer be able to check the true pressure zero frequently; in order to do so the computer must be able to control the opening and closing of the valves in a simple valving arrangement. If measurements are to be made as a function of pressure, then the computer must also be able to control the pressure, not merely measure it.

As of this writing, the MSU photoionization mass spectrometer includes only those items mentioned above as being absolutely necessary -- photon and ion data acquisition, bidirectional wavelength control, and

control of a shutter before the ion source. A valve control and pressure measurement interface has also been completed recently; however, the solenoid valves originally used were found to have unacceptably high leak rates. This capability is temporarily unused pending the arrival of new valves. The hardware necessary to implement the other capabilities discussed above is in various stages of design.

This chapter describes the hardware and electronics used to implement the computer control and data acquisition capabilities of the MSU PIMS instrument, and characterizes their performance. The computer is a Digital Equipment Corporation (DEC) PDP 8/I minicomputer [96], which uses a 12-bit word length and is equipped with 12K of memory. Data and program storage peripherals include a dual DEC-Tape drive and a dual floppy disc drive (Sykes 7200 series) [97]. Interaction between the user and computer takes place via a Tektronix 4010 graphics display terminal [98] or an ASR 35 Teletype [99]. Graphic output from the computer can be plotted not only on the Tektronix terminal, but also on a Heath EU-205 strip chart recorder [100] which is interfaced to the computer.

Nearly all of the electronic circuits described in this chapter are constructed on printed circuit boards that are mounted in a card cage in the computer rack. The card cage and basic computer interfacing techniques used are described in Appendix B. The real-time clock which is used by the computer for a wide variety of timing functions is described in Appendix C. Several conventions have been adopted for the schematic diagrams of all these circuits. Almost all of the logic circuits use standard 7400 series TTL integrated circuits (ICs). These are not specified except when the type of IC is not obvious from its symbol, in which

case the IC type number is shown in parentheses (e.g., a simple box used to represent a counter might be labelled with (74161)). All ICs use standard totem-pole outputs, except those marked with an asterisk (*), which have open collector outputs. Small numbers are sometimes shown just outside the IC symbol; these refer to pin numbers (for the dual in-line package, unless otherwise specified). The large numbers within the IC symbol are for reference only. Any resistor shown without a specified value is simply used as a pull-up resister, and has a value between 1000-10,000 ohms (not critical).

The wavelength drive is described in Section B of this chapter, the shutter control in Section C, and Section D contains a description of the interface used to control the capacitance manometer valves. The remaining sections of the chapter are devoted to the electronics used in data acquisition. The two approaches which have been used most commonly to measure the output of electron multiplier devices are DC current measurement (DC) and pulse counting techniques (PC). The two approaches have different merits, and which approach is more advantageous is determined by the characteristics of the transducers, the photon and ion arrival rate and the limitations of the electronics used. Their relative merits have been amply discussed in the literature (see reference [101] and other literature cited in Section F), to which the reader is referred. Either type of measurement system can be used with the MSU instrument. The electronics used for DC measurements are described in Section E. The novel circuit developed for pulse counting measurements is described and evaluated in Section F, and in Section G the counter circuits which interface both DC and PC electronics to the computer are described.

B. The Wavelength Drive

The wavelength of the McPherson 225 monochromator is scanned by rotating the drive screw of its modified sine drive mechanism, the digital-to-shaft angle conversion being accomplished with a high resolution stepping motor (Responsyn HDM 150-1000-4) [102], which is directly coupled to the drive screw. The stepping motor has an angular resolution of 0.36° (1000 steps/revolution), which with a 1200 line/mm grating is equivalent to 0.025 Å/step. At the maximum rated speed of 1500 steps/second, a region of 1000 Å can be scanned in less than 30 seconds. A set of 10:1 reduction gears can be inserted between the stepping motor and drive screw to obtain finer steps for high resolution work, although this reduces the maximum effective scan rate by a factor of ten.

The motor is driven by the computer via a commercial indexer (Responsyn PSD-4-3) which can also be controlled manually. The interface between the computer and the indexer is very simple, as shown in Figure IV-1. The computer sends the indexer either a "step forward"

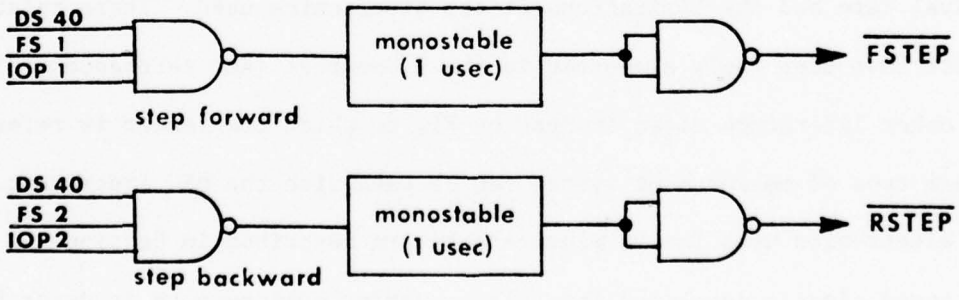


FIGURE IV-1. Stepping Motor Interface.

($\overline{\text{FSTEP}}$) or "step backward" ($\overline{\text{BSTEP}}$) command, the pulses being lengthened by the monostables in order to meet the input pulse width requirements of the indexer.

The wavelength drive screw could be damaged if the stepping motor attempts to drive it past its upper or lower limits. To prevent this possibility, the limit switches on the slave screw of the monochromator (located outside the vacuum) have been disconnected from the synchronous motor supplied with the monochromator (and not used by us). The stepping motor indexer has been modified to accept signals derived from these switches so that if the upper limit switch is actuated, or disconnected, the stepping motor will no longer respond to commands from either the computer or operator to move toward higher wavelength, although it will still move toward lower wavelength. The action of the lower limit switch is just the reverse.

No optical shaft encoder is used on the wavelength drive screw, nor is there any electrical feedback from the stepping motor to the computer, i.e., this is an open loop system. The computer keeps track of the wavelength by maintaining a step count in a software register which is incremented or decremented each time the computer issues a STEP instruction. This system is simpler than a closed loop system, but high wavelength accuracy depends on absolute reliability of the interface and stepping motor. Many stepping motors, however, tend to miss steps if they are started or stopped suddenly at full speed, and must instead be accelerated more gradually to full speed, and then decelerated before stopping. In addition, there may exist certain resonant frequencies in the system (motor plus load) which cause the motor to misstep

when run at the corresponding step rate. It is important that these problems be avoided if good accuracy is to be attained.

Figure IV-2 shows eight repetitive scans of the atomic nitrogen emission lines near 1134 Å, obtained with the reducing gears in place. Between each scan, the monochromator was scanned without acceleration at a rate of 1200 steps/second to a wavelength of 1034 Å and back, a total of 80,000 steps. Any missteps should show up as an apparent shift in wavelength of the emission peaks. Table IV-1 summarizes the apparent peak locations of the scans shown in Figure IV-2, and Table IV-2 summarizes results from two similar series of scans recorded on different days. In order to ascertain whether the small apparent wavelength shifts were due to lost steps, the reducing gears were removed and several further scans of the same lines were recorded (again with an 80,000 step round trip to lower wavelength in between scans). If the observed deviations were in fact due to lost steps, they should be ten times as large without the reducing gears. In fact, the results (also summarized in Table IV-2) are different only by a factor of 2-3, most of which can be attributed to the difficulty of precisely measuring peak positions by eye when only a few points could be obtained over the width of the peak. Thus the observed wavelength shifts are not attributed to lost steps, but instead to the limit of reproducibility of the wavelength drive system of the monochromator. This limit of reproducibility is assumed to be about 0.03 Å.

Since there is no evidence for lost steps, there is no need to accelerate the stepping motor to its maximum scan rate. Although the programs used (see Chapter V) include provisions for such acceleration,

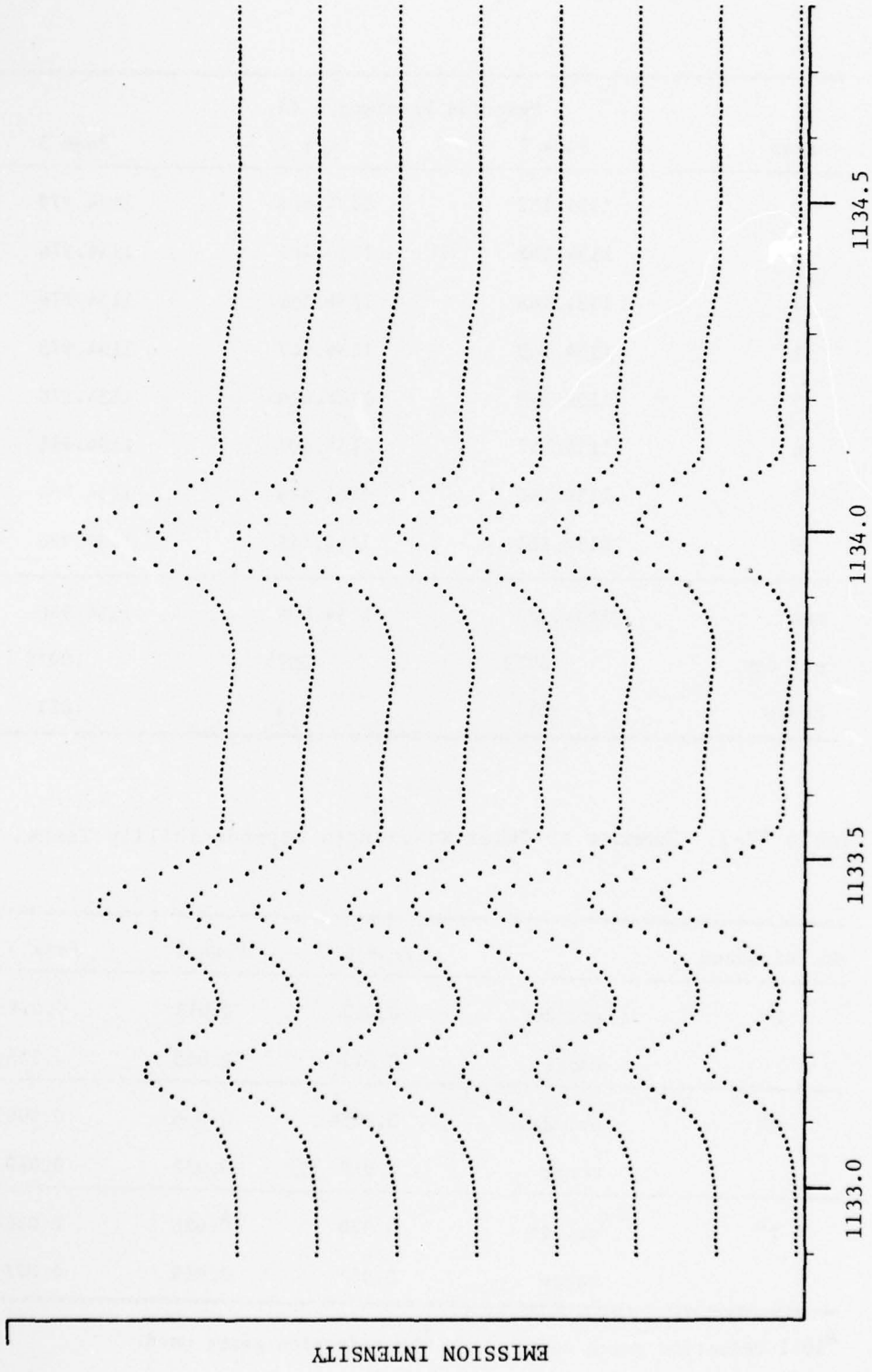


Figure IV-2. Eight Successive Scans of the Atomic Nitrogen Lines at 1134 Å.

Table IV-1. Wavelength Reproducibility.

	Measured Wavelength (Å)		
Scan	Peak 1	Peak 2	Peak 3
1	1134.152	1134.407	1134.979
2	1134.152	1134.407	1134.976
3	1134.146	1134.395	1134.976
4	1134.149	1134.407	1134.973
5	1134.149	1134.410	1134.976
6	1134.157	1134.407	1134.981
7	1134.160	1134.419	1134.984
8	1134.163	1134.418	1134.996
mean	1134.154	1134.409	1134.980
st. dev.	.0059	.0075	.0073
range	.017	.024	.023

Table IV-2. Summary of Other Wavelength Reproducibility Tests.

No. of Scans		Peak 1	Peak 2	Peak 3
8[a]	st. dev.	0.013	0.012	0.014
	range	0.042	0.035	0.035
8[a]	st. dev.	0.0054	0.0062	0.0063
	range	0.017	0.022	0.020
7[b]	st. dev.	0.020	0.026	0.026
	range	0.043	0.059	0.075

[a]10:1 reduction gears used. [b]No reduction gears used.

Table IV-3. Wavelength Accuracy.

Known λ	Measured λ	Difference	Known λ	Measured λ	Difference
948.6855	948.606	.080	1097.2372	1097.161	.076
949.7430	949.662	.081	1098.0951	1098.016	.079
950.1121	950.033	.079	1098.2599	1098.178	.082
950.7327	950.669	.064	1100.3597	1100.289	.071
950.8846	950.825	.060	1134.1653	1134.147	.018
952.3178	952.252	.066	1134.4149	1134.396	.019
953.4152	953.386	.029	1134.9803	1134.973	.007
953.6549	953.640	.015	1163.8836	1163.840	.044
953.9699	953.948	.022	1164.3246	1164.295	.030
963.9903	964.051	-.061	1167.4485	1167.394	.055
964.6256	964.691	-.065	1168.3344	1168.298	.036
965.0413	965.116	-.075	1168.5358	1168.479	.057
971.7381	971.774	-.036	1176.5098	1176.378	.132
972.5368	972.551	-.014	1177.6948	1177.571	.124
973.2342	973.235	-.001	1199.5496	1199.420	.130
973.8852	973.890	-.005	1200.2233	1200.109	.114
976.4481	976.481	-.033	1200.7098	1200.583	.127
977.9594	978.006	-.047	1215.6701	1215.581	.089
988.7734	988.875	-.102	1243.178	1243.112	.066
990.8010	990.927	-.126	1243.307	1243.234	.073
1027.4307	1027.439	-.008	1302.1685	1301.991	.178
1028.1571	1028.172	-.015	1304.8576	1304.699	.159
1039.2304	1039.323	-.093	1306.0286	1305.901	.128
1040.9425	1041.018	-.076	1310.5403	1310.446	.094
1041.6876	1041.742	-.054	1319.675	1319.541	.134

Standard deviation of differences: 0.073 Å.
range of differences: 0.304 Å.

they are rarely used.

It should also be noted that when measurements such as those described above are made immediately after re-lubrication of the drive screw (when the lubricating oil is relatively "thick" on the threads), the first few scans show a monotonic shift toward lower wavelength of about about 0.03 Å per scan. This is in the direction that would correspond to a thinning of the oil between the drive screw and nut threads. After five or six scans, no further changes are observed larger than those reported in Tables IV-1 and IV-2. When one considers that 0.01 Å corresponds to a linear travel of only 5×10^{-5} cm along the wavelength drive screw, a reproducibility limit of 0.03 Å is not too surprising.

In order to test the accuracy of the wavelength drive system, several lamp emission spectra were recorded at high resolution over the wavelength region from 940 to 1320 Å, with a "dirty" helium lamp as the light source. This region contains many atomic emission lines whose wavelengths are well known [103]. Table IV-3 compares the known and measured wavelengths of 50 of these lines. The observed deviations fall in a range of 0.15 Å over the entire region, which is typical of all scans recorded. This is indicative of the (maximum) wavelength error to be expected when no atomic lines exist nearby for calibration. When such lines are nearby, the wavelength accuracy can be considerably higher.

C. Shutter

The small flap valve just behind the exit slit assembly of the monochromator is used not only as a vacuum valve, but also as the optical shutter. Its control knob has been removed and replaced with an extension

shaft capped with a small lever. The lever is attached to a pneumatic piston which extends and thereby closes the shutter whenever compressed air is admitted to it via a small 3-way solenoid valve. When this valve is de-energized, an internal spring in the piston opens the shutter. The position of the piston is adjusted so that when it is fully extended, the flap valve is closed far enough to block all radiation from reaching the exit slit, but not far enough to engage the detent which keeps it closed tightly. The pin connecting the piston to the lever is easily removed, allowing the flap valve to be closed all the way manually when it is necessary to use it as a vacuum seal.

The solenoid-actuated air valve operates on 115 VAC power, which is controlled by a small solid state relay (Teledyne 675-4). The relay is in turn controlled by a 5 volt signal from the shutter interface near the computer. The interface circuits are shown in Figures IV-3 and IV-4.

Whether the shutter is open or closed is determined by the state of JK flip-flop 4. Its output is buffered by the 75450 which is an AND "peripheral driver", capable of supplying sufficient current to operate reliably the solid state relay which is located some 50 feet away, near the shutter. The output of the flip-flop is also used to activate a light emitting diode (LED) on the front panel when the shutter is open. The INIT pulse, which is received whenever the computer is started, is used to open the shutter, which is thereafter controlled by the signals transmitted by the and-or-invert (AOI) gates 3 and 7. These AOI gates are included to allow either manual or computer control of the shutter. The computer generates requests to open or close the shutter via NAND

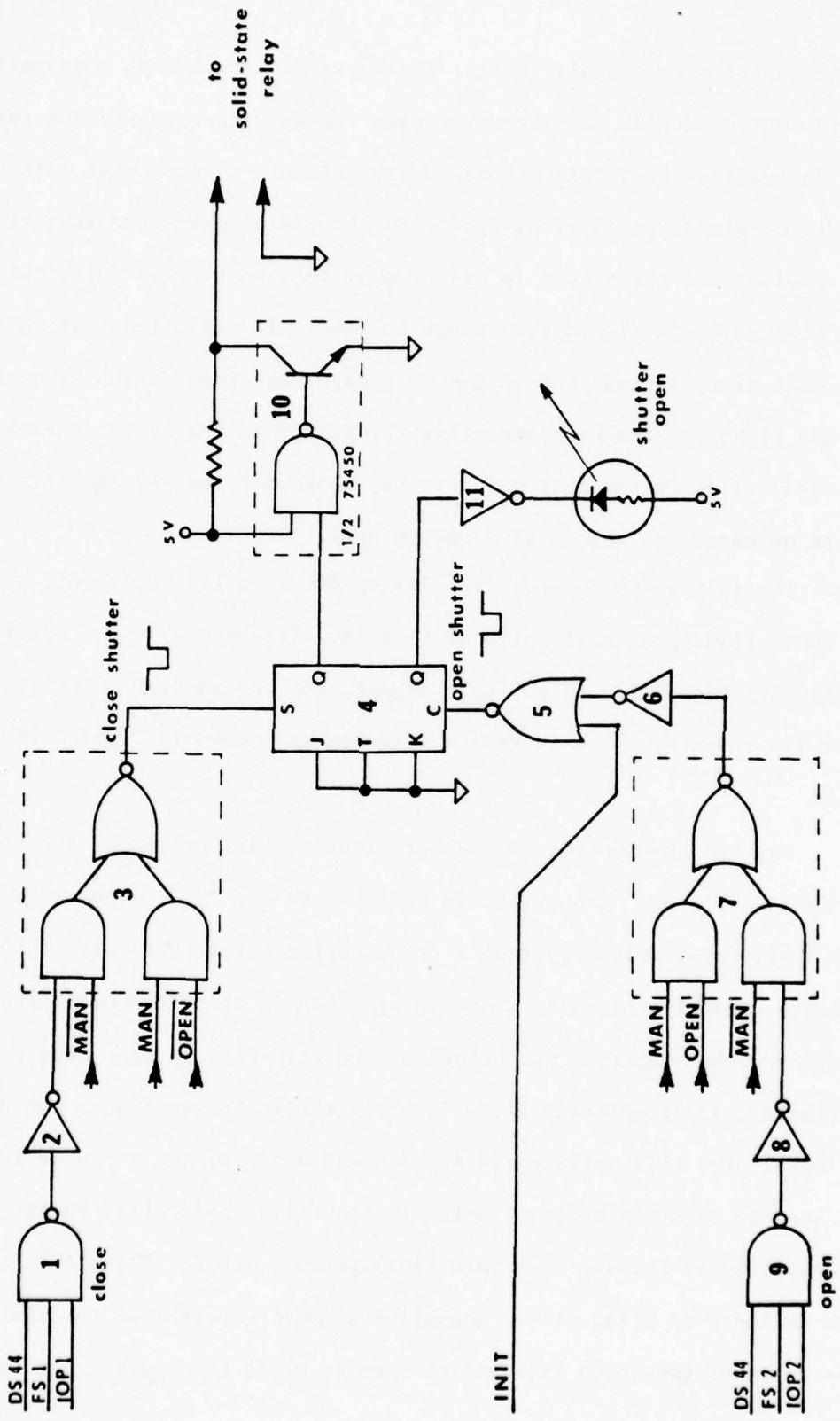


Figure IV-3. Shutter Control Interface.

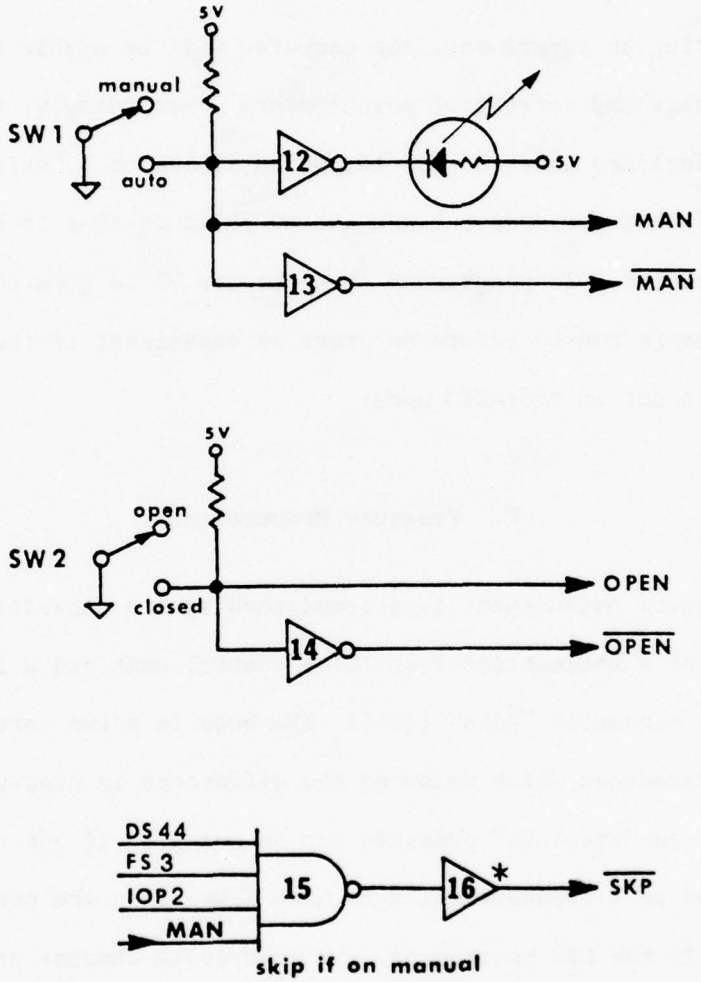


Figure IV-4. Auxiliary Shutter Control Circuits.

gates 1 and 9 and the user can generate similar requests via front panel switch SW2. The AOI gates will transmit only one of these two sets of signals, with the choice determined by front panel switch SW1.

The inclusion of manual shutter control creates a potential problem. If the user inadvertently leaves SW1 in the MANUAL position after starting an experiment, the computer will be unable to make the desired background correction measurements. Accordingly, the shutter interface includes gates 15 and 16, which implement a "skip if on manual" instruction that the computer can use to check whether it has control or not. The computer is programmed (see Chapter V) to give the user a warning message and to refuse to start an experiment if the shutter interface is not in the AUTO mode.

D. Pressure Measurement

Pressure measurement is accomplished with a capacitance manometer consisting of a Datametrics type 1014A control unit and a 571D-IT-1B2-H5 capacitance manometer "head" [104]. The head is a two port, differential pressure transducer which measures the difference in pressures between the two ports. An "absolute" pressure can be measured if one side of the head is connected to a pressure which is much lower than the pressure being measured. In the MSU instrument, the quadrupole chamber pressure serves as this reference. With an eye toward future double-chamber ion-molecule reaction studies, the pressure measurement interface was designed to allow the single head to be used to measure the pressure in either of two separate chambers. The valving arrangement is shown in Figure IV-5.

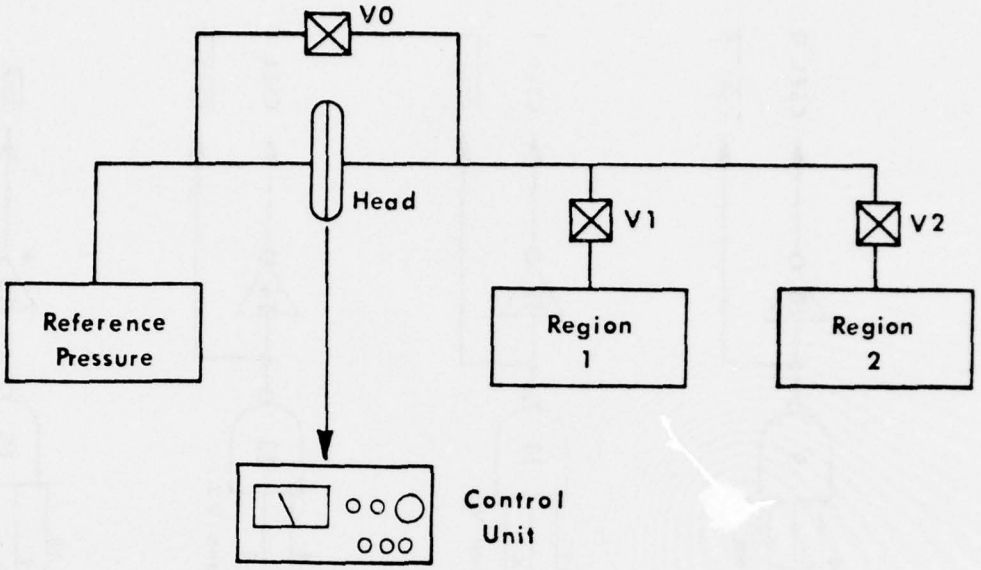


FIGURE IV-5. Sample Pressure Measurement System.

When only valve V0 is open, the pressures on either side of the head equilibrate, which allows the zero output level from the control unit to be checked. When only V1 is open, the pressure in region 1 is measured: when only V2 is open the pressure in region 2 is measured. The actual acquisition of pressure data is accomplished by measuring the voltage output of the control unit with a V/F converter and counter arrangement identical to that described in Sections E and G of this chapter. This section describes only the circuits which control the valves shown in Figure IV-5.

The valve control interface, like the shutter control, is operated either manually or under computer control, depending on the position of SW2 (Figure IV-6). Similarly, the computer can check (via gates 15 and 16) to see whether it has control of the interface.

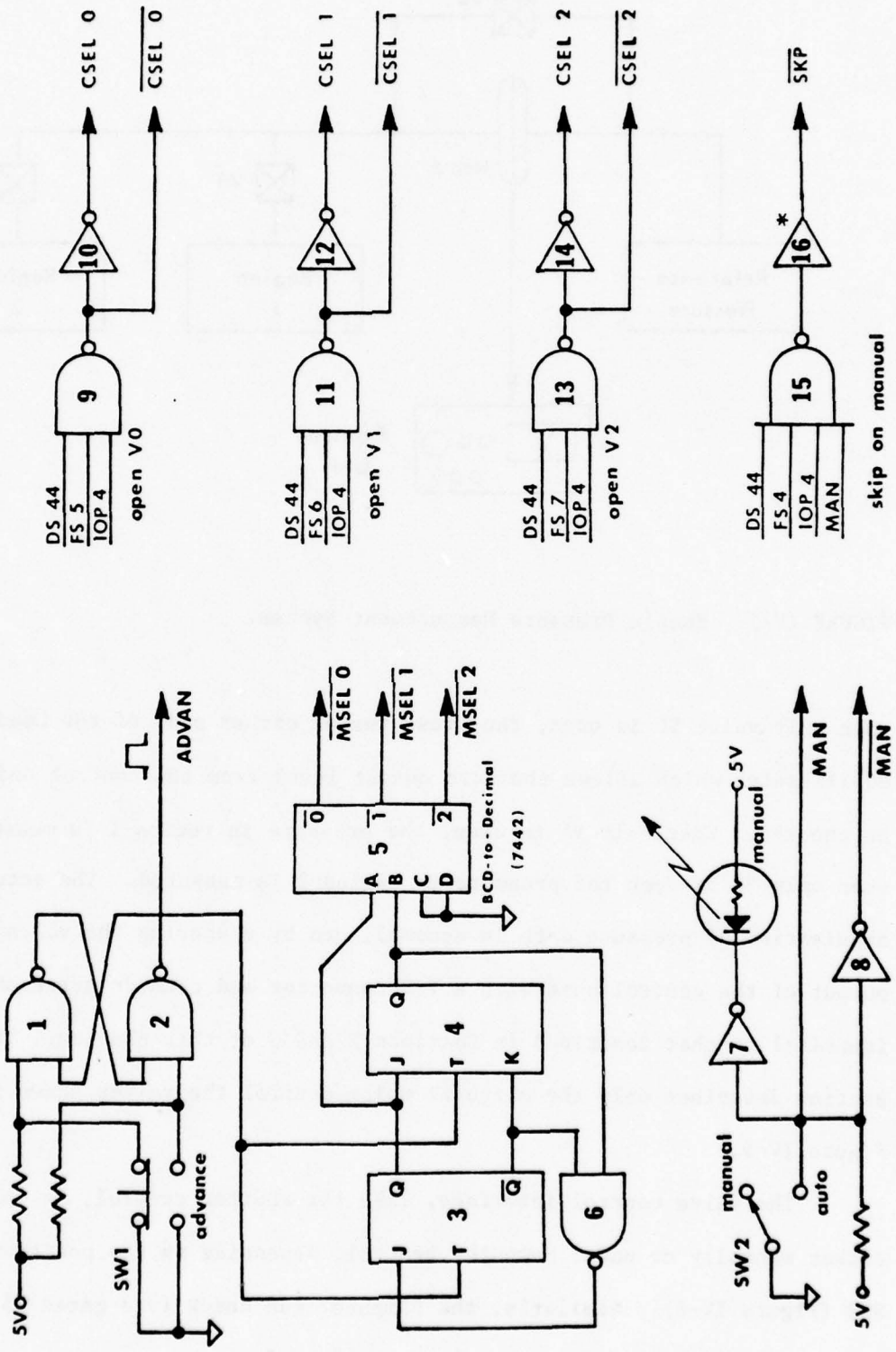


Figure IV-6. Valve Control Signal Generation.

It is both unnecessary and undesirable to have more than one of the three valves open at any given time, and the interface is designed to prevent this. When the interface is requested to open a given valve, it first closes all valves, waiting about a half a second to give any open valve time to close, and then opens the appropriate valve. As with the shutter, the valves are powered by 115 VAC, which is controlled by solid state relays. The solid state relays are driven by gates 25, 27 and 29 shown in Figure IV-7. These gates as well as the front panel indicator LEDs are controlled by JK flip-flops 21-23.

Assume that SW2 is in the manual position. When the advance pushbutton (SW1) is pushed, the ADVANCE signal ("debounced" by gates 1 and 2) will be passed by AOI gate 18, creating the CLOSE VALVES pulse which closes all valves. That same signal also triggers monostable 19, which 0.5 seconds later causes monostable 20 to emit a short OPEN VALVES pulse which goes to the toggle input of all three valve control flip-flops. Any flip-flop which has a logical 1 at its J input (ENABLE n, n=0,1,2) will be set by this pulse, opening the corresponding valve.

Flip-flops 3 and 4 (Figure IV-6) are wired as a modulo-3 binary counter which advances one every time an advance signal is received. The binary output is decoded by the BCD-to-decimal decoder 5 so that only one of the $\overline{\text{MSELn}}$ signals will be low. AOI gates 36-38 (Figure IV-8) insure that these signals control the ENABLEn lines during manual operation. Thus only one of the ENABLEn lines will be high, and the OPEN VALVES pulse will cause only one valve to open. Each time the advance push-button is pushed, a different valve will be opened.

It is possible to open valves out of sequence manually if the

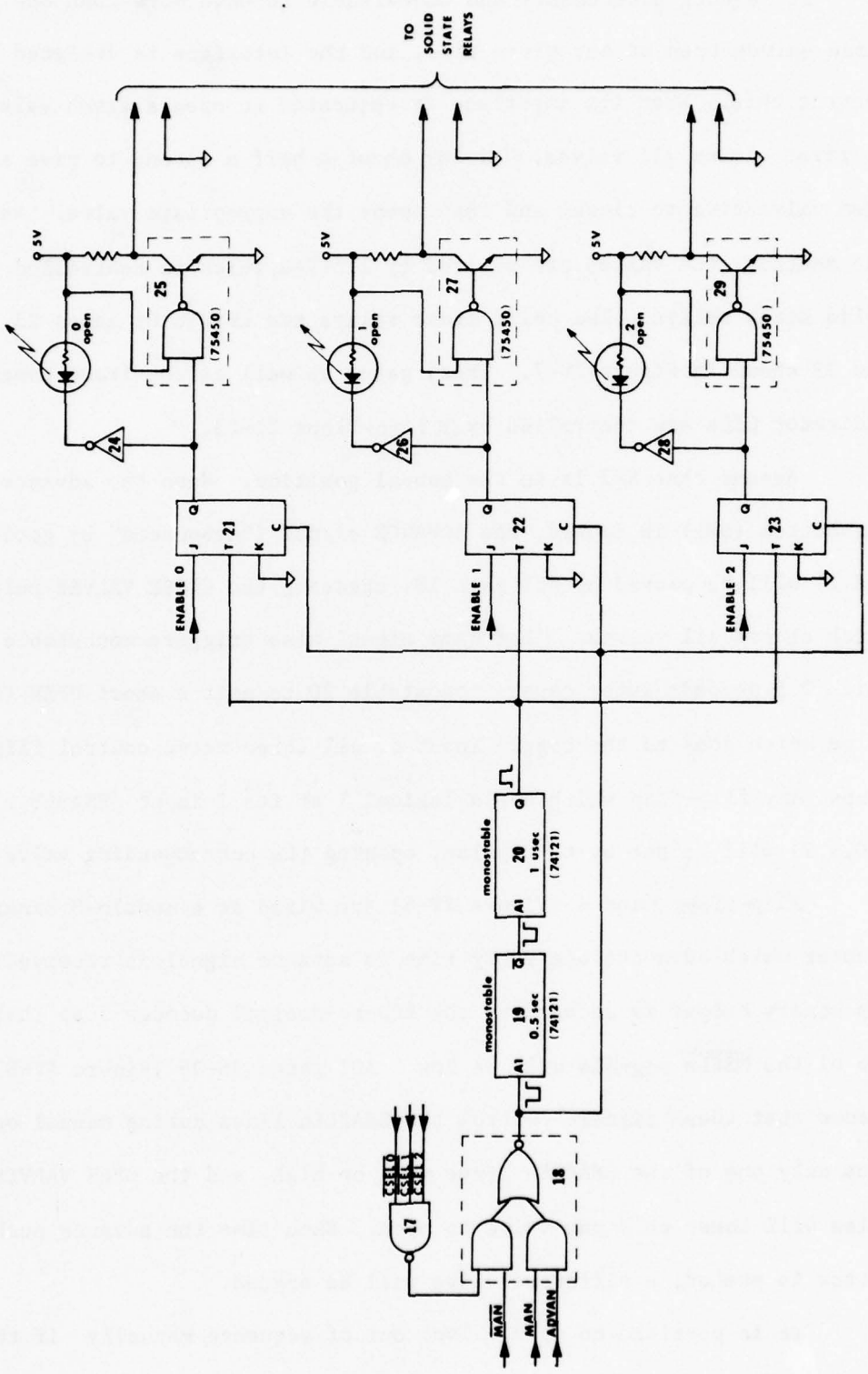


Figure IV-7. Valve Timing and Control.

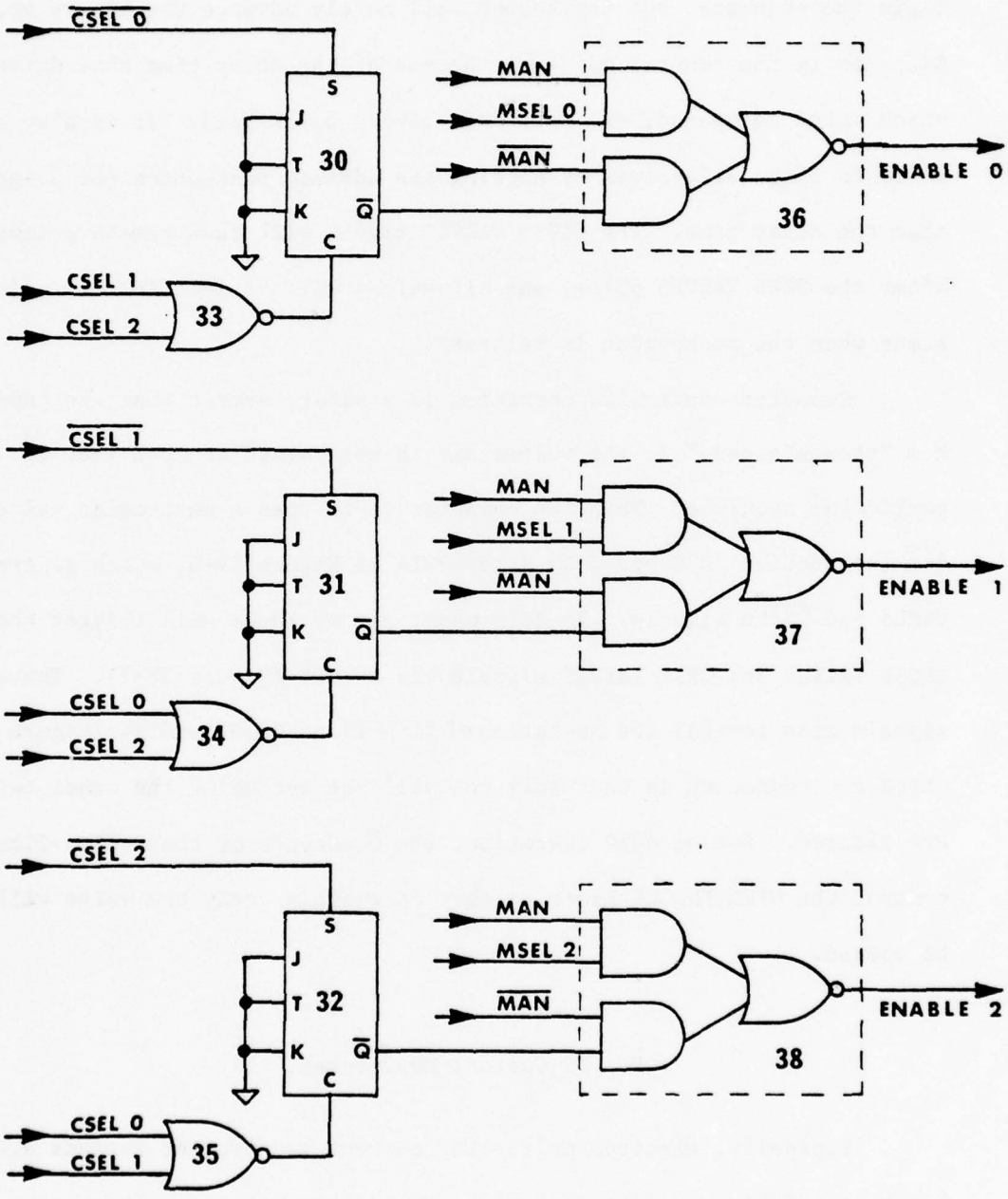


Figure IV-8. Valve Enable Signal Selection.

advance pushbutton is pressed an additional time during the delay between the CLOSE VALVES and OPEN VALVES signals. The first advance signal will begin the sequence, but the second will merely advance the binary counter. Since it is the counter value at the end of the delay time that determines which valve is opened, one valve can easily be skipped. It is also possible to close all valves by holding the advance pushbutton for longer than the delay time. The CLOSE VALVES signal will then remain active after the OPEN VALVES pulse, and all valves will be left in their closed state when the pushbutton is released.

Computer-controlled operation is similar, except that the computer has "random access" to the valves and is not forced to open them in any particular sequence. When the computer is to open a particular valve, its instruction is decoded by gates 9-14 of Figure IV-6, which generate the CSELn and $\overline{\text{CSELn}}$ signals. In AUTO mode, any of these will trigger the CLOSE VALVES and OPEN VALVES signals via AOI 18 (Figure IV-7). These signals also control the operation of flip-flops 30,32 and 34 (Figure IV-8), which are connected so that only one will be set while the other two are cleared. During AUTO operation, the $\overline{Q}$ outputs of these flip-flops control the OPEN ENABLE lines so that once again, only one valve will be opened.

E. DC Current Measurement

Typically, electron multiplier current measurement systems are built around high quality current-to-voltage converters. The output voltage from such a converter can be measured with an analog device such as a meter or chart recorder, or it can be converted to a digital

signal and displayed or recorded. When, as in PIMS, the current must be integrated over some period of time, the integration can be performed in either the analog or digital domains, although the latter is more accurate for integration times longer than a few seconds.

One of the simplest methods of achieving such digital current integration is shown in Figure IV-9. The voltage output of the I-to-V

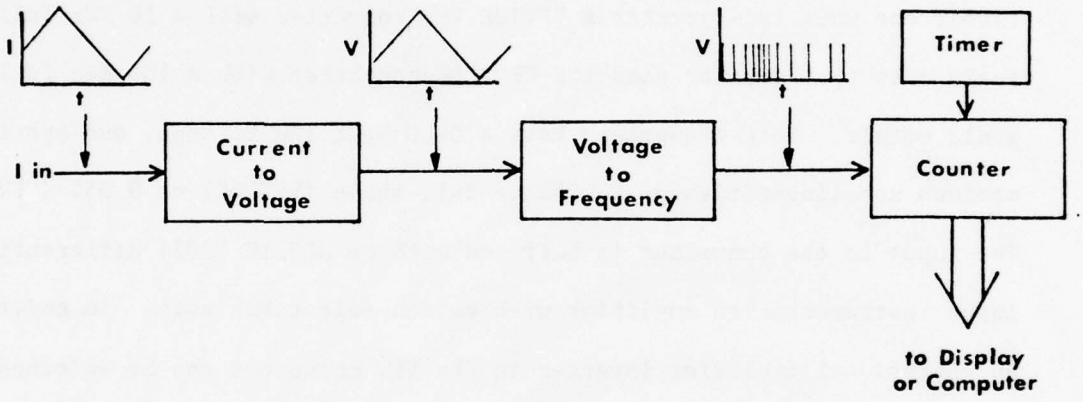


FIGURE IV-9. V-F Current Integration Method.

converter is converted to a frequency which is proportional to that voltage. The pulses from the V-F converter are counted with a digital counter, which at the end of the measurement interval contains a count proportional to the integral of the current over that same period. This is the system used in most automated photoionization mass spectrometers, including tne MSU instrument.

Two different current-to-voltage converters have been used. One, a Kiethley Instruments Model 417 high-speed picoammeter [105] has a 3V full scale output, which is switch-selectable, and may correspond to a

current between 1.0×10^{-13} amps to 3.0×10^{-5} amps. The other, a Kiethley 427 current amplifier, has a full scale output of 10V and a gain selectable between 10^4 and 10^{11} volts/ampere. The digital counter and its interface to the computer are described in Section G of this chapter. The remainder of this section is devoted to the V-F converter unit.

Two very similar V-F units have been built. The circuit used is shown in Figure IV-10. It is based on the Datel VFV series converter [106]; one unit incorporates a VFV10K V-F converter with a 10 KHz full scale output, the other uses the VFV100K converter with a 100 KHz full scale output. Both converters have a 0-10 Volt input range, and specified maximum non-linearities of 0.005% of full scale (VFV10K) or 0.05% (VFV100K). The input to the converter is buffered with an AD521K [107] differential input instrumentation amplifier with switch-selectable gain. In addition, an operational amplifier inverter in the VFV converter can be switched into the circuit so that inputs of either polarity may be used. Full scale output from the V-to-F converters can thus be obtained for inputs of 1, 2, 3, 5, 10 or 20 volts, with either positive or negative polarity. This versatility is required because these units are used to interface a wide variety of voltage sources to the computer when not in use with the PIMS instrument.

The output pulses from the V-F converter are fed to a 75450 AND driver integrated circuit, which is connected as a differential voltage mode line driver [109]. When coupled with the line receiver circuit described in Section G, this circuit is capable of providing communication over very long lines (5000 ft.) with excellent noise immunity [14]. Thus the V-to-F units may be located close to the voltage source whose output

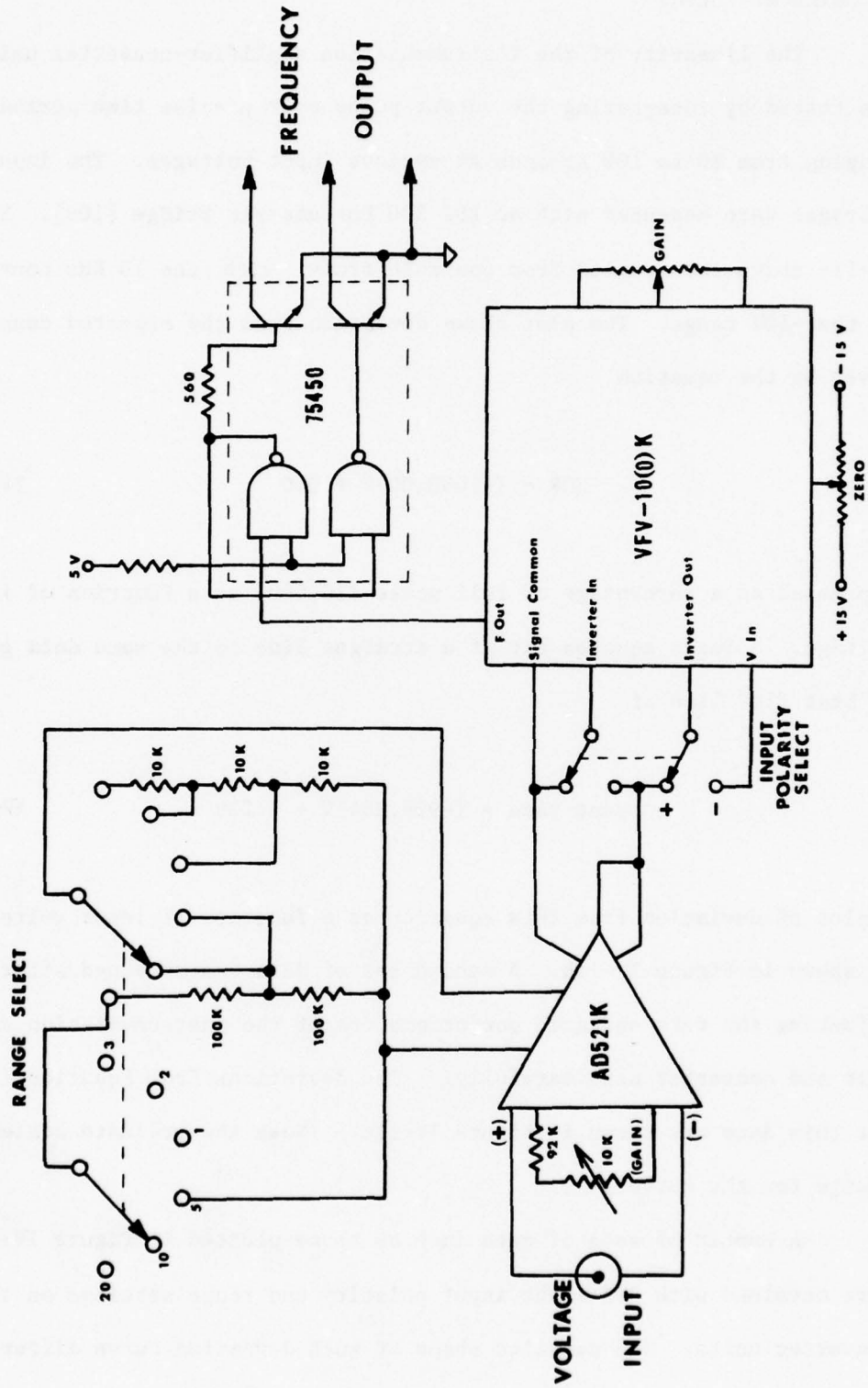


Figure IV-10. V-F Converter Module Circuit.

is being measured.

The linearity of the instrumentation amplifier-converter units was tested by integrating the output pulse over precise time periods ranging from 10 to 100 seconds at various input voltages. The input voltages were measured with an ESI 300 Portametric bridge [108]. Figure IV-11a shows the results from one such study, with the 10 KHz converter on the -10V range. The plot shows deviation from the expected count rate given by the equation

$$ECR = (-1000.00)V + 0.0 \qquad \text{IV-1}$$

expressed as a percentage of full scale (10,000) as a function of input voltage. A least squares fit of a straight line to the same data gave a "best fit" line of

$$\text{count rate} = (-999.164)V + 2.239 \qquad \text{IV-2}$$

A plot of deviation from this equation as a function of input voltage is shown in Figure IV-11b. A second set of data was obtained after adjusting the zero and gain potentiometers of the instrumentation amplifier and converter more carefully. The deviations from Equation (IV-1) for this data are shown in Figure IV-11c. (Note the ordinate scale change for the curve.)

A number of sets of data such as those plotted in Figure IV-11 were obtained with different input polarity and range settings on the converter units. The detailed shape of such deviation curve differed

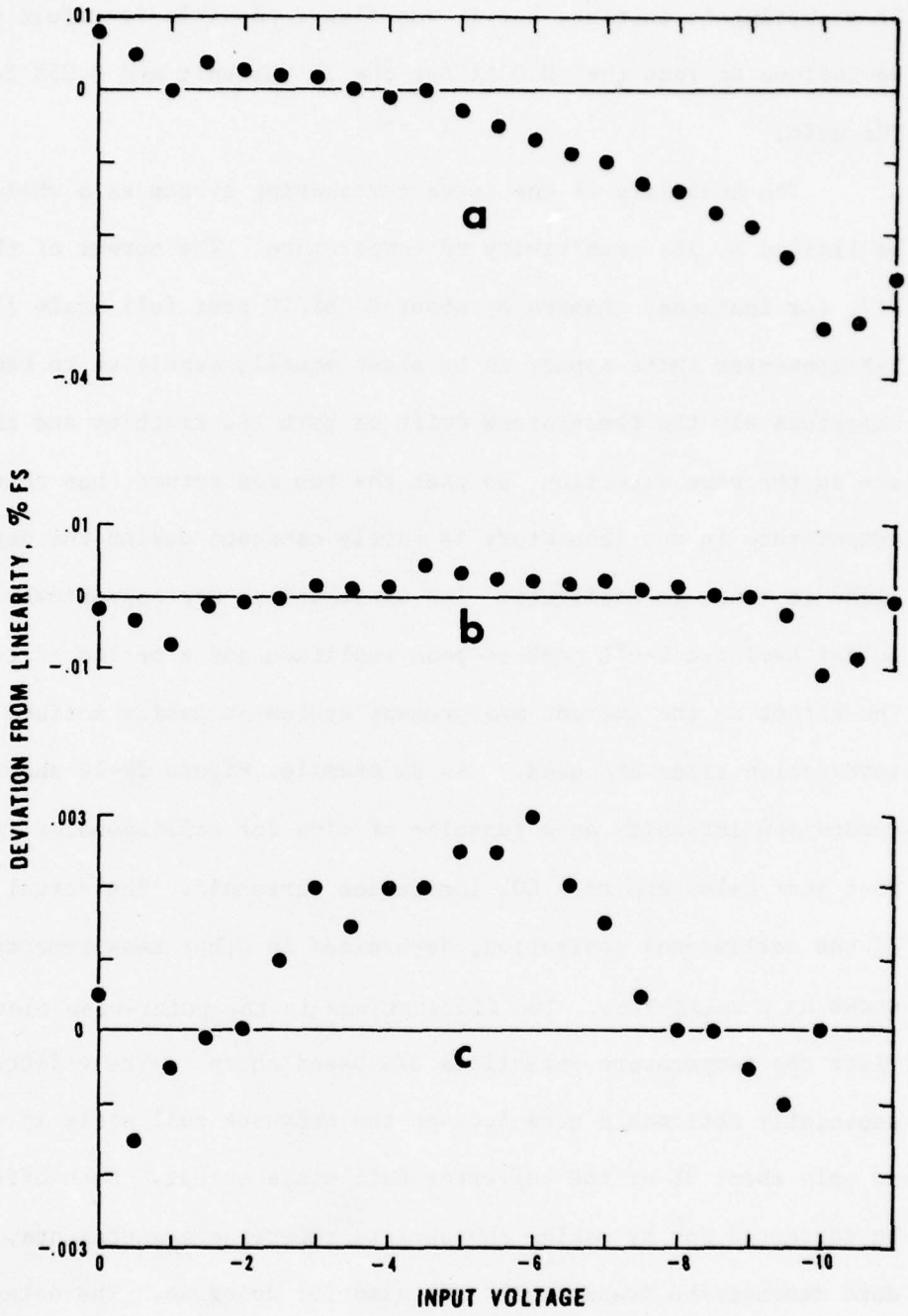


Figure IV-11. Linearity of the V-F Converter Module. The module was on the -10V range for all measurements shown here. Plots a and b were obtained before final adjustment; deviations are from equations IV-1 and IV-2, respectively. Plot c (note scale change) shows deviations from equation IV-1 after more careful adjustment.

from setting to setting, but it was always possible to adjust the maximum deviations to less than 0.005% for the 10 KHz unit and 0.05% for the 100 KHz unit.

The stability of the current measuring system as a whole seems to be limited by its sensitivity to temperature. The output of the Keithley 417, for instance, changes by about 0.16%/°C near full scale [110]. The V-F converter units appear to be about equally sensitive to temperature. Unfortunately the temperature drift of both the Kiethley and the converter are in the same direction, so that the two add rather than cancel. The temperature in our laboratory is fairly constant during the day, but at night it tends to oscillate. The oscillations are approximately sinusoidal having a 2-4°C peak-to-peak amplitude and a period of 1-2 hours. The effect on the current measurement system is easily noticed when long integration times are used. As an example, Figure IV-12 shows the recorded ion intensity as a function of time for collisionally ionized CO_2^+ ions just below the true CO_2 ionization threshold. The actual behavior of the collisional ionization, determined in other measurements, is shown as a solid line. The fluctuations in the point-wise plot reflect the temperature variations discussed above. The effects are especially noticeable here because the ordinate full scale in the figure is only about 3% of the converter full scale output. Such effects can be corrected for by making appropriate reference measurements, and these data demonstrate dramatically the need for doing so. The data also suggest that significant improvements could be made in the overall system performance by placing the current-to-voltage and voltage-to-frequency converters in a more stable temperature environment.

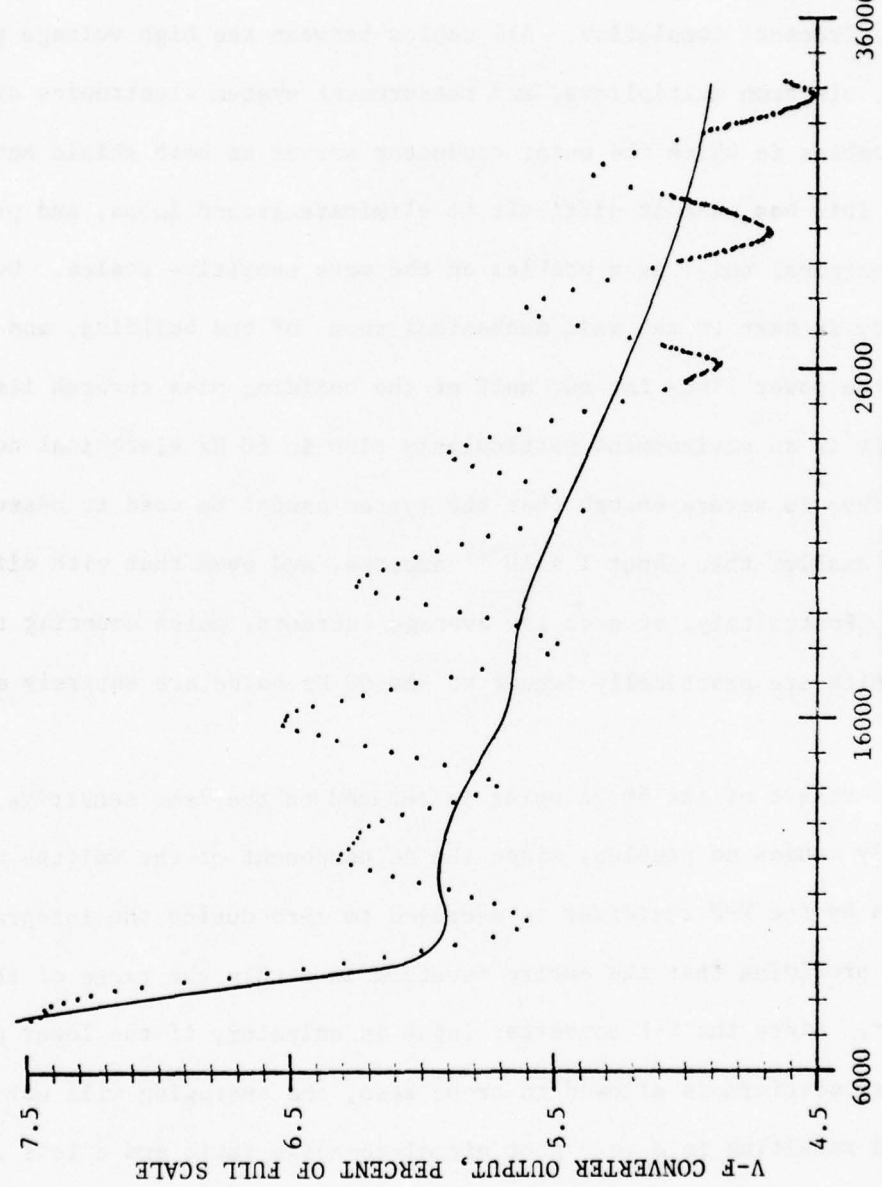


Figure IV-12. Effect of Temperature on the Analog Measurement System. The apparant oscillations in the ion intensity (points) are caused by room temperature oscillations of several degrees. The solid line shows the expected behavior of the ion intensity curve, determined in other measurements.

The V-F systems described here have been used to measure both photon and ion intensities, although the ion counter described in the next section has been used almost exclusively to measure ion intensities since its (recent) completion. All cables between the high voltage power supplies, electron multipliers, and measurement system electronics are coaxial cables in which the outer conductor serves as both shield and common. This has made it difficult to eliminate ground loops, and pick up of electrical noise is a problem on the more sensitive scales. Our laboratory is next to the main mechanical room of the building, and most of the power lines for our half of the building pass through its walls. It is an environment particularly rich in 60 Hz electrical noise. Noise pickup is severe enough that the system cannot be used to measure currents smaller than about 1×10^{-11} amperes, and even that with difficulty. Fortunately, at such low average currents, pulse counting techniques which are practically immune to the 60 Hz noise are entirely adequate.

The effect of the 60 Hz noise is reduced on the less sensitive scales. It usually causes no problem, since the AC component of the voltage waveform seen by the V-F converter is averaged to zero during the integration process, providing that the entire waveform is within the range of the converter. Since the V-F converter input is unipolar, if the lower part of a noisy waveform is allowed to cross zero, the averaging will not be performed resulting in a very poor signal-to-noise ratio and a loss of accuracy. The user must make sure that enough offset is added to the electrometer output to keep the noise signal always above zero.

Perhaps the most serious limitation of the present system is that

the range of the current-to-voltage converter must be set manually. Since it cannot be adjusted during an automated (operator-less) run, it must be set to a range which will keep all signals during the run on scale. If, as is often the case, one feature in the photon or ion intensity curve is much stronger than the rest, then the remainder of the data may have to be acquired using only the lower 10 percent of the electrometer range. While the resolution of the V-F converters, especially with long integration times, is more than adequate even if only 10% of their range is being used, their accuracy is not as good. Many of the errors involved in the measurement (non-linearities, zero drifts, etc.) are typically relatively constant and small when expressed as a percentage of full scale. However, if expressed as a percentage of the measured value, the errors become much larger for measurements near the bottom end of the range. As an example, consider deviations from linearity of the V-F converter. Figure IV-13 shows deviation measurements similar to those described earlier, plotted both as a percentage of full scale and as a percentage of the measured value. The disadvantage of obtaining most of the data at the lower end of the range is obvious; if the experiment were performed manually, the range of the I-V converter would be changed as often as necessary to maintain the lowest possible error. This cannot be done with the present system without losing the advantages of automated operation. However, a new current measurement system incorporating an I-to-V converter with remotely-selectable range is in the process of being designed.

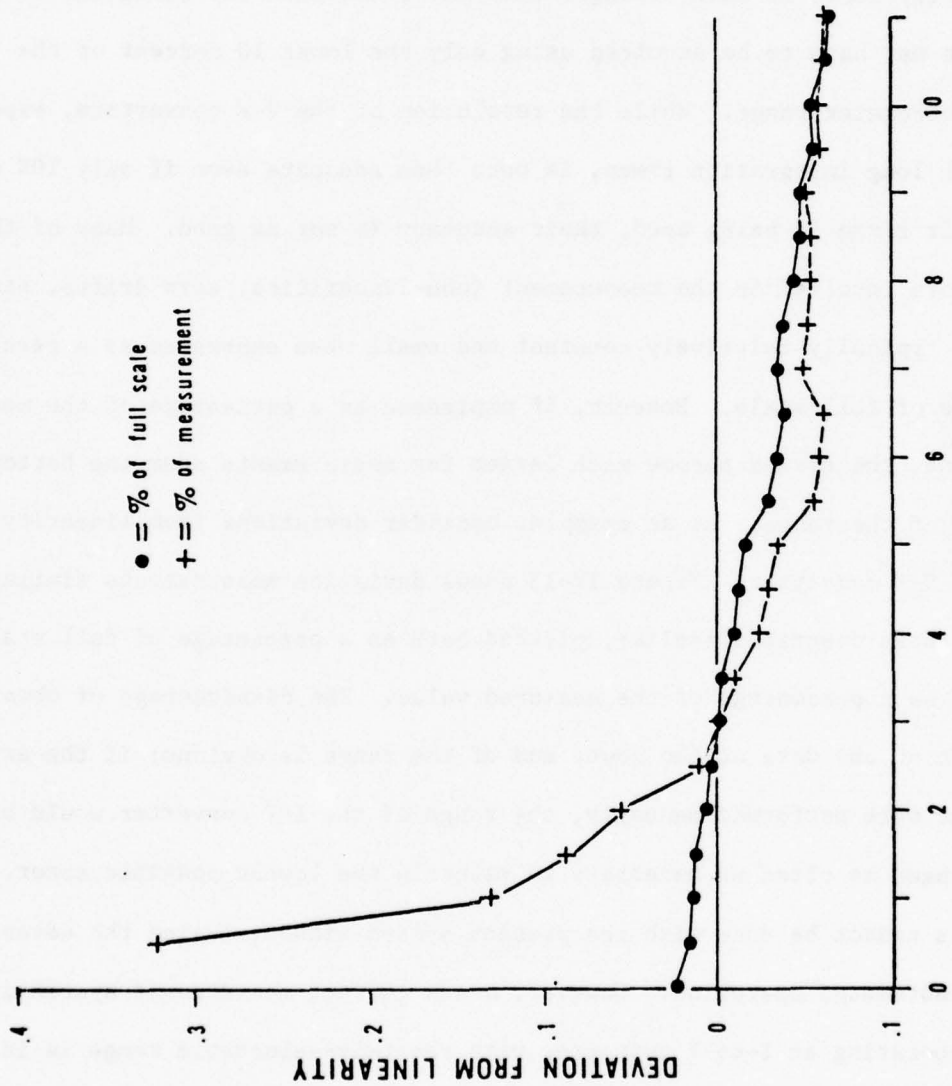


Figure IV-13. V-F Non-linearity as a Percentage of Full Scale and of Reading. V-F range, +10 V; assumed transfer function is Counts = 1000 V + 0.0.

F. The Pulse Counter

1. Introduction

Electron multipliers are widely used as particle flux transducers. Whether incorporated into a photomultiplier for measuring photon flux, or used "bare" for detecting electron, ion, or VUV photons, the output of the multiplier is usually measured with either pulse counting (PC) or direct current (DC) techniques. When the particle flux is extremely low, such as in PIMS experiments where only a few ions per second are generated, pulse counting techniques must be used [89]. At the other extreme, when the flux is very high, pulse overlap counting loss precludes use of pulse counting, and DC measurement techniques must be used [101]. Examples of this latter situation include measurement of photon intensity in PIMS, or in analytical absorption spectroscopy with bright light sources. In between these two extremes is a range where either technique may be used. The relative merits of PC and DC within this range depend on many factors, and the reader is referred to the paper by Ingle and Crouch [101], which examines these factors in detail. The exact limits of the range in which either PC or DC may be used are quite variable, since they depend on the characteristics of the PC and DC measurement systems[3] as well as the accuracy and precision required of the measurement. For instance, the upper limit of PC utility depends on the speed of the overall pulse counting system, as well as the magnitude of pulse overlap

---

[3] When making an evaluation of these limits, it is important to use the characteristics of the entire PC or DC measurement system, since the capabilities of each often depend as much on the transducer and power supplies as on the actual PC or DC electronics.

loss that can be tolerated.

In spite of the fact that DC measurement systems which are adequate for high flux measurements are readily available, there has been a continued interest in developing pulse counting systems which can operate at ever higher count rates, for several practical reasons. For instance, pulse counting systems often have significant signal-to-noise ratio and stability advantages over DC systems at equivalent fluxes [101]. Furthermore, PC is an inherently digital technique; PC measurements require fewer data domain conversions than DC measurements, and are thus less susceptible to the inevitable errors which accompany such conversions [101,111]. The development of faster PC systems not only extends these advantages to measurements made at higher fluxes, but also has important consequences in terms of cost and convenience. In order to retain the advantages mentioned above, one should use PC whenever possible, and DC only when necessary. If the measurements to be made span a range of fluxes which extends above the upper limit for the PC system, this may require switching back and forth between measurement systems rather frequently, which is often extremely inconvenient or even impossible (e.g., during an unattended experiment). Furthermore, high-quality DC current measurement instrumentation is expensive, and although many pulse counter designs have been reported in the literature [112] or are available commercially [113]; those designs which excel in speed, sensitivity and stability also tend to be fairly expensive. It is therefore desirable to use a PC system which is as fast as possible, so as to increase the probability that all necessary measurements (or at least an entire series of measurements) can be made without resorting to DC

techniques.

Unfortunately, no matter how fast the pulse counting electronics are, pulse overlap within the electron multiplier itself will eventually cause unacceptable counting losses.[4] Although dead-time compensation (DTC) [114] or post-experiment count loss formula corrections (CLFC) [115,116] can be used to extend the linearity of the system well into the region of pulse overlap, neither can be employed without compromising other potential advantages of the PC technique [101,115]. Optimum use of PC requires that the user be able to evaluate the trade-offs involved. Even if DTC or CLFC are employed, there may well exist some upper limit beyond which the use of DC measurement techniques becomes mandatory, and economic considerations then make it desirable that the pulse counter employed be as inexpensive as possible, while retaining high speed, sensitivity, and stability.

A block diagram of the pulse counter developed for use with the MSU PIMS instrument is shown in Figure IV-14. The digital counter (which is also used with the V-F converter modules described in Section E of this chapter) is described in Section G. The real-time clock used by the computer for timing purposes is described in Appendix C. The remainder of the circuitry (amplifier, discriminator, prescaler and line driver) is described and characterized in this section. For the sake of brevity, these four units will henceforth be termed the "pulse counter", although it should be realized that some sort of digital counter and timer are necessary to make a complete pulse counter.

---

[4] See Part 2 for a fuller discussion of this point.

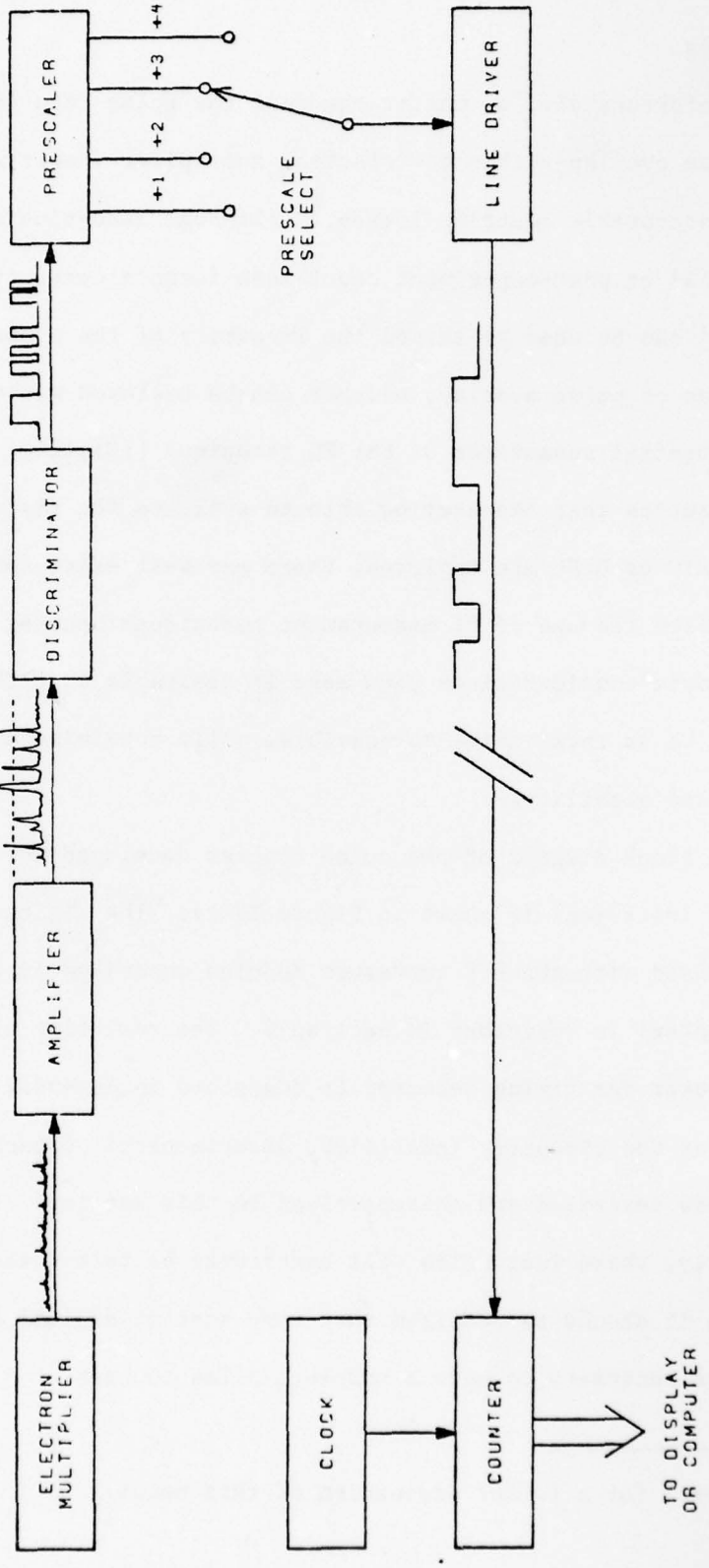


Figure IV-14. Block Diagram of the Pulse Counter.

The pulse counter described here has performance characteristics approaching those of state-of-the-art pulse counters, but it can be built for a small fraction of the cost of a commercial pulse counting system. It makes pulse counting an affordable alternative to DC measurement techniques. The pulse counter has high sensitivity as well as easily adjusted gain and discriminator levels, which are very stable as a function of time and temperature, and independent of pulse rate. These properties make it possible to perform an accurate characterization of the entire pulse counting system relatively quickly, and under the exact conditions to be used in the actual measurements. This provides the user with the information necessary to determine the optimum measurement system parameters for any given experiment. For instance, the user can easily obtain quantitative information on the benefits and disadvantages of using DTC for a given application, thus considerably simplifying the decision about whether to use DTC (and if so, how much). Furthermore, the discriminator level is voltage programmed and the amount of prescaling can be selected remotely. These features create the possibility of real-time computer control of the measurement system parameters, which could be automatically optimized to meet changing experimental conditions.

A pulse counting system consisting of the pulse counter described here and the RCA 8850 photomultiplier [69] used as part of the sodium salycilate photon transducer, described in Chapter II, has been thoroughly characterized. This system has attained maximum counting rates of greater than 35×10^6 photons sec^{-1}. With optimum dead time compensation, the system is linear to within ±0.5% up to a counting rate of 12 MHz, which

corresponds to a DC current of about 3×10^{-6} amperes. The results of these studies also indicate that, at least for this photomultiplier and for counters of similar sensitivity, the stability of the pulse counting electronics is more important than often assumed, but that the loss of stability inherent in the use of DTC is not necessarily as serious as often assumed. Similar, though less thorough, characterizations have been performed on systems employing an RCA 1P28 photomultiplier [69] and a Johnston MM1 electron multiplier [91]. Results for these systems were usually very similar to those for the 8850 system, and will be alluded to only briefly.

The circuitry of the pulse counter is described in Part 2 of this section, and its performance is characterized in Part 3. Part 4 contains several recommendations for modifications which should improve the performance of the pulse counter even further. The experiments used to characterize the 8850 system are described in Part 5, and their results and implications are discussed. Finally, this rather lengthy section is summarized in Part 6.

2. The Pulse Counter

i. Design Requirements:

The pulse counter described here was intended for use not only with the PIMS instrument, but also with a wide variety of computer-interfaced spectrometric instrumentation in other laboratories as well as our own. The primary design goals were high speed and sufficient sensitivity for use with common photomultiplier tubes, such as the 1P28.

The speed of the counter is important since pulse overlap in the

counter is usually the limiting factor in determining the maximum count rate at which accurate data can be obtained. State-of-the-art counters are capable of counting periodic pulses at up to about 100 MHz, i.e., they can resolve pulses separated by as little as 10 nsec. Unfortunately, the photon arrival rate is random, and a significant fraction of the pulses are separated by less than 10 nsec, even at much lower average rates than 100 MHz. For example, a 100 MHz counter with its discriminator set to pass all the pulses is expected to miss about 1% of the pulses at an average count rate of only 1 MHz.

Faster pulse counting electronics could help the pulse overlap problem only up to a point. Even relatively fast electron multipliers operated at moderate voltages have anode pulse rise times of about 1.5 - 3 nsec [117]. Fall times depend on the impedance and capacitance of the connection between the anode and the input to the pulse amplifier, but will certainly be longer than the rise times, and the FWHM of the pulse observed at the counter input will thus be on the order of 2-3 nsec. The width of the pulse near its base (where the discriminator is usually set to obtain best stability) might be expected to be several times the FWHM, or roughly 10 nsec. Thus, a 100 MHz pulse counter with a 10 nsec dead-time approaches the practical limit set by pulse overlap within the electron multiplier itself, and count rate improvements of more than a factor of 2 or so are probably not possible with the great majority of currently available photomultipliers. Therefore, 100 MHz was adopted as a speed goal which would be adequate if met, and which was felt to be quite ambitious enough.

The sensitivity of the counter is important for two reasons.

Pulse heights from a typical electron multiplier have a random and broad distribution. If the counter is not sensitive enough to count the smallest pulses, then some of the signal is wasted, increasing the measurement time or lowering the signal-to-noise ratio of the measurement. Furthermore, the stability often assumed for pulse counting systems is based on the assumption that there is more than enough sensitivity to count all the anode pulses. If this is true, then neither changes in the discriminator setting of the counter nor variations in the pulse height distribution due to power supply fluctuations or changes in the electron multiplier will alter the count rate, and the system will exhibit very good stability.

Ease of use and restricted space within the photomultiplier housings dictated that the pulse counter not be mounted inside the housing, but rather in a separate enclosure connected to the electron multiplier or photomultiplier with a short length of common 50 ohm coaxial cable. To minimize reflections, an anode load resistor of 50 ohms must be used. The amplitude of the voltage pulses generated across this resistor by the anode current pulses determines the sensitivity that the rest of the circuit must have. A Tektronix 7623A storage oscilloscope [98] was used to observe the voltage pulses developed across a 50 ohm load by anode current pulses from the 1P28, 8850 and MM1 multipliers. Of the three multipliers, the 1P28 produced the smallest pulses when run at normal operating voltages (<1000 V), the results shown in Figure IV-15 being typical. These measurements indicated that, although many pulses were as large as 5-10 mV, many were smaller than 1 mV. Therefore, a design goal of sub-millivolt sensitivity was adopted.

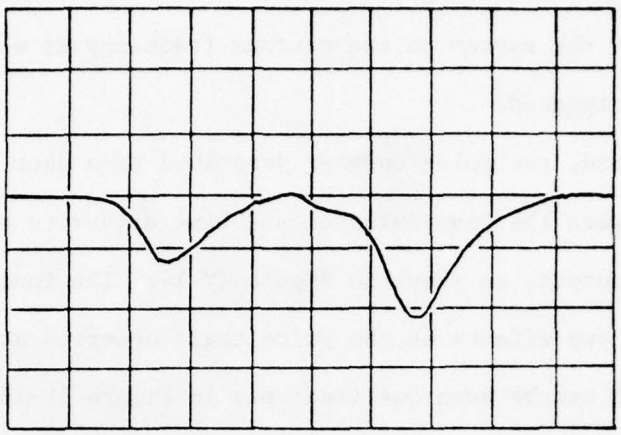


FIGURE IV-15. Anode Pulses from a 1P28 Photomultiplier. 50Ω load. Vertical: 5 mV/div. Horizontal: 5 nsec/div. PMT voltage: 900 V.

To minimize broadening of the anode pulse by excess cable capacitance, the pulse counter must be located near the multiplier. Often, however, the digital counter is located some distance further away (about 50 feet in the case of the PIMS instrument/computer). To increase the versatility of the counter, it must therefore include circuitry capable of transmitting the signal to the digital counter over long distances (e.g., 100 feet or more) with good noise immunity. Commonly available integrated-circuit line drivers are incapable of responding to pulses as short as those expected at the output of the discriminator (ca. 10 nsec) [109], so that some sort of signal conditioning is required between the discriminator and line driver. A common solution to this problem is simply to insert a monostable "pulse stretcher" between the two, to make certain

that the pulses at the line driver input are slow enough for it and the succeeding circuitry to handle. However, this approach limits the overall speed of the system to the maximum frequency at which the monostable can be re-triggered.

Instead, the pulse counter described here uses a fast binary counter between the discriminator and line driver to prescale the discriminator output, as shown in Figure IV-14. The inclusion of such prescaling has two effects on the pulse train observed at the line driver input, which can be seen qualitatively in Figure IV-16. After division by eight, the average pulse rate is reduced by a factor of eight, so that succeeding circuitry does not have to be so fast. Perhaps even more important is the fact that the prescaling exerts more of an influence on the high-frequency end of the pulse arrival time distribution than on the low frequency end. This has the effect of reducing the "randomness" of the pulse train--the maximum instantaneous pulse rate is much closer to the mean rate after prescaling than before, so that the line driver and succeeding circuitry need to be able to respond to pulse rates only a little higher than the average rate.

While prescaling does not limit the maximum count rate, it does limit the maximum attainable count resolution. At high count rates, when prescaling is most needed, the loss in resolution should be negligible, but at low rates, it may be important. Fortunately, at low count rates, less prescaling is needed and, if the amount of prescaling can be changed, the count resolution can be improved when necessary.

ii. Preamplifier/Discriminator Circuit:

The preamplifier-discriminator portion of the pulse counter is

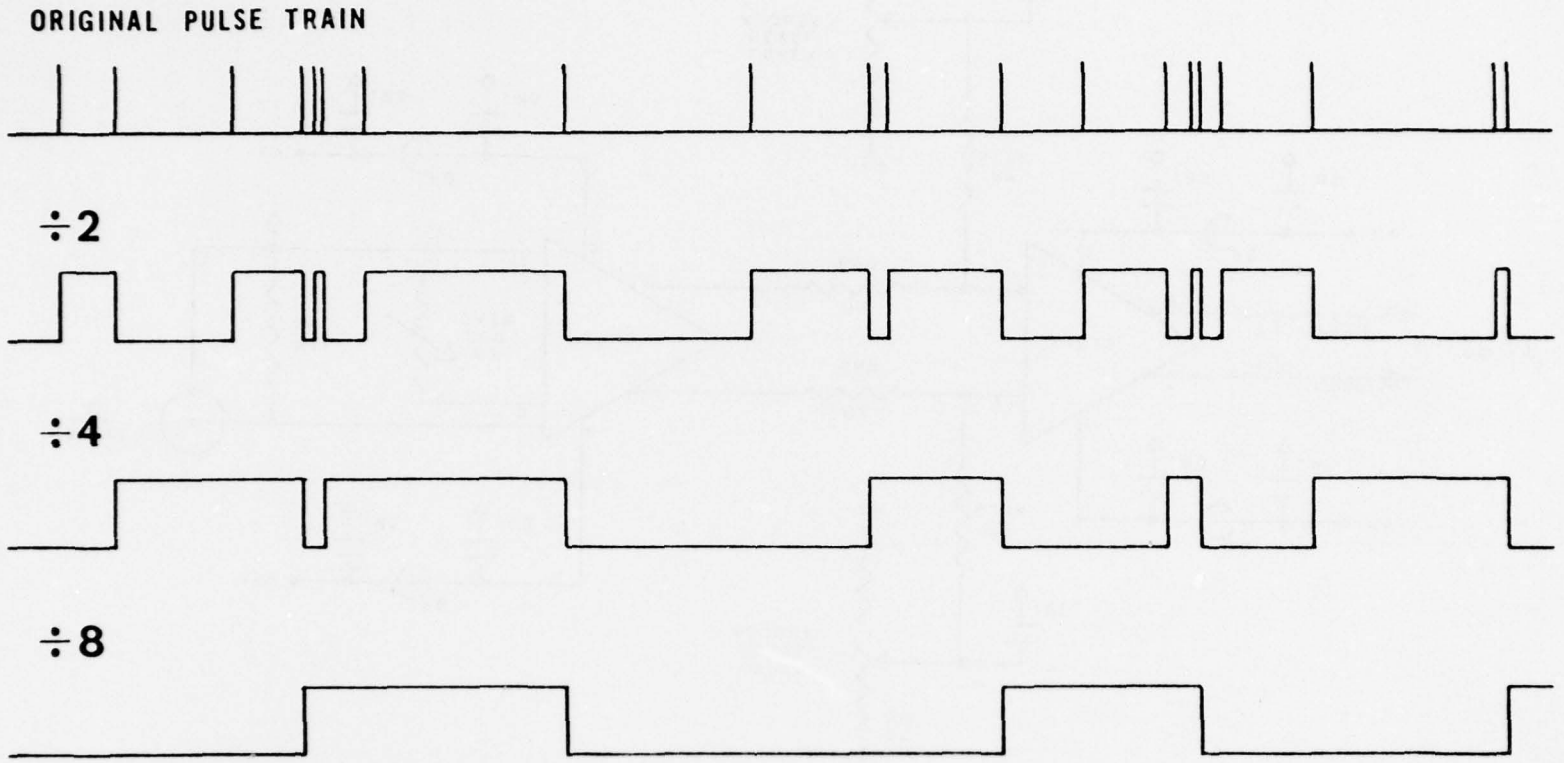


Figure IV-16. The Effect of Prescaling on a Random Pulse Train.

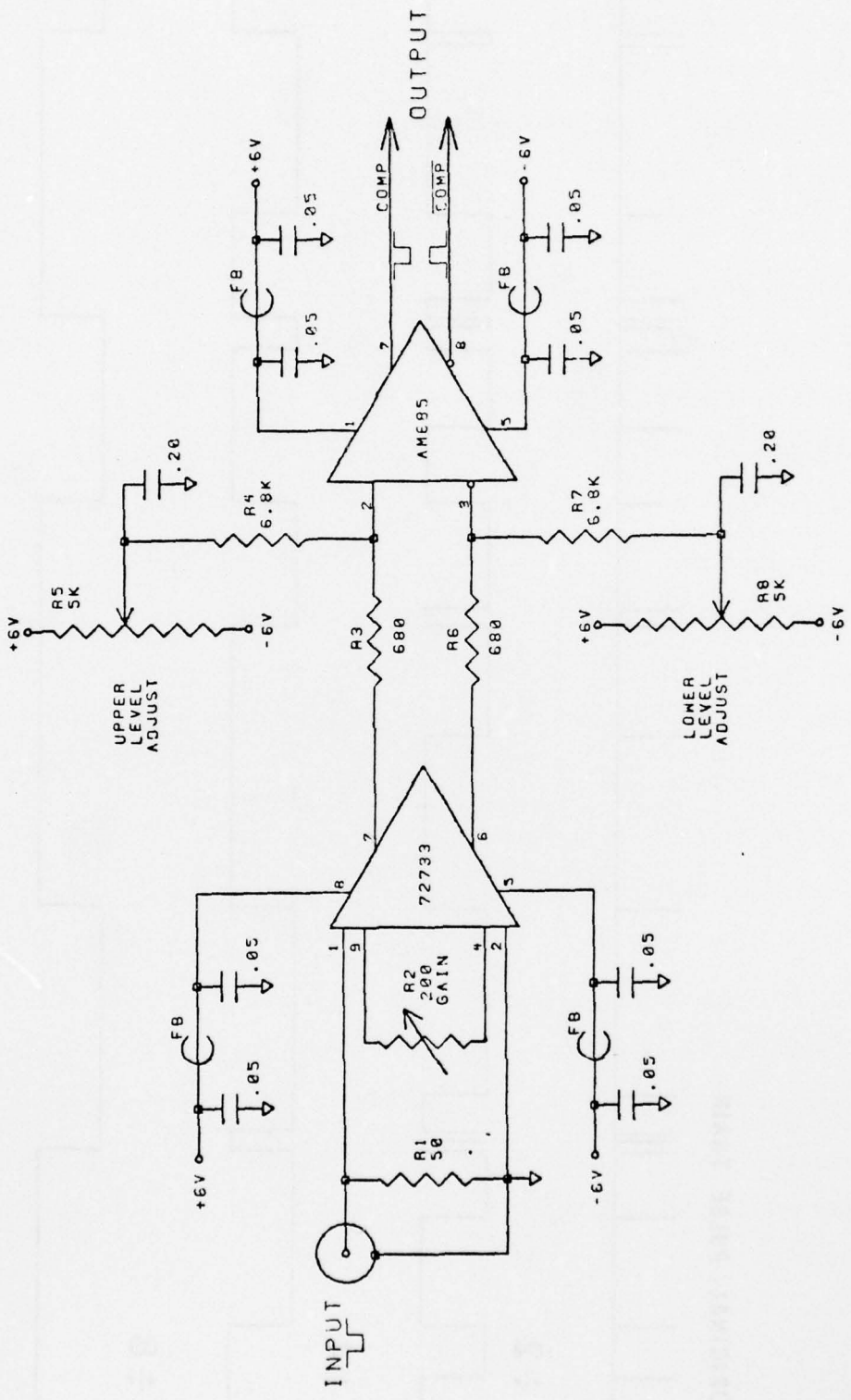


Figure IV-17. Preamplifier / Discriminator Circuit. All resistor values in ohms, all capacitor values in microfarads. FB = ferrite bead.

very simple, being based on only two integrated circuits, as shown in Figure IV-17. A high-speed comparator (Advanced Mirco Devices type AM 685 [118]) with differential inputs and emitter-coupled logic (ECL) outputs is used as the discriminator. The preamplifier is a Texas Instruments SN72733 adjustable gain, high-speed differential video amplifier[5] [119]. When the counter is in its quiescent state (both amplifier inputs at essentially zero volts), the amplifier outputs have a common mode voltage, V_{Acm}, which is typically about 2.9 volts, and are separated by an offset voltage, V_{Ao}, which depends on the gain of the amplifier, but is typically 0.6 V at a gain of 400. A negative pulse at the input of the amplifier causes the outputs to move closer together, and for sufficiently large input pulses, the outputs will cross (see Figure IV-18).

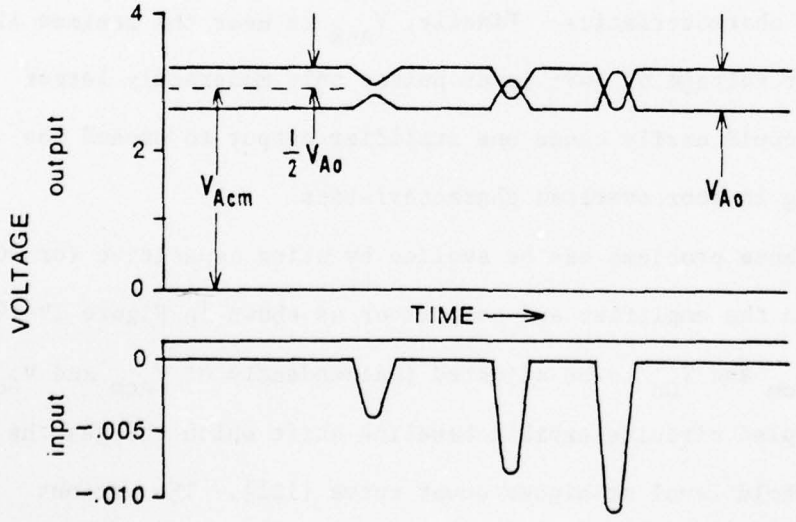


FIGURE IV-18. Response of Amplifier to Input Pulses.

[5]Also manufactured by Motorola [120], and perhaps others.

A quiescent comparator input common mode voltage, V_{Ccm}, and an input offset voltage, V_{Co}, can be defined which are analogous to V_{Acm} and V_{Ao}. The comparator is triggered whenever its inputs cross, i.e., when the input pulse to the comparator is larger than V_{Co}:

If the amplifier outputs are connected directly to the comparator inputs, then $V_{Acm} = V_{Ccm}$ and $V_{Ao} = V_{Co}$. In this case, the threshold of the counter is given simply by the minimum pulse amplitude necessary to make the amplifier outputs cross, or V_{Ao}/G, where G is the gain of the amplifier. Though conceptually simple, such a design is undesirable for several reasons. An amplifier gain of more than 600 is necessary to obtain sub-millivolt sensitivity, and the maximum gain of the amplifier is only 400. The only way of adjusting the threshold of the counter is to change the gain of the amplifier, which also changes its bandwidth and temperature characteristics. *Finally*, V_{Acm} is near the maximum allowed comparator input voltage of +4V; input pulses only moderately larger than threshold could easily cause one amplifier output to exceed the limit, resulting in poor overload characteristics.

All of these problems can be avoided by using capacitive (or AC) coupling between the amplifier and comparator, as shown in Figure IV-19, which allows V_{Ccm} and V_{Co} to be adjusted independently of V_{Acm} and V_{Ao}. However, AC coupled circuits exhibit baseline shift which changes the effective threshold level at higher count rates [121]. The various diode clamp techniques which are commonly used to limit baseline shift do not completely eliminate it [122], and design of baseline correction circuits suitable for use at 100 MHz is a problem which is far from trivial.

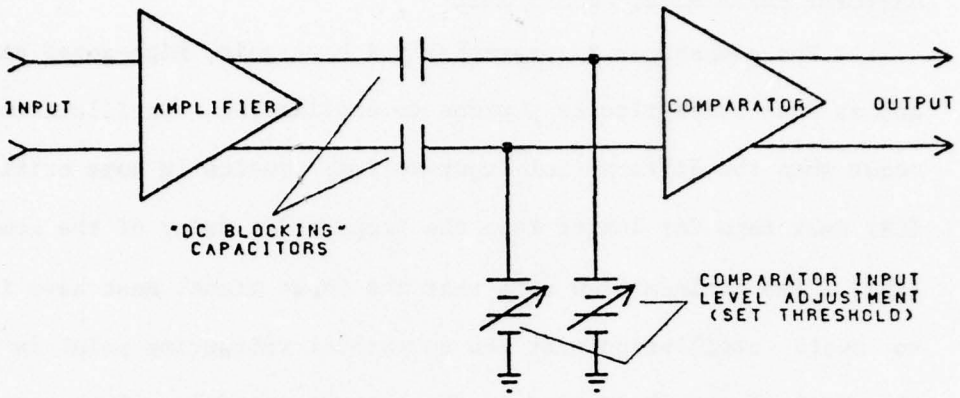


FIGURE IV-19. AC Coupling of Amplifier and Comparator.

This pulse counter, therefore, retains DC coupling, but through two simple resistor networks as seen in Figure IV-17. Resistors R3 and R4 (and similarly R6 and R7) act as simple voltage dividers, transmitting a large fraction of the amplifier output pulse to the comparator input. However, R5 and R8 allow the voltage at one end of each divider to be varied independently over a range of +6V to -6V, which in turn allows independent control of the quiescent values of the comparator input voltages. With the component values shown, V_{Ccm} can be reduced to approximately 1V, which yields much improved overload characteristics. V_{Co} can be adjusted continuously within a range of approximately ±300 mV. A typical value might be 60 mV, resulting in a tenfold gain in sensitivity compared with the directly coupled amplifier and comparator. Both V_{Ccm} and V_{Co} can be varied independently of the gain of the amplifier, which can be set so as to obtain the best compromise between bandwidth and temperature stability (see Part 3). Furthermore, <u>there is no</u>

baseline shift at any count rate.

The comparator is essentially a high-gain, high-speed amplifier, and as such is particularly prone to oscillation. Oscillations will occur when the differential input voltage remains in some critical range (CR) near zero for longer than the propagation delay of the comparator [123]. The minimum slew rate that the input signal must have in order to avoid oscillation near the comparator triggering point is simply the width of the CR divided by the propagation delay of the comparator. Fortunately, the slew rate of the amplified anode pulses is much higher than the minimum necessary slew rate, so that hysteresis (which can only limit sensitivity and maximum speed) is unnecessary.[6]

The tendency to oscillate does limit the overall sensitivity of the counter, however, since the CR limits the minimum useful value of V_{Co}. The width of the CR (which may be as small as a few mV or as large as several hundred mV) depends on the (fixed) gain of the comparator, the extent to which the comparator's output is coupled back to its input via stray capacitance, and the source impedance seen by the comparator at its inputs [123]. Careful construction techniques can help minimize the stray capacitance between comparator output and input. The use of a comparator with ECL outputs is also advantageous, since the voltage swing for an ECL logic transition is only about one-fifth of that for a TTL logic transition, and thus there is less signal to couple back to

---

[6]The pulse counter was in fact constructed so that various amounts of comparator hysteresis could be added, to study their effect. Hysteresis was found necessary for preventing oscillation only with input frequencies less than 1 MHz. Since anode pulses with FWHMs less than 50 nsec have no frequency components below about 20 MHz, hysteresis is unnecessary for electron multiplier pulse counting application, no matter how low the input count rate.

the inputs. The width of the CR is also found to be smallest when the comparator is driven by a balanced source with an output impedance of about a thousand ohms or a little larger.[7] The differential outputs of the video amplifier used in this design provide a balanced source for the comparator, although they have a low output impedance (about 20 ohms [124]). The coupling resistors R3 and R6 serve not only to provide easily adjustable V_{Co} and V_{Ccm}, but also to increase the source impedance seen by the comparator inputs.

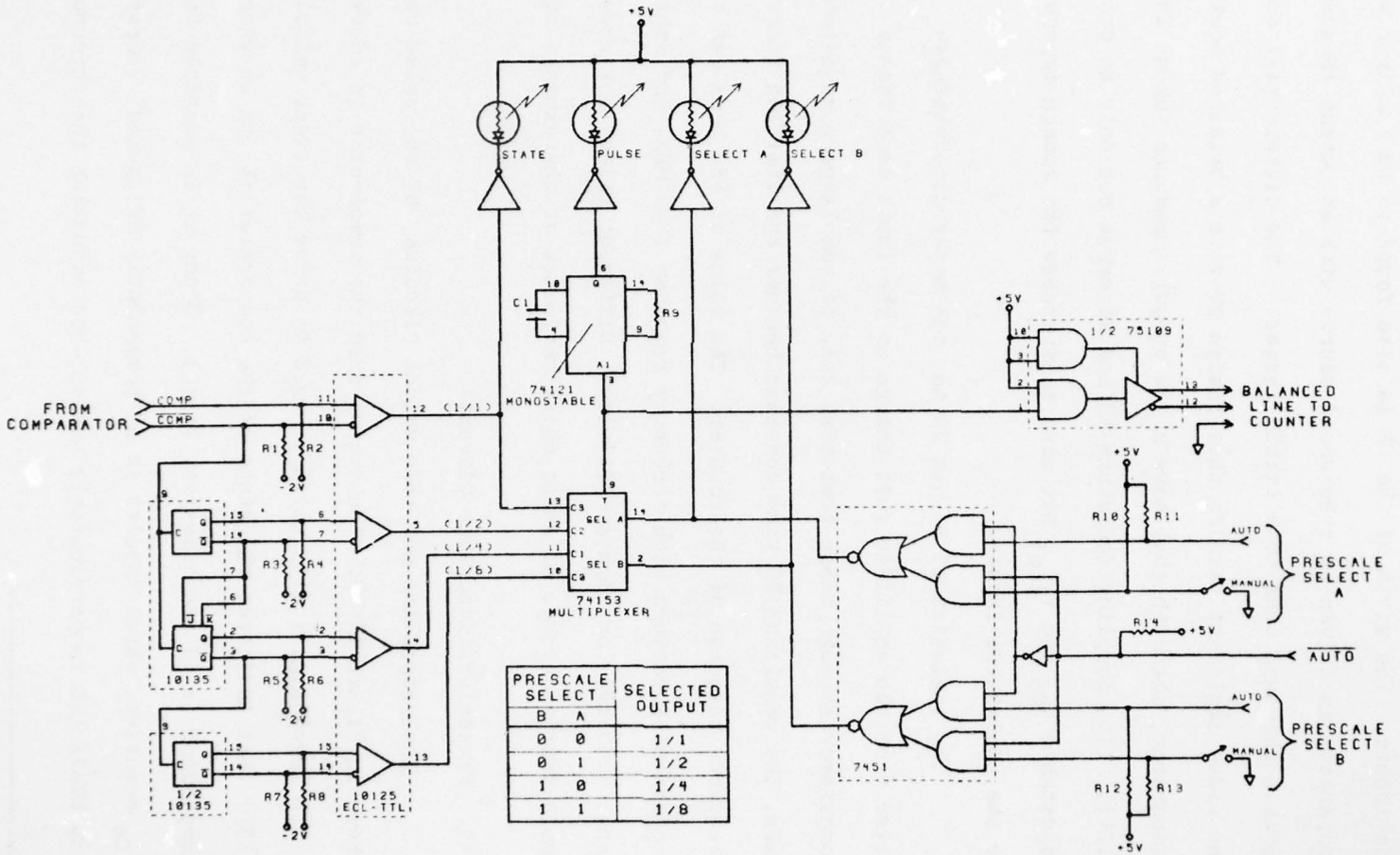
The inclusion of R3 and R6 has one major disadvantage. Every pulse from the amplifier must charge up the input capacitance of the comparator through these resistors and, if too large a resistance is used, the resulting RC time constant becomes the limiting factor in the frequency response of the counter. The value of 680 ohms was chosen as a compromise between high frequency response (>90 MHz) and small critical range (≃30 mV), or high sensitivity. Different values for these resistors could improve either of these characteristics at the expense of the other.

iii. Prescaler/Linedriver Circuit:

The prescaling and line driver circuits of the pulse counter are shown in Figure IV-20. The signal from the comparator is converted into a TTL level signal (÷1) which is used to drive the light emitting diode (LED) that indicates the state of the comparator (it is on when the comparator is in its quiescent state). Since it is possible to make V_{Co} negative, which results in a "permanently triggered" comparator, the STATE LED is particularly useful when adjusting the threshold level

---

[7] This applies to the metal can package. The DIP package may have its smallest CR at different input impedances.



PRESCALE SELECT		SELECTED OUTPUT
B	A	
0	0	1/1
0	1	1/2
1	0	1/4
1	1	1/8

Figure IV-20. Prescaler / Line Driver Circuit. Pulldown resistors (R1-R8) are 50Ω, pullup resistors (R10-R14) are 3KΩ. Values of R9 and C1 are not critical (see text).